2013

Power System State Estimation Using Phasor Measurement Units

Jiaxiong Chen
University of Kentucky, jchen208@hotmail.com

STUDENT AGREEMENT:

I represent that my thesis or dissertation and abstract are my original work. Proper attribution has been given to all outside sources. I understand that I am solely responsible for obtaining any needed copyright permissions. I have obtained and attached hereto needed written permission statements(s) from the owner(s) of each third-party copyrighted matter to be included in my work, allowing electronic distribution (if such use is not permitted by the fair use doctrine).

I hereby grant to The University of Kentucky and its agents the non-exclusive license to archive and make accessible my work in whole or in part in all forms of media, now or hereafter known. I agree that the document mentioned above may be made available immediately for worldwide access unless a preapproved embargo applies.

I retain all other ownership rights to the copyright of my work. I also retain the right to use in future works (such as articles or books) all or part of my work. I understand that I am free to register the copyright to my work.

REVIEW, APPROVAL AND ACCEPTANCE

The document mentioned above has been reviewed and accepted by the student's advisor, on behalf of the advisory committee, and by the Director of Graduate Studies (DGS), on behalf of the program; we verify that this is the final, approved version of the student's dissertation including all changes required by the advisory committee. The undersigned agree to abide by the statements above.

Jiaxiong Chen, Student

Dr. Yuan Liao, Major Professor

Dr. Caicheng Lu, Director of Graduate Studies

POWER SYSTEM STATE ESTIMATION USING PHASOR MEASUREMENT UNITS

DISSERTATION

A dissertation submitted in partial fulfillment of the requirements for the degree of Doctor of Philosophy in the College of Engineering at the University of Kentucky

By

Jiaxiong Chen

Lexington, Kentucky

Director: Dr. Yuan Liao, Associate Professor of Electrical and Computer Engineering

Lexington, Kentucky

2013

ABSTRACT OF DISSERTATION

POWER SYSTEM STATE ESTIMATION USING PHASOR MEASUREMENT UNITS

State estimation is widely used as a tool to evaluate the real time power system prevailing conditions. State estimation algorithms could suffer divergence under stressed system conditions. This dissertation first investigates impacts of variations of load levels and topology errors on the convergence property of the commonly used weighted least square (WLS) state estimator. The influence of topology errors on the condition number of the gain matrix in the state estimator is also analyzed. The minimum singular value of gain matrix is proposed to measure the distance between the operating point and state estimation divergence.

To study the impact of the load increment on the convergence property of WLS state estimator, two types of load increment are utilized: one is the load increment of all load buses, and the other is a single load increment. In addition, phasor measurement unit (PMU) measurements are applied in state estimation to verify if they could solve the divergence problem and improve state estimation accuracy.

The dissertation investigates the impacts of variations of line power flow increment and topology errors on convergence property of the WLS state estimator. A simple 3-bus system and the IEEE 118-bus system are used as the test cases to verify the common rule. Furthermore, the simulation results show that adding PMU measurements could generally improve the robustness of state estimation.

Two new approaches for improving the robustness of the state estimation with PMU measurements are proposed. One is the equality-constrained state estimation with PMU measurements, and the other is Hachtel's matrix state estimation with PMU

measurements approach. The dissertation also proposed a new heuristic approach for optimal placement of phasor measurement units (PMUs) in power system for improving state estimation accuracy. In the problem of adding PMU measurements into the estimator, two methods are investigated. Method I is to mix PMU measurements with conventional measurements in the estimator, and method II is to add PMU measurements through a post-processing step. These two methods can achieve very similar state estimation results, but method II is a more time-efficient approach which does not modify the existing state estimation software.

KEY WORDS: Weighted Least Square, Phasor Measurement Unit, Topology Error, Load Increment, Optimal Placement

Jiaxiong Chen

November 6, 2013

POWER SYSTEM STATE ESTIMATION USING PHASOR MEASUREMENT UNITS

By

Jiaxiong Chen

Dr. Yuan Liao

_____

Director of Dissertation

Dr. Cai-Cheng Lu

_____

Director of Graduate Studies

November 1, 2013

_____

Date

ACKNOWLEDGEMENTS

I wish to acknowledge and thank those people who helped me complete this dissertation:

Dr. Yuan Liao, my academic advisor, who gave me the chance to do research in this field and guided me through my studies by his valuable help and encouragement. I could not have imagined a better mentor than Dr. Liao. His insightful experience and assistance have always been helpful to my research. I also gratefully acknowledge Dr. Bei Gou for his invaluable suggestions during the research.

Special thanks are also extended to members of the committee, Dr. Yu-Ming Zhang, Dr. Paul Dolloff, Dr. Alan Male and Dr. Zongming Fei for their insightful advice and willingness to serve in the Dissertation Advisory Committee.

I would also like to thank my parents for their endless love, support and understanding.

Table of Contents

ACKNOWLEDGEMENTS iii

List of Tables vii

List of Figures viii

Chapter 1 Introduction 1

1.1 Background 1

1.2 Phasor Measurement Unit 3

1.3 Lessons of Northeast Blackout in 2003 5

1.4 Contribution of This Dissertation 6

1.5 Dissertation Outline 8

Chapter 2 Impacts of Load Levels and Topology Error on WLS State Estimation Convergence 10

2.1 WLS State Estimation Algorithm 10

2.1.1 Numerical Formulation 10

2.1.2 The Measurement Jacobian 12

2.1.3 Ill-conditioned Problem 15

2.2 Overall Description of the Performed Studies 17

2.3 Results of Divergence Characteristics Study 19

2.4 Analysis of the Converged $cond(G)$ 22

2.5 Gain Matrix Stability Index 35

2.5.1 Singular Value Decomposition of Gain Matrix 35

2.5.2 Testing Results of σ_n 36

2.6 Conclusion 37

Chapter 3 Convergence Property of the State Estimation Considering Two Types of Load Increment and PMU Measurements 39

3.1 Introduction 39

3.2 State Estimation Considering Load Increment for All the Load Buses 40

3.2.1 Adding Conventional Voltage Magnitude Measurements in Measurement Vector 42
3.2.2 Adding PMU Voltage Phasor Measurements 44
3.3 Simulation Results Considering Single Load Increment 46
3.4 Effect of Adding PMU Measurements on State Estimation Accuracy 51
3.5 Conclusion 53

Chapter 4 Convergence Property of State estimation with Load Increment on a Specific Line .. 54
4.1 Introduction 54
4.2 Formulation of Topology Error in WLS State Estimation 55
4.3 Simulation results 57
4.3.1 Test on a Simple 3-bus System 58
4.3.2 Test on the IEEE 118-bus system 62
4.4 Effect of PMU measurements on WLS State Estimation convergence 65
4.5 Future work 67
4.6 Conclusion 69

Chapter 5 Incorporation of PMU Measurements in WLS State Estimation 70
5.1 Introduction 70
5.2 Equality-constrained State Estimation with PMU Measurements Approach 72
5.3 Hachtel's Matrix State Estimation With PMU Measurements Approach 74
5.4 Simulation result of the IEEE 14-bus system 75

Chapter 6 Optimal Placement of Phasor Measurement Units for Improving Power System State Estimation Accuracy 80
6.1 Introduction 80
6. 2 State estimation with PMU measurements 82
6.2.1 Method I: Mixing PMU Measurements with Conventional Measurements in the Estimator 83
6.2.2 Method II: Incorporating PMU measurements through a post-processing step 85
6. 3 Heuristic PMU placement algorithm 88
6.4 Simulation results 93
6.5 Conclusion 97

Chapter 7 Conclusion 98
Appendix A 101
Appendix B 107
References 109
VITA 115

List of Tables

2.1 Four sets of values of measurement standard deviation 20
3.1 Standard deviation setting of the measurement errors 41
3.2 Simulation results of adding voltage magnitudes 43
3.3 Comparison of the number of divergence cases for running 1000-time state estimation with random topology errors 45
3.4 Experiment results of state estimation accuracy improvement 52
4.1 Standard deviation setting of measurement errors 59
4.2 Impacts of PMU measurements on loadability 66
5.1 Standard deviation setting of the measurement errors 77
5.2 Simulation results of the condition number of gain matrix G 77
5.3 Simulation results for 0.1% of the standard deviation of PMU measurements 77
5.4 Simulation results for 0.01% of the standard deviation of PMU measurements 78
6.1 The corresponding data table of the above figure. 95
6.2 Time comparison of two methods running on the 4 case studies 97

List of Figures

1.1 State estimation block diagram 2
1.2 Functional blocks of a generic PMU 4
2.1 The divergence rate versus the load increment 20
2.2 The zoom-in curve of case 2 21
2.3 The converged $cond(G)$ for 20% load increment 24
2.4 The converged $cond(G)$ for 30% load increment 24
2.5 The converged $cond(G)$ for 40% load increment 25
2.6 The converged $cond(G)$ for 50% load increment 25
2.7 The converged $cond(G)$ for 60% load increment 26
2.8 The converged $cond(G)$ with load increment 26
2.9 Comparison of the converged $cond(G)$ 28
2.10 Comparison of iteration number 28
2.11 The mean of the converged $cond(G)$ 30
2.12 Iteration number for measurement 30
2.13 The mean of the converged $cond(G)$ 31
2.14 Iteration number for measurement 32
2.15 The mean of the converged $cond(G)$ 33
2.16 Iteration number for measurement 33
2.17 The mean of the converged $cond(G)$ 34
2.18 Iteration number for measurement 34
2.19 Minimum singular value versus load increment with a random topology error 37
3.1 Overall change of the divergence rate 41
3.2 Zoom-in variation of the divergence rate 42
3.3 Comparison of 3 case studies 44
3.4 Change of divergence rate for running 1000-time state estimation with different number of PMUs 46
3.5 The network with topology error in branch 98-100 47
3.6 Voltage magnitudes of bus 98 and 100 without topology error 48

3.7 Voltage angles of bus 98 and 100 without topology error 49
3.8 Voltage magnitudes of bus 98 and 100 with topology error 50
3.9 Voltage angles of bus 98 and 100 with topology error 50
3.10 Voltage magnitudes of bus 98 and 100 with topology error 51
4.1 Topology error: a) shows the true situation; b) shows the situation modeled in state estimation 55
4.2 A simple 3-bus system 59
4.3 Voltage magnitudes of 3-bus system 60
4.4 Voltage angles of 3-bus system 61
4.5 Voltage magnitude of bus 3 61
4.6 The topology error in branch 60-61 of the IEEE 118-bus system 63
4.7 Voltage magnitudes of bus 60 and 61 63
4.8 Voltage angles of bus 60 and 61 64
4.9 Voltage magnitude of bus 98 and 100 65
4.10 Voltage angles of bus 98 and 100 65
4.11 Comparison of voltage magnitude of bus 88 68
4.12 Comparison of voltage magnitude of bus 89 68
5.1 Two-port π-circuit model for a network 71
5.2 IEEE 14-bus system with PMU measurements 76
6.1 IEEE 14-bus system with initial measurements 94
6.2 Simulation results of 4 case studies 95

Chapter 1 Introduction

1.1 Background

Power system state estimation is an essential tool used by system operators for real time analysis of the power system. It is able to estimate the optimal voltage magnitudes and angles at the system bus-bars based on the redundant raw measurements available. The idea of state estimation applied into power system was first introduced by MIT professor Fred Schweppe in 1970s, and now has been widely applied in the energy control centers (ECCs) of electric utilities and independent system operators (ISOs) [1-3]. It has constituted the backbone of the Energy Management System (EMS), which plays an important role in monitoring and controlling power systems for reliable operations.

The state estimation block diagram is shown in Fig. 1.1. Monitoring and control of power system is conducted by the supervisory control and data acquisition (SCADA) system, which collected the measurement data in real time from the remote terminal units (RTUs) installed at the substations across the power system network. The term SCADA consists of two parts. Supervisory control indicates that the operators in ECC have ability to control the RTUs. Data acquisition indicates that the data gathered by RTUs are sent to the operators for monitoring purpose [4-7]. Typical RTU measurements include bus voltage magnitudes, line current magnitudes, power injections and flows (both real and reactive). In addition to these measurements, RTUs also record the on/off status of switching devices, such as circuit breakers and transformer taps. This set of the measurement and status information is telemetered to the energy control center through a

periodic scan of all RTUs. A typical scan cycle is usually 2 or 4 seconds. The traditional types of SCADA telemetry includes telephone wire and microwave radio. A more recent development of communication technologies has taken advantage of fiber optic cable, satellites, spread spectrum radio, and internet/intranet systems, which have improved the communication reliability and speed, although the cost is still higher than the conventional mediums [8].

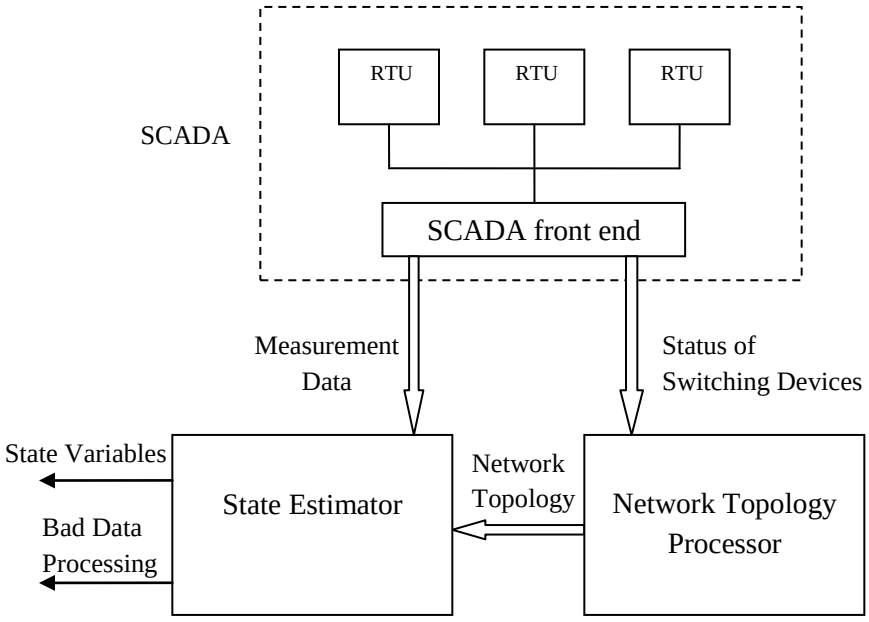

Fig. 1.1 State estimation block diagram

By processing the RTU status information of switching devices, the network topology processor in EMS determines the topology of the network, which characterizes the connectivity between buses (nodes), the shunt elements at each bus, and which generators and loads are connected to these buses by using one-line diagram. The status information of switching devices coming to topology processor is referred to as the bus section-breaker-switch data. It provides the on/off information at each substation and how they

are connected. Different bus sections connected with closed breakers and switches can be recognized as an electrical bus. The topology processor converts the bus section-breaker-switch data into so-called bus-branch in one-line diagram, which is an appropriate approach for modeling transmission line and transformer connections at each substation, rather than the precise bus-section connections at each substation [9].

The network topology must reflect the actual network condition in order for the state estimator to determine the optimal operating state of the current system. Unfortunately, to obtain an accurate network topology is not always available. Many current topology processors are not capable to acquiring the status change of circuit breakers automatically due to the destruction of communication mediums. Besides, equipment status of remote substations is usually managed manually through telephone call to report to the ECC. Hence, it is common to have topology errors occurred in the network models.

1.2 Phasor Measurement Unit

The conventional SCADA measurements do not include phase angle measurements of voltage and current phasors. With the invention of the phasor measurement unit (PMU), the phase angle was first directly measured. A PMU is a digital device that can provide synchronized voltage and current phasor measurements. The phasor is a vector representation of the magnitude and phase angle of an AC waveform. Phase angles in different sites can be determined when the measurements are synchronized to a common time source. The global positioning satellite (GPS) is capable to provide the common timing signal of the order of 1 microsecond, which can obtain highly accurate PMU voltage and current phasors [10].

Fig. 1.2 provides the function blocks of a generic PMU [11]. The analog inputs include voltages and currents obtained from the secondary windings of the voltage and current transformers. The anti-aliasing filter is used to attenuate the frequencies that are higher than the Nyquist frequency. The phase-locked oscillator converts GPS 1 purse per second into a sequence of high speed timing purses that will be used in waveform sampling. The A/D converter can convert the analog voltage and current signals to digital signals, which are imported into the phasor microprocessor to execute the Discrete Fourier Transform

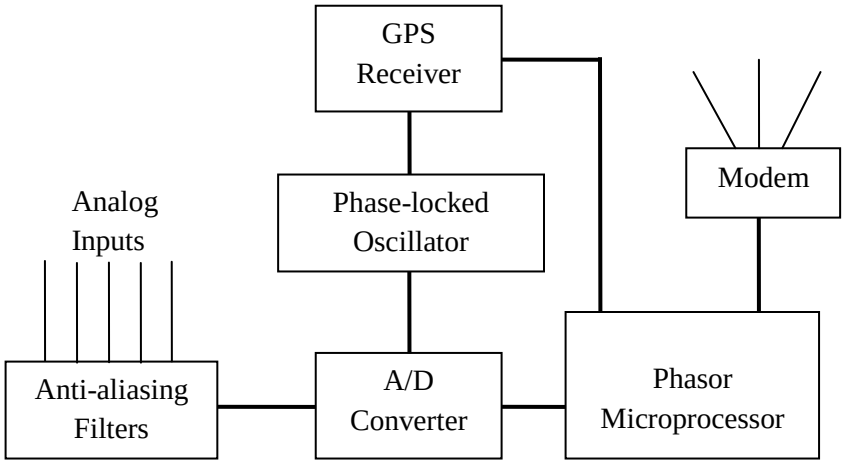

Fig. 1.2 Functional blocks of a generic PMU

(DFT) phasor calculations. The computed string of phasors is assembled in a phasor data concentrator (PDC) and this phasor stream is then transmitted to the modems. The IEEE standard for synchrophasor formulates real time phasor data transmission.

In the recent years, PMUs are gradually applied in the monitoring and control of power systems. The current and potential benefits are discussed in [12-15]. The widespread applications of PMUs also bring about the beneficial impacts to the state estimation,

which includes the improvement of network observability and state estimation accuracy, etc [16-21].

1.3 Lessons of Northeast Blackout in 2003

The Northeast blackout of 2003 was one of the most severe power outages occurred in North American history. It took place in eight Northeastern states of the United States and one Canadian province on August 14, 2003. More than 50 million people lost power for up to two days. This severe event resulted in at least 11 death and cost the economic loss of about $6 billion. After that, a team consisting of the national experts from the U.S. and Canada was built immediately to investigate the reasons of the blackout, and their final report of the U.S.-Canada Power System Outage Task Force was released in April, 2004 [22].

This Task Force report helped people open the Pandora's box of electric utility problems. The primary cause of the blackout was that overgrown trees came into contact with a strained high voltage transmission line owned by FirstEnergy Corp in the state of Ohio. Cascaded outage propagated through the system and caused the widespread blackout. To make the situation even worse, the monitoring computer running the state estimation program in Ohio was not working due to the software glitch. The operators became 'blind' to the crisis and unable to take any effective actions at early stage to prevent the widespread blackout.

The blackout gives people a proof that how fragile the interconnected power system really is. Each day roughly 500,000 Americans encounter at least two hours without electricity in their daily life, and these outages cost the economy $150 billion a year.

Although no one has investigated that how many of these blackouts are due to the failure of computer monitoring function, many power grid control centers acknowledge that computer glitches occur regularly -weekly or monthly [23].

State estimation is a critical tool for monitoring and control of power system. It is tuned to be effective under normal load conditions and may fail under conditions of high transmission line loads. The weighted least square (WLS) state estimation method is most commonly used in the control centers. The inherent flaws, as discussed in next chapter, cause the solution of state estimation to be inaccurate and unavailable. Researchers have made continuous efforts to solve this challenge for decades, and fortunately a lot of revolutionary approaches have been proposed and applied to improve the reliability and robustness of the state estimator.

1.4 Contribution of This Dissertation

As discussed in the previous section, the WLS state estimator did not work properly in the blackout. When the load level becomes severe, the state estimator may not converge to a solution. Besides, a topology error in state estimation model could worsen the convergence of the state estimator, which is the motivation for this dissertation. The main contributions of this dissertation are listed as follows:

- The simulation of the blackout is created to investigate the impacts of the topology errors and the load levels on the commonly used WLS state estimator by using the IEEE 118-bus system. The influence of the topology errors on the system is also studied from the point view of the condition number of the gain

matrix. Besides, the minimum singular value of gain matrix *G* is proposed to measure the distance between the operating point and state estimation divergence.

- The convergence property of WLS state estimation under two types of load increment is studied, one is load increment of all load buses, and the other one is a single load increment. Simulation shows that adding PMU measurements can finally solve state estimation divergence problem. In addition, the effect of topology error on state estimation when there is a single load increment is also studied. The voltage magnitude of generator bus will increase if there is a topology error in the state estimation. It is also found that adding PMU measurements in state estimation can reduce the error of voltage magnitude and angle estimation.
- The impact of topology error on a line with increasing power flow on the WLS state estimator is investigated. It is found that the voltage magnitude of the load bus will decrease at first and then increase until the state estimator diverges. For other buses including the generator buses, the voltage magnitudes will always increase. Besides, the simulation shows that PMU measurements could make the WLS state estimation more robust when the topology error occurs.
- Novel approaches of incorporating PMU measurements into the state estimation are proposed. These approaches can reduce the condition number of the coefficient matrix in state estimation, and thus are able to improve the robustness of the state estimation.
- A heuristic PMU placement approach is proposed to improve state estimation accuracy. The obtained PMU placement table and figure could help planning

engineers determine the optimal placement of PMUs when they have only a limited number of PMUs to place in the system. In addition, two methods for calculating state estimation results are utilized in the PMU placement approach. It is observed that the method for adding PMU measurements through a post-processing step can significantly improve the computation efficiency of the proposed approach.

1.5 Dissertation Outline

The dissertation is organized as follows. Chapter 2 will start with the review of the WLS state estimation method, and then explore the impact of the load level and topology errors on the convergence property of the WLS state estimation from the point view of condition number of the gain matrix. Besides, it also proposes a method of the minimum singular value of gain matrix to measure the distance between the current operating point and state estimation divergence. Chapter 3 further studies the convergence property of the WLS state estimation through considering load increment of all load buses and single load increment. It also illustrates the effect of adding PMU measurements on state estimation accuracy. Chapter 4 firstly presents the formulation of the topology error in state estimation, and describes the simulation results using a simple 3-bus system and the IEEE 118-bus system. It also studies the effect of PMU measurements to convergence of WLS state estimation. Chapter 5 presents two approaches of adding PMU measurements into state estimation, including the equality-constrained approach and the Hachtel's matrix approach. The comparison of these two methods and conventional WLS state estimation method using the IEEE 14-bus system is also illustrated. Chapter 6 proposes a heuristic optimal PMU placement approach to improve state estimation accuracy. The

IEEE 14-bus system is used to test the proposed approach. Chapter 7 provides the conclusion for the whole dissertation.

Chapter 2 Impacts of Load Levels and Topology Error on WLS State Estimation Convergence

This chapter is organized as follows. Section 2.1 gives a review of the weighted least square (WLS) state estimation algorithm and the ill-conditioned problem. Section 2.2 presents the overall description of the performed studies. Section 2.3 describes the results of the divergence characteristic study. Section 2.4 provides the analysis of the converged $cond(G)$. Section 2.5 proposes the minimum singular value of the gain matrix as the gain matrix stability index, followed by the conclusion [63].

2.1 WLS State Estimation Algorithm

In the past decades, various methods have been proposed to solve the power system state estimation problem [24-26]. The WLS state estimation algorithm is the most commonly used in the electric utility industry. We will review this algorithm consisting of numerical formulation, the measurement Jocobian and ill-condition problem in this section.

2.1.1 Numerical Formulation

For a given set of measurements, the measurement equation is given as follows [27]:

$$z = \begin{bmatrix} z_1 \\ z_2 \\ \vdots \\ z_m \end{bmatrix} = \begin{bmatrix} h_1(x_1, x_2, \cdots x_n) \\ h_2(x_1, x_2, \cdots x_n) \\ \cdots \\ h_m(x_1, x_2, \cdots x_n) \end{bmatrix} + \begin{bmatrix} e_1 \\ e_2 \\ \vdots \\ e_m \end{bmatrix} = h(x) + e \tag{2.1}$$

where,

$z = [z_1, z_2, \cdots, z_m]^T$ is the measurement vector (m x 1);

$h(x) = [h_1(x), h_2(x), \cdots, h_m(x)]^T$ is a vector of nonlinear functions that relate the states to the measurements;

$x = [x_1, x_2, \cdots, x_n]^T$ is the state vector (n x 1) to be estimated;

$e = [e_1, e_2, \cdots, e_m]^T$ is the measurement error vector (m x 1). It is necessary that $m \geq n$ and the Jacobian matrix of $h(x)$ has a rank of n.

The optimal state estimate vector x can be determined by minimizing the sum of weighted squares of residuals

$$Min \quad J(x) = [z - h(x)]^T R^{-1} [z - h(x)] \tag{2.2}$$

where, R is a diagonal matrix with the measurement variance σ_i^2, with i being the measurement index.

$J(x)$ is a non-linear function, and thus the first derivative is set equal to zero to find a minimum.

$$g(x) = \frac{\partial J(x)}{\partial x} = -H^T(x) R^{-1} [z - h(x)] = 0 \tag{2.3}$$

where $H(x)$ is the measurement Jacobian matrix with dimension m by n

$$H(x) = \frac{\partial h(x)}{\partial x} \tag{2.4}$$

The nonlinear function $h(x)$ is linearized

$$h(x + \Delta x) \approx h(x) + H(x) \Delta x \tag{2.5}$$

The iterative approach is used to solve equation (2.3) as follows:

$$(H^T R^{-1} H)\Delta x = H^T R^{-1}[z - h(x)] \tag{2.6}$$

$$x^{k+1} = x^k + \Delta x \tag{2.7}$$

where,

The symmetric matrix $G = H^T R^{-1} H$ is called gain or information matrix. k is the iteration index.

Equation (2.6) is the so-called normal equation of the WLS state estimation algorithm. A flat start for the state variables is usually utilized, where all bus voltages are assumed to be 1.0 per unit and in phase with each others. The iteration will be terminated when the measurement mismatch reaches a prescribed threshold, e.g. 1e-4, or the maximum number of iterations is reached.

2.1.2 The Measurement Jacobian

For a system containing N buses, bus 1 is usually considered as the reference bus, thus the phase angle of bus 1 is set equal to 0 degree. The state vector x has $(2N-1)$ elements, including N bus voltage magnitudes and $(N-1)$ phase angles, expressed as follows:

$$x^T = [\delta_2, \delta_3, \cdots \delta_N, V_1, V_2, \cdots, V_N] \tag{2.8}$$

The measurement vector usually includes voltage magnitudes, real and reactive power injections and flows, the structure of the measurement Jacobian H will be as follows [28]:

$$H = \begin{bmatrix} 0 & \frac{\partial V_{mag}}{\partial V} \\ \frac{\partial P_{inj}}{\partial \delta} & \frac{\partial P_{inj}}{\partial V} \\ \frac{\partial Q_{inj}}{\partial \delta} & \frac{\partial Q_{inj}}{\partial V} \\ \frac{\partial P_{ij}}{\partial \delta} & \frac{\partial P_{ij}}{\partial V} \\ \frac{\partial Q_{ij}}{\partial \delta} & \frac{\partial Q_{ij}}{\partial V} \end{bmatrix} \tag{2.9}$$

where,

V_{mag} is the voltage magnitude.

P_{inj} and Q_{inj} are the real and reactive power injections, respectively.

P_{ij} and Q_{ij} are the real and reactive power flow from bus *i* to *j*, respectively.

The expressions for each partition are given below:

- Elements corresponding to voltage magnitude measurements V_i:

$$\frac{\partial V_i}{\partial \delta_i} = 0 \text{ for all } i \text{ and } j,\ \frac{\partial V_i}{\partial V_i} = 1,\ \frac{\partial V_i}{\partial V_j} = 0 \tag{2.10}$$

- Elements corresponding to real power injection measurements P_{inj}:

$$\frac{\partial P_{inj}}{\partial \delta_i} = \sum_{j=1}^{N} V_i V_j \left(-G_{ij} \sin \delta_{ij} + B_{ij} \cos \delta_{ij} \right) - V_i^2 B_{ii} \tag{2.11}$$

$$\frac{\partial P_{inj}}{\partial \delta_j} = V_i V_j \left(G_{ij} \sin \delta_{ij} - B_{ij} \cos \delta_{ij} \right) \tag{2.12}$$

$$\frac{\partial P_{inj}}{\partial V_i} = \sum_{j=1}^{N} V_j \left(G_{ij} \cos \delta_{ij} + B_{ij} \sin \delta_{ij} \right) + V_i G_{ii} \tag{2.13}$$

$$\frac{\partial P_{inj}}{\partial V_j} = V_i \left(G_{ij} \cos \delta_{ij} + B_{ij} \sin \delta_{ij} \right) \tag{2.14}$$

- Elements corresponding to reactive power injection measurements Q_{inj}:

$$\frac{\partial Q_{inj}}{\partial \delta_i} = \sum_{j=1}^{N} V_i V_j \left(G_{ij} \cos \delta_{ij} + B_{ij} \sin \delta_{ij} \right) - V_i^2 G_{ii} \tag{2.15}$$

$$\frac{\partial Q_{inj}}{\partial \delta_j} = V_i V_j \left(- G_{ij} \cos \delta_{ij} - B_{ij} \sin \delta_{ij} \right) \tag{2.16}$$

$$\frac{\partial Q_{inj}}{\partial V_i} = \sum_{j=1}^{N} V_j \left(G_{ij} \sin \delta_{ij} - B_{ij} \cos \delta_{ij} \right) - V_i B_{ii} \tag{2.17}$$

$$\frac{\partial Q_{inj}}{\partial V_j} = V_i \left(G_{ij} \sin \delta_{ij} - B_{ij} \cos \delta_{ij} \right) \tag{2.18}$$

- Elements corresponding to real power flow measurements P_{ij}:

$$\frac{\partial P_{ij}}{\partial \delta_i} = V_i V_j \left(g_{ij} \sin \delta_{ij} - b_{ij} \cos \delta_{ij} \right) \tag{2.19}$$

$$\frac{\partial P_{ij}}{\partial \delta_j} = - V_i V_j \left(g_{ij} \sin \delta_{ij} - b_{ij} \cos \delta_{ij} \right) \tag{2.20}$$

$$\frac{\partial P_{ij}}{\partial V_i} = - V_j \left(g_{ij} \cos \delta_{ij} + b_{ij} \sin \delta_{ij} \right) + 2 g_{ij} V_i \tag{2.21}$$

$$\frac{\partial P_{ij}}{\partial V_j} = - V_i \left(g_{ij} \cos \delta_{ij} + b_{ij} \sin \delta_{ij} \right) \tag{2.22}$$

- Elements corresponding to reactive power flow measurements Q_{ij}:

$$\frac{\partial Q_{ij}}{\partial \delta_i} = - V_i V_j \left(g_{ij} \cos \delta_{ij} + b_{ij} \sin \delta_{ij} \right) \tag{2.23}$$

$$\frac{\partial Q_{ij}}{\partial \delta_j} = V_i V_j \left(g_{ij} \cos \delta_{ij} + b_{ij} \sin \delta_{ij} \right) \tag{2.24}$$

$$\frac{\partial Q_{ij}}{\partial V_i} = - V_j \left(g_{ij} \sin \delta_{ij} - b_{ij} \cos \delta_{ij} \right) - 2 b_{ij} V_i \tag{2.25}$$

$$\frac{\partial Q_{ij}}{\partial V_j} = -V_i\left(g_{ij}\sin\delta_{ij} - b_{ij}\cos\delta_{ij}\right) \tag{2.26}$$

where,

V_i and δ_i are the voltage magnitude and phase angle at bus i, respectively;

$\delta_{ij} = \delta_i - \delta_j$;

$G_{ij} + jB_{ij}$ is the *i*th row and *j*th column of the complex bus admittance matrix.

$g_{ij} + jb_{ij}$ is the admittance of the series branch connecting buses *i* and *j*.

$\frac{Bs_{ij}}{2}$ is the line-charging susceptance.

2.1.3 Ill-conditioned Problem

A whole complete set of state estimation process typically includes the following functions [28]:

- Topology processing: Obtains the one line diagram of network topology for state estimation based on the information of circuit breaker/switch statuses.
- Observability analysis: Tests whether or not the available set of measurements is sufficient to obtain the solution of state estimation. Identifies the observable islands and adds pseudo-measurements to make the whole network observable [29-36].
- State estimation: Solves a set of nonlinear equations to obtain the system states based on the network model and available measurements. Also provides the estimates of the line flows, loads and generator outputs.

- Bad data processing: Detects if there exists bad data in the measurements. Identifies and removes the bad data so that the state estimation solution will not be biased [37-43].

There are many hot research topics for each function of state estimation, and it will be hard to cover over 40 years of active researches in the theory and practice of power system state estimation. Hence, we have chosen to review the numerical problem that is directly related to this dissertation. As mentioned in section 2.1.1, the normal equation of Equation (2.6) is the common approach to the solution of the WLS state estimation. To deal with the inverse of the gain matrix $G = H^T R^{-1} H$, the Choleskey decomposition is applied to factor the matrix G in the normal equation, and then followed by forward/backward substitutions to obtain the solution.

However, the difficulty in implementing normal equation approach is that the gain matrix may be ill-conditioned, which causes the state estimation to fail to converge to a solution. The condition number is used to represent the degree of system ill-conditioning. The more singular a matrix is, the more ill-conditioned its associated system will be. For the WLS state estimation, the main reasons of ill-conditioned gain matrix are described as follows [28]:

- Very accurate measurements (i.e. virtual measurements)
- A large number of injection measurements
- Long and short lines connected to the same bus

Virtual measurements are zero injections at the switching buses, and they represents perfect measurements with very large weights in the WLS state estimation, which renders the gain matrix G ill-conditioned [44-45]. Orthogonal factorization, also known as *QR*

factorization, is proposed to prevent computation of the gain matrix. This method is based on column-wise Householder transformation and Givens rotations. It turns a zero element of a sparse gain matrix to a nonzero elements in the process of factorization called a fill-in. The time-consuming process in dealing with extensive fill-ins prevents the method from being widely applied [46-47]. The alternative method, called approach of Peters and Wilkinson, performs *LU* composition on matrix *H*. Although it is computationally more expensive than the normal equation approach, this method is a tradeoff between speed and stability. The improvement of numerical conditioning compared with the normal equation approach is shown in [48].

2.2 Overall Description of the Performed Studies

The convergence property of the WLS state estimator is a critical issue for real time monitoring and control of power grids. In addition to the three reasons mentioned in the last section that cause ill-conditioned gain matrix, the topology error can also cause the WLS state estimator to diverge without reaching a solution. The Northeast blackout of 2003 is a well-known example. The fact that the WLS did not converge due to the existence of a topology error was an indirect factor leading to the blackout. Besides, it is known that the load levels became severe before the blackout. In this section, we will study the impact of topology errors on the convergence characteristics of the WLS state estimator during the blackout when the loads gradually increase.

Topology errors can be broadly classified in two categories: branch status errors and substation configuration errors. Branch status errors include branch exclusion error and

branch inclusion error. This simulation utilizes the branch exclusion error, which takes place when a line, actually in service, is excluded from the formulation of the state estimator [49]. The IEEE 118-bus system is used as the test case [50]. Various standard deviation settings for measurements are utilized, which play a significant role in dictating the divergence characteristics of the state estimation. The detailed study procedures are described below.

First, the measurements for state estimation are generated. The Matpower tool is used to generate the power flow results of the IEEE 118-bus system by using the Newton Raphson load flow method [51]. Then, the power flow results are contaminated with normal distribution noises to form the measurements for state estimation. The measurements comprise all the bus voltage magnitudes and angles, and real and reactive power injections.

To obtain the measurements corresponding to prescribed load levels, real and reactive power of all the loads and real power of generators in the 118-bus system are increased in proportion, e.g. 10%, and the power flow program is run to check if it can converge or not. The experiments show that the maximum load increment under which the power flow program still converges is 218%. Thus, the measurements below 218% load increment will be considered for application in state estimation.

Second, branch exclusion errors are applied on state estimation. The 118-bus system has 186 branches. The Matlab function *randint* is used to generate a vector of 1000 random integers ranging from 1 to 186. The vector is used to represent the branch error index, and each value in the vector represents the branch index that will have branch error in state estimation.

Each time when the state estimator is run, a value from the branch error index vector is selected. For example, a number 10 is selected from the branch error index. Then, this 10^{th} branch will be removed from the system and will not be considered in constructing the bus admittance matrix. Meanwhile, the real and reactive power flow measurements of the 10^{th} branch are also excluded from the measurement vector. The state estimation program is run to check convergence. In this study, the maximum iteration number is set to be 50; if the state estimator does not converge within 50 iterations, it is considered to be diverged. In total, state estimation is run 1000 times for each load increment to check how many topology errors will cause state estimation to diverge under a specific load increment, from which the divergence rate is calculated.

2.3 Results of Divergence Characteristics Study

It has been found that the standard deviation of measurements can significantly affect the divergence rate of state estimation. Thus, four different sets of standard deviation settings are chosen to find out the divergence rates. The notations of standard deviations of measurements are defined as follows.

σ_{V_m} : Standard deviation of voltage magnitude measurements.

σ_{V_a} : Standard deviation of voltage angle measurements.

σ_p : Standard deviation of real power injection measurements.

σ_Q : Standard deviation of reactive power injection measurements.

The standard deviation settings are shown in Table 2.1. The divergence rates of the four cases are plotted in Fig. 2.1 and 2.2. Fig. 2.1 depicts the overall change of the divergence

rate versus load increment. Fig. 2.2 illustrates the zoom-in variation of the divergence rate versus load increment between 60% and 70% for case 2.

Table 2.1 Four sets of values of measurement standard deviation

	Standard deviation settings
Setting 1	$\sigma_{Vm}=1e-3, \sigma_{Va}=1e-3, \sigma_P=1e-2$ and $\sigma_Q=1e-2$
Setting 2	$\sigma_{Vm}=1e-2, \sigma_{Va}=1e-2, \sigma_P=1e-3$ and $\sigma_Q=1e-3$
Setting 3	$\sigma_{Vm}=1e-2, \sigma_{Va}=1e-3, \sigma_P=1e-3$ and $\sigma_Q=1e-2$
Setting 4	$\sigma_{Vm}=1e-3, \sigma_{Va}=1e-2, \sigma_P=1e-2$ and $\sigma_Q=1e-3$

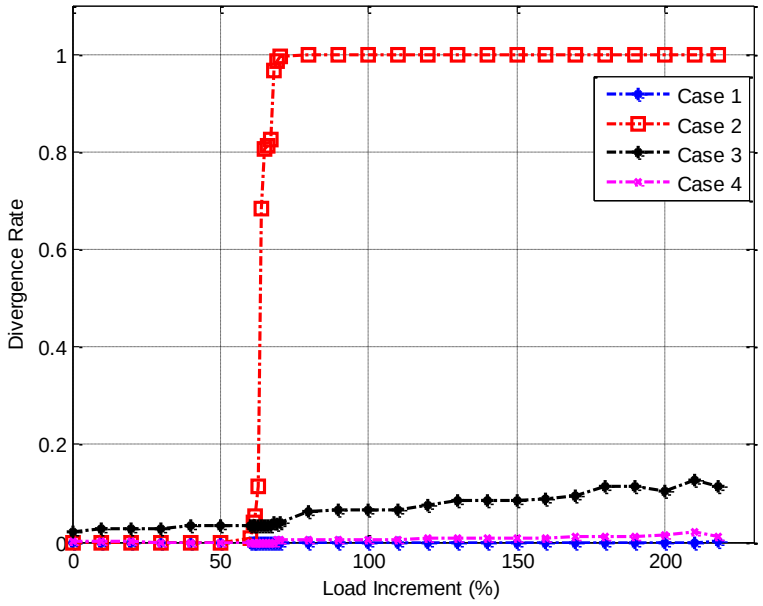

Fig. 2.1 The divergence rate versus the load increment

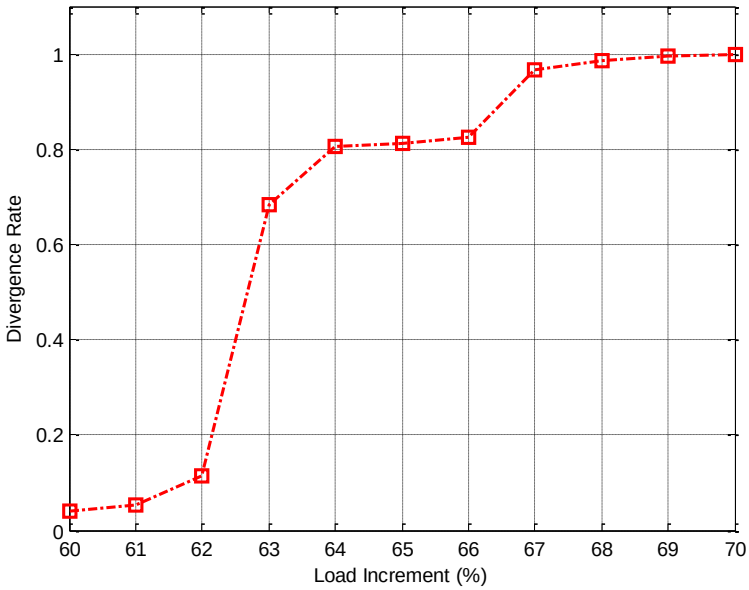

Fig. 2.2 The zoom-in curve of case 2

As seen in Fig. 2.1 and 2.2, the standard deviation values of the measurements can significantly affect the divergence rate with elevated load levels. It is observed that when both real and reactive power injection measurements have relatively small standard deviations, such as 1e-3 in case 2, the divergence rate with the existence of topology errors will reach 1.0, or 100%, when the load increment equals to 70%. A load increment of 70% means that the load level of the system increases by 70% compared to the base load level. For the other 3 cases, the divergence rates are relatively small. For example, case 1 has the minimum value of divergence rate, which is 0.003 at 218% load increment, while case 3 has less than 0.2 of divergence rate at 218% load increment.

In addition, simulation results show that the state estimator without topology error in case 2 will diverge when the load increases to 63%. For other 3 cases, the state estimators will converge at any load increment if no topology error occurs. It is observed that when the

divergence rate with topology error is low, e.g. less than 0.2, the state estimator will converge when no topology errors are present. If the divergence rate reaches a high value, like 0.7, the state estimator will diverge even when there are no topology errors.

2.4 Analysis of the Converged $cond(G)$

The condition number is used to measure the degree to which a matrix is ill-conditioned, and is defined as [52]

$$cond(A) = \|A\| \bullet \|A^{-1}\| \tag{2.27}$$

where, A is a given matrix. $\|\bullet\|$ represents a given matrix norm. A large condition number indicates an ill-conditioned matrix.

This section studies the influence of the topology errors on the condition number of the gain matrix G, denoted as $cond(G)$. In subsection A, a set of 10 cases with random topology errors is used to study the variation of the $cond(G)$ versus load increment under measurement standard deviation setting 2, and certain phenomena are obtained. In subsection B, a set of 1000 cases with random topology errors are utilized to further investigate the variation of the $cond(G)$.

A. Test results of 10 cases with random topology errors under measurement standard deviation setting 2

The loci of the $cond(G)$ for the 10 cases, each of which has a random topology error, versus load increment for standard deviation setting 2 are depicted in Fig. 2.3 to 2.7. When the state estimation converges, the convergence iteration count is a known limited number, and the $cond(G)$ will converge to a certain value for a specific load increment.

While for a diverged case, the condition number might oscillate between two values, or diverge, as shown in Fig. 2.7, similar to what is reported in [53-54]. In this work, the maximum iteration number is set to be 50; if the state estimator does not converge after 50 iterations, it is considered to be diverged.

As seen from Fig. 2.3 to 2.7, as the load increases, the iteration numbers of certain cases significantly increase. For the load increment of 20%, 30% and 40%, all the cases converge. For the load increment of 50%, one case diverges, as shown in Fig. 2.6. For the load increment of 60%, one case oscillates, where the condition number oscillates around the value of 0.5*1e8, as shown in Fig. 2.7, and the same case that diverges under load increment of 50% still diverges with load increment of 60%.

Fig. 2.8 plots the changes of the converged $cond(G)$ of these two cases for the ranges of load increment under which the two cases converge. It is observed that the converged $cond(G)$ will increase when the load level increases for the oscillated case and diverged case.

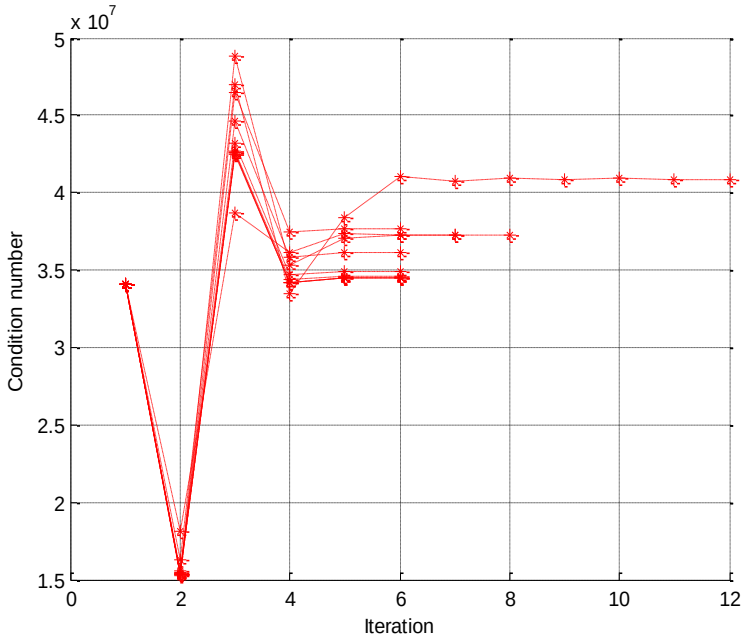

Fig. 2.3 The converged $cond(G)$ for 20% load increment

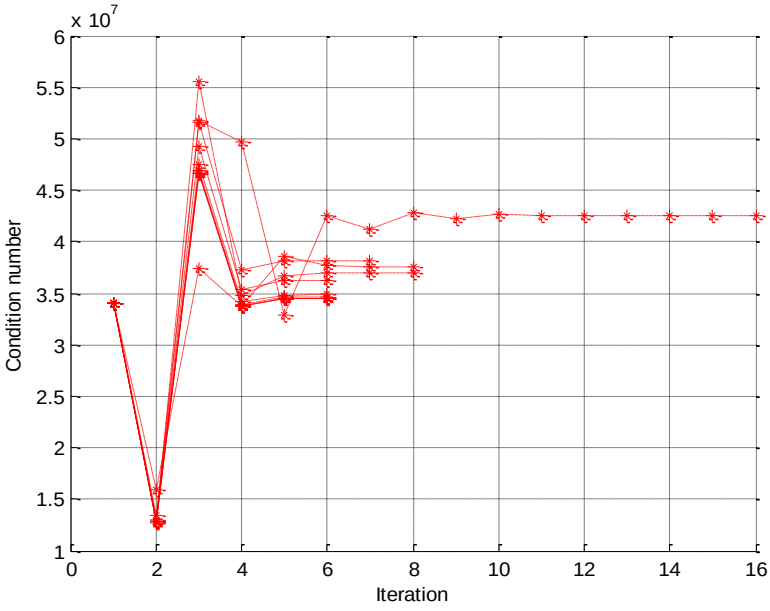

Fig. 2.4 The converged $cond(G)$ for 30% load increment

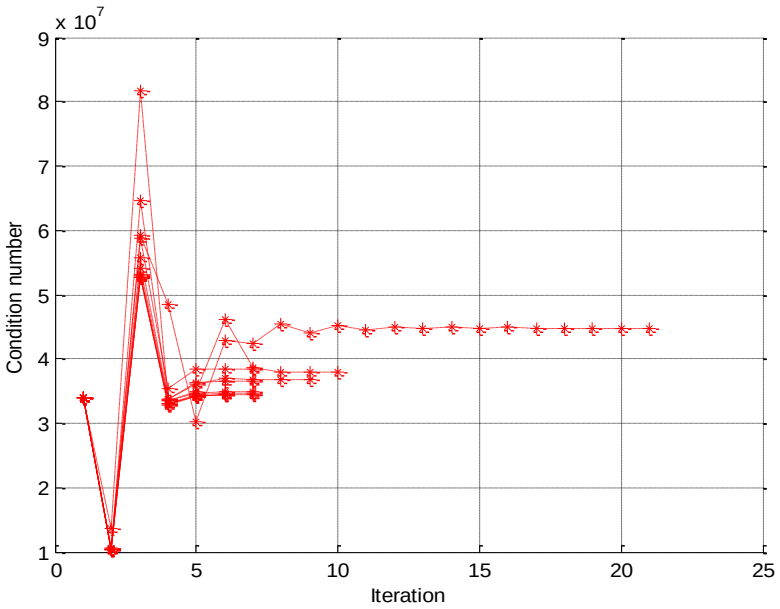

Fig. 2.5 The converged $cond(G)$ for 40% load increment

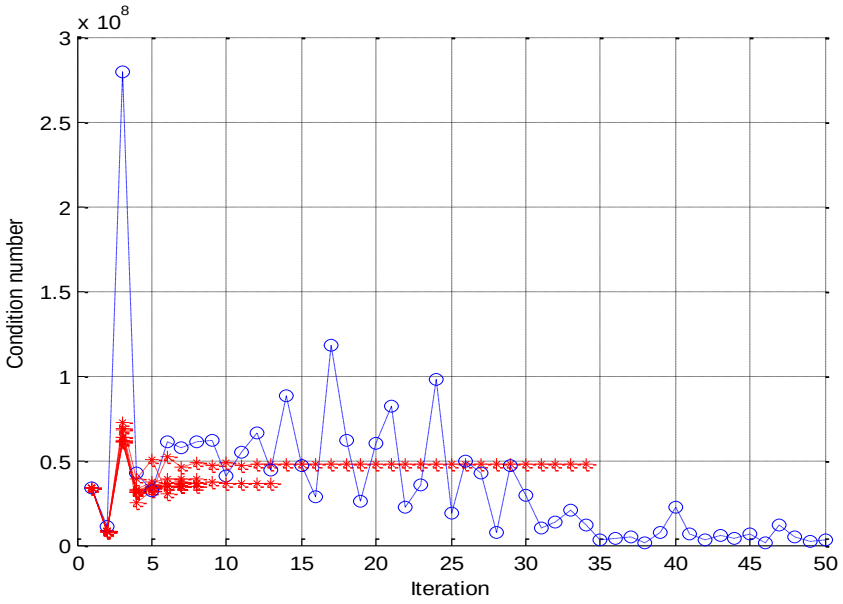

Fig. 2.6 The converged $cond(G)$ for 50% load increment

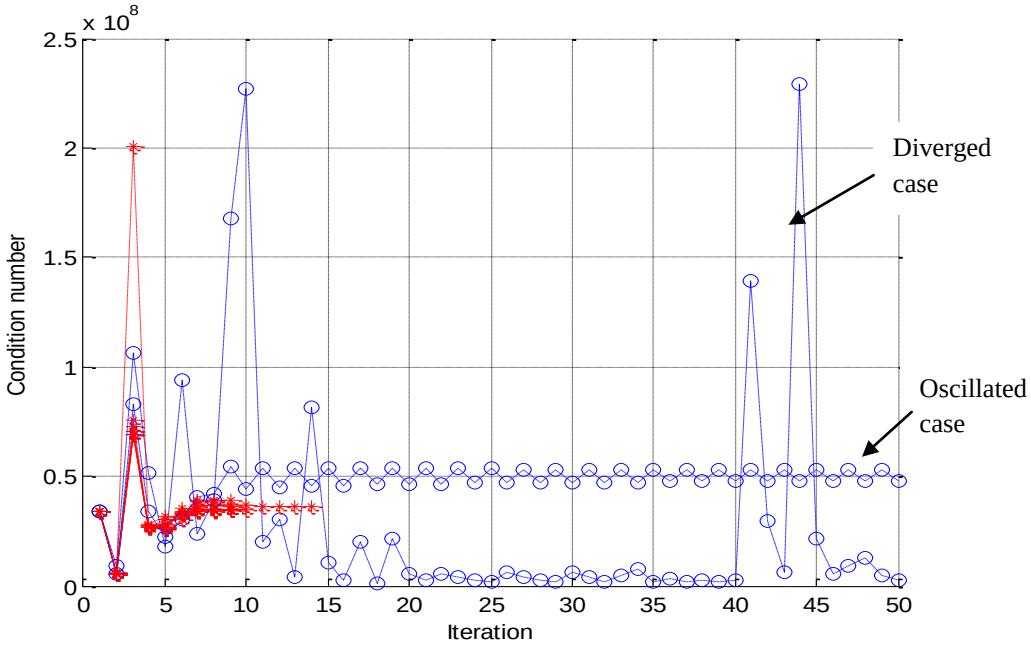

Fig. 2.7 The converged $cond(G)$ for 60% load increment

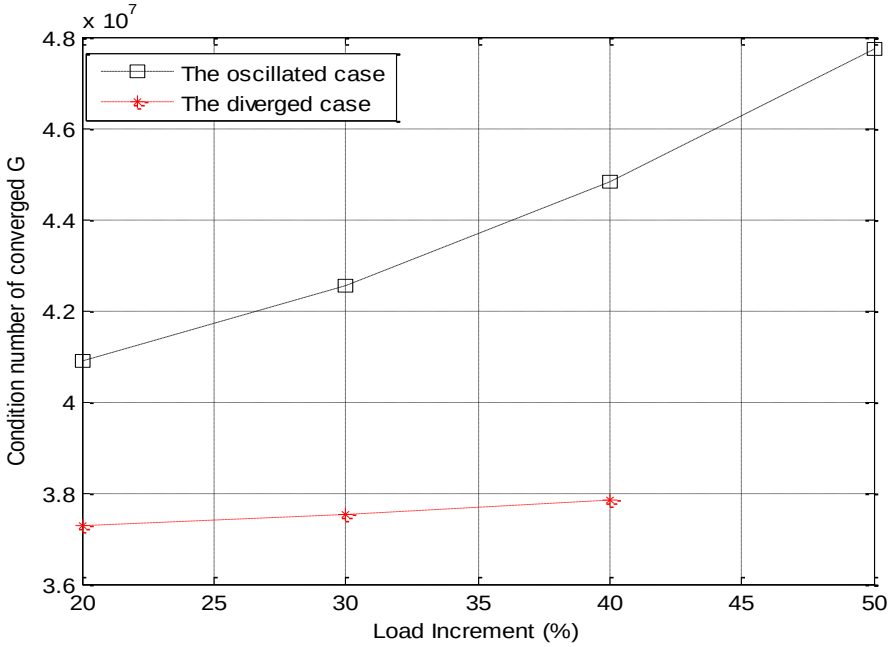

Fig. 2.8 The converged $cond(G)$ with load increment

The results for the other 8 cases with random topology errors are illustrated as follows. For 5 of the cases, the converged $cond(G)$ will increase when the load level increases if the case converges. For the other 3 cases with topology errors, the converged $cond(G)$ decreases with load increment.

The mean of the converged $cond(G)$ for the 10 cases, each of which has a topology error, at each load increment is calculated to measure the impact of topology errors on the converged $cond(G)$ with load increment. If a case does not converge, this case will be excluded from the calculation of the mean of the converged $cond(G)$. As a comparison, the values of the converged $cond(G)$ for cases without topology errors with load increment are also calculated. The values of the converged $cond(G)$ are plotted in Fig. 2.9, and the change of the curves can be explained as follows. As mentioned earlier, the converged $cond(G)$ will increase for some cases, and decrease for other cases. From load increment of 20% to 50%, the total increase of the converged $cond(G)$ for the cases whose condition number increases exceed the total decrease of the converged $cond(G)$ for the cases whose condition number decreases. As a result, the mean of the $cond(G)$ increases for load increment of 20% to 50%. When the load increment goes beyond 50%, the decrease of the converged $cond(G)$ surpasses the increases, and thus the mean value of the condition number decreases versus the load increment.

Fig. 2.10 depicts the iteration number required to reach convergence for cases with and without topology errors for measurement deviation setting 2. It is shown that the cases with topology errors require more iterations than the cases without topology errors.

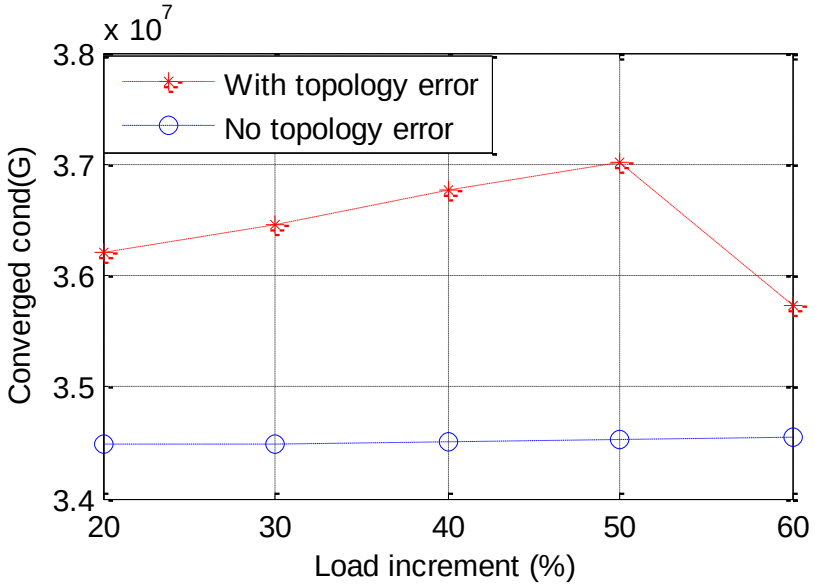

Fig. 2.9 Comparison of the converged $cond(G)$

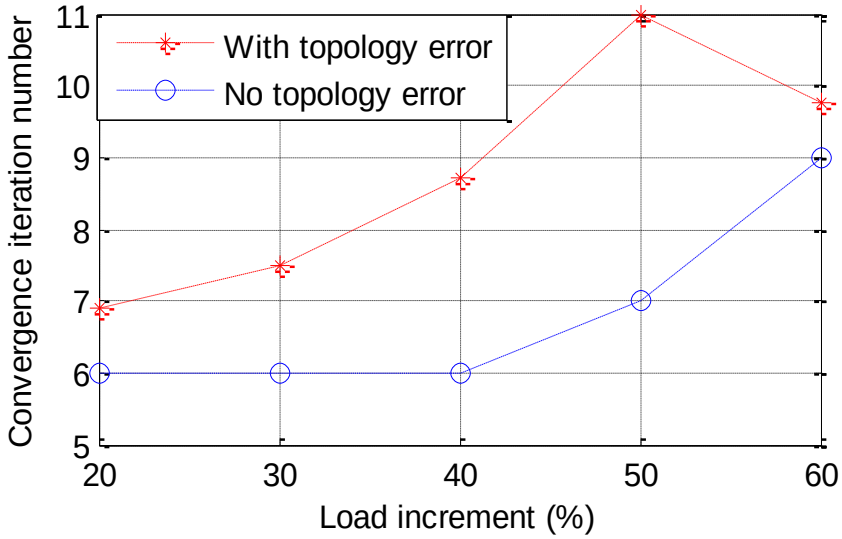

Fig. 2.10 Comparison of iteration number

B. Test results of 1000 cases with random topology errors under different deviation settings

In this section, under each set of the measurement standard deviations as shown in Table 2.1, the changes of the converged $cond(G)$ under 1000 random topology errors are

studied. The divergence rates of the 4 case studies are plotted in Fig. 2.1 and 2.2. It is known that as load level keeps increasing, the divergence rate of case 2 reaches 1.0, while the other 3 cases are under 0.2. In the following studies, similar to the previous 10 random topology error tests, the mean of the converged $cond(G)$ under 1000 random topology errors for a specified load increment is calculated. For those diverged state estimation cases, the condition numbers are not converged and unpredictable, thus are not considered in the mean calculation of the converged $cond(G)$.

(1) Results for measurement deviation setting 1

Fig. 2.11 depicts the converged $cond(G)$ for cases with measurement deviation setting 1. The mean of the converged $cond(G)$ for the cases with topology errors has a similar trend as that for the cases without topology errors. They both increase at first to the maximum condition number, and then decrease with load increment. Through the analysis of the curves of converged $cond(G)$ of 1000 random topology errors, 90.2% of the curves follow this trend of the curve without topology error. Though 9.8% of curves of 1000 random topology errors do not follow this trend, they do not affect the trend of the curve with topology error. Moreover, it is observed that it takes more iterations for the state estimation to converge for the cases with topology errors than the cases without topology errors, as shown in Fig. 2.12.

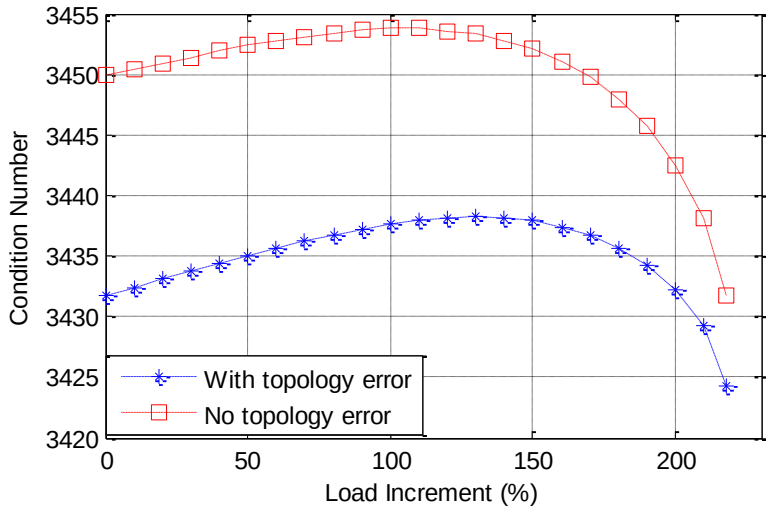

Fig. 2.11 The mean of the converged $cond(G)$

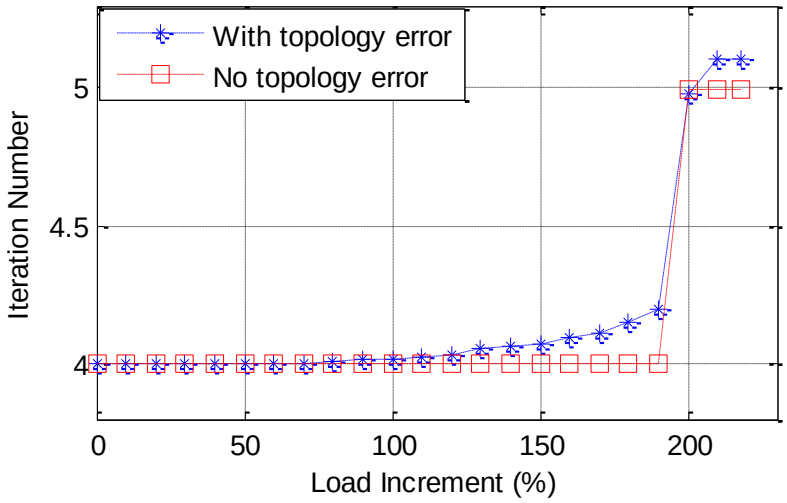

Fig. 2.12 Iteration number for measurement

(2) Results for measurement deviation setting 2

Fig. 2.13 shows the converged $cond(G)$ for cases with measurement deviation setting 2. As shown in Fig. 2.13, the mean of converged $cond(G)$ for cases with topology errors is larger than that without topology errors, and it oscillates during 60% - 70% load

increment. For 92.7% of the 1000 cases with topology errors, the converged $cond(G)$ increases with load increment; for the other cases with topology errors, the converged $cond(G)$ decreases with load increment. Because the amount of increase and decrease of the condition number for each case is different, the mean value of the condition number may increase or decrease with different load levels and thus oscillate when load level varies. It is noted that the diverged cases are excluded from the calculation of the mean value of the converged $cond(G)$. It is also observed that the case without topology error diverges at about 62% load increment. In addition, the topology error will lead to a larger iteration number than that without errors, as shown in Fig. 2.14.

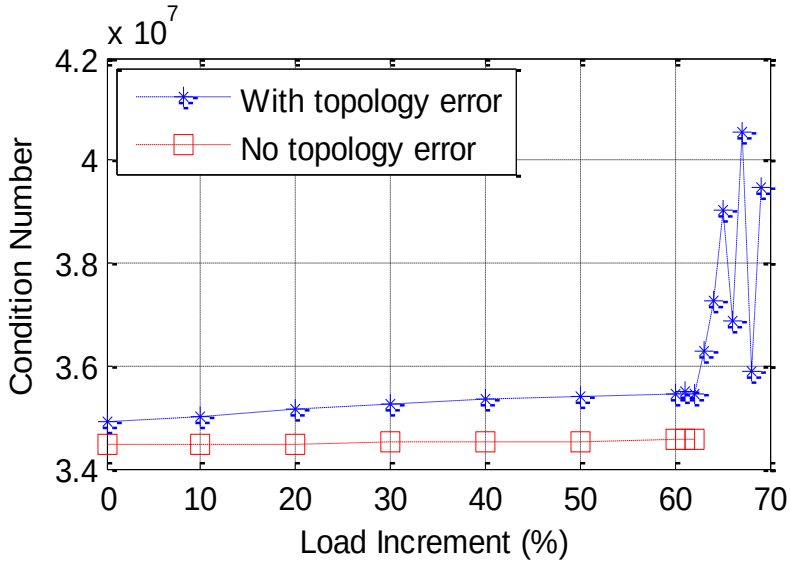

Fig. 2.13 The mean of the converged $cond(G)$

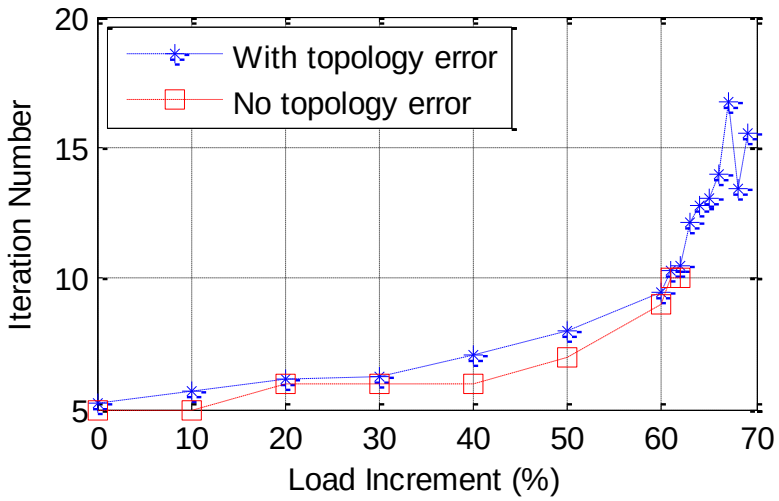

Fig. 2.14 Iteration number for measurement

(3) Results for measurement deviation setting 3

Fig. 2.15 depicts the converged $cond(G)$ for cases with measurement deviation setting 3. Fig. 2.16 shows the comparison of iteration number required to converge for the cases with and without topology errors.

As shown in Fig. 2.15, as the load level increases, the condition number first reaches the maximum value, and then decreases with load increment. 97.4% of 1000 cases with topology errors follow this trend.

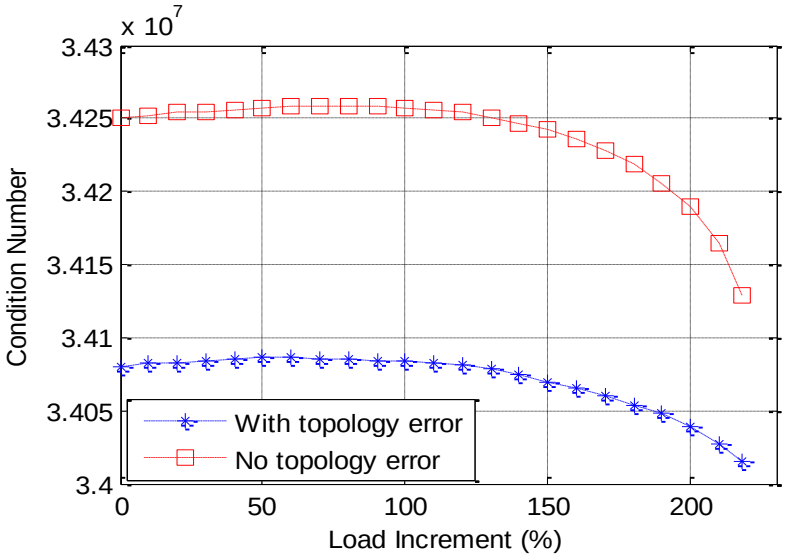

Fig. 2.15 The mean of the converged $cond(G)$

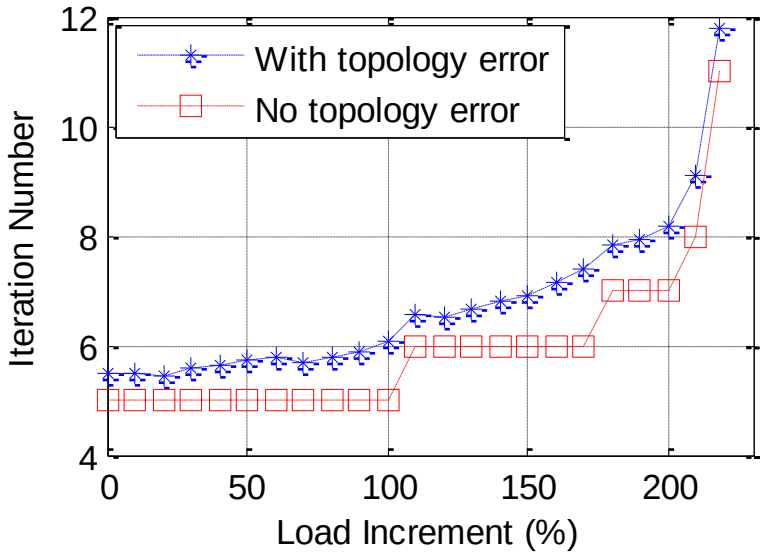

Fig. 2.16 Iteration number for measurement

(4) Results for measurement deviation setting 4

Fig. 2.17 plots the converged $cond(G)$ for cases with measurement deviation setting 4. Fig. 2.18 shows the comparison of iteration number required to converge for the cases with and without topology errors.

The two curves in Fig. 2.17 monotonically decrease with load increment. 94.9% of the 1000 cases with topology errors follow this trend. Fig. 2.18 gives the comparison of the iteration number required to converge between the cases with and without topology errors.

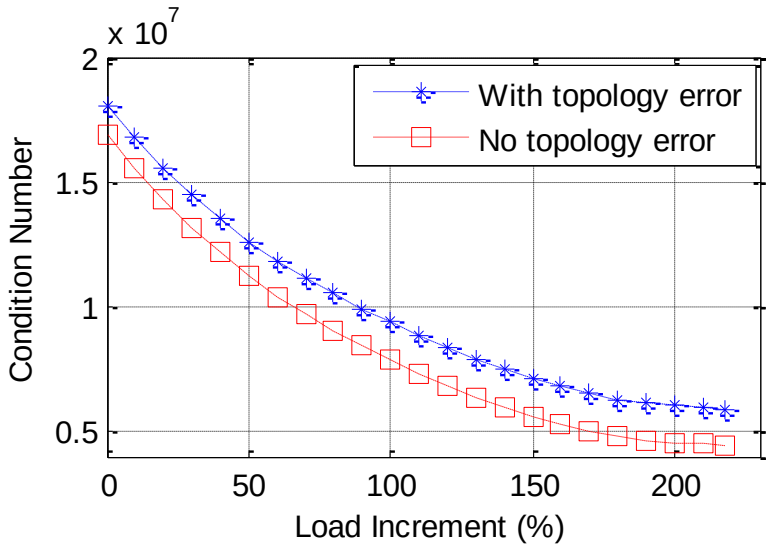

Fig. 2.17 The mean of the converged $cond(G)$

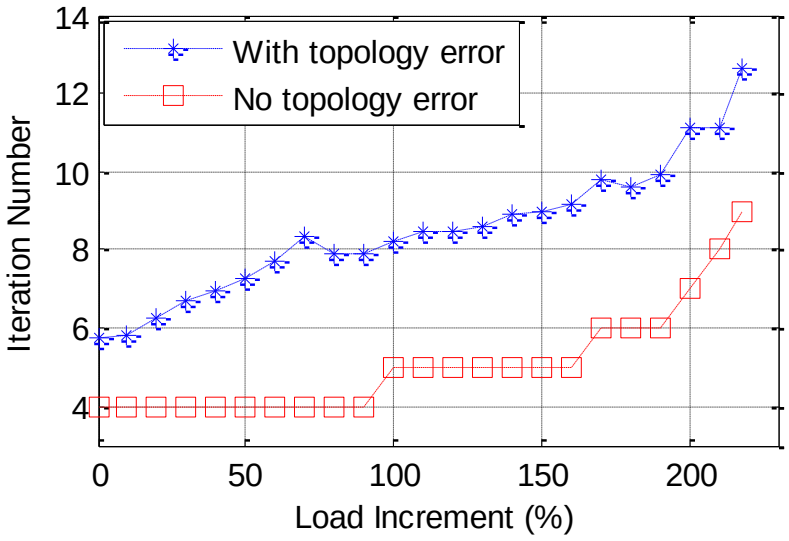

Fig. 2.18 Iteration number for measurement

Based on the variation of the converged $cond(G)$ versus load increment as shown in Fig. 2.11, 2.13, 2.15 and 2.17, it can been seen that the mean of the converged $cond(G)$ for the cases with topology errors is not necessarily larger than that for the cases without topology errors. The mean of the converged $cond(G)$ also depends on the standard deviation values of the measurements. Moreover, the iteration number to reach convergence for cases with topology error is larger than cases with no topology error.

2.5 Gain Matrix Stability Index

The minimum singular value of the gain matrix is used as the gain matrix stability index, indicating the distance between the studied operating point and state estimation divergence. The singular value decomposition is first introduced, followed by the simulation on the IEEE 118-bus system.

2.5.1 Singular Value Decomposition of Gain Matrix

The singular value decomposition is an important orthogonal decomposition method in matrix computation [55]. Consider the gain matrix G with dimension n by n, where n is the number of the state variables. Matrix G can be decomposed by using singular value decomposition method as follows [56]:

$$G = U\Sigma V^T = \sum_{i=1}^{n} \sigma_i u_i v_i^T \tag{2.28}$$

where U and V are n by n orthonormal matrices. The singular vectors u_i and v_i are the columns of the matrices U and V respectively. Matrix Σ is a diagonal matrix with

$$\sum(G) = diag\{\sigma_i(G)\} \qquad i = 1,2,\cdots,n \tag{2.29}$$

where $\sigma_i \geq 0$ for all *i*. The diagonal elements of matrix Σ are usually ordered so that $\sigma_1 \geq \sigma_2 \geq ... \geq \sigma_n \geq 0$.

The smallest singular value of the matrix *G* is a measure of the distance, in the l_2-norm, between *G* and the singular matrix with no full rank [57]. Moreover, the singular value decomposition is well-conditioned since the singular values are fairly insensitive to the permutations in the matrix elements. If the smallest singular value σ_n is close or equal to zero, the corresponding matrix *G* could be singular. This property can be used in the WLS state estimation to measure the distance between the operating point to the state estimation divergence.

2.5.2 Testing Results of σ_n

The IEEE 118-bus system is used as the test case, and a random topology error is applied in the state estimation. The standard deviation setting of measurement errors utilizes setting 3 of Table 2.1. The simulation process is similar to section 2.3. In order to study the convergence property of state estimation versus load increment, we need to obtain the measurements corresponding to prescribed load levels. Let real and reactive power of all the loads and real power of generators in the 118-bus system increase in proportion, e.g. 10%, then the power flow program is run to check if it can converge or not. The experiments show that the maximum load increment under which the power flow program still converges is 218%. Thus, the measurements below 218% load increment will be considered for application in state estimation.

The following figure plots minimum singular value versus load increment with a random topology error. As can be seen in Fig. 2.19, the minimum singular value decreases

gradually at first, then it oscillates to a point, with 202% load increment. At this point, the state estimator still converges. When the minimum singular value reduces below 1000, the state estimator diverges. Thus, the minimum singular value of gain matrix can be used as convergence index to judge if the state estimator converge or not. If this value is close to zero, the state estimator will diverge.

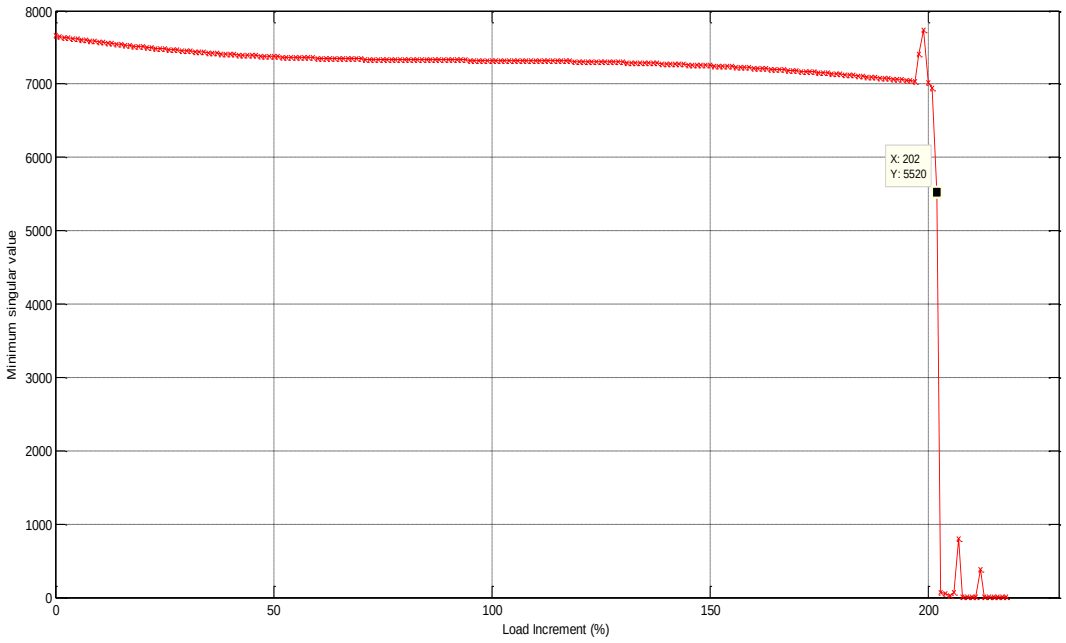

Fig. 2.19 Minimum singular value versus load increment with a random topology error

2.6 Conclusion

This chapter first reviews the WLS state estimation method and reasons that cause ill-conditioned gain matrix. It then investigates the impacts of the topology errors and the load levels on the commonly used WLS state estimator. As the load level increases, the divergence rate of the state estimation may increase to 1.0 if the standard deviations of

the measurements take certain values. The influence of the topology errors on the system is also studied from the point view of the condition number of the gain matrix. If the state estimator diverges due to a topology error, the condition number of the gain matrix is unable to converge and reach a certain value. Case studies show that the topology errors and measurement standard deviations have impacts on the converged $cond(G)$. Moreover, the impacts of the topology errors on the condition number of the converged gain matrix will differ case by case. The locus of the condition number versus the load increment follows a similar trend for the cases with and without topology errors, and the state estimation for cases with topology error will need more number of iterations to converge than cases without topology error. Besides, the minimum singular value of gain matrix G is proposed to measure the distance between the operating point and state estimation divergence. Its effectiveness has been verified by the simulation on the IEEE 118-bus system.

Chapter 3 Convergence Property of the State Estimation Considering Two Types of Load Increment and PMU Measurements

This chapter is organized as follows. Section 3.1 briefly introduces the background knowledge. Section 3.2 describes the state estimation considering load increment of all load buses. Section 3.3 simulates the scenario when there is a single load increment. Section 3.4 illustrates the effect of adding PMU measurements on state estimation accuracy, and followed by the conclusion.

3.1 Introduction

In the power system, the buses are classified as three types: load bus, generator bus and slack bus. The load bus, known as PQ bus, does not connect to a generator, and the real and reactive power of the load are specified. The generator bus, known as PV bus, connects a generator with specified real power and voltage magnitude. The slack bus is a special generator bus serving as the reference bus for the power system. Both voltage magnitude and angle are assumed to be fixed (for instance, $1.0\angle 0^0$ per unit). The real and reactive powers are uncontrolled: the bus supplies whatever real or reactive power is necessary to make the power flows in the system balance.

Two types of load increment in real power system operation are considered: one is the load increment for all the load buses, and the other is a single load increment. The real and reactive power of the load bus are increased in proportion, where the power factor of the load is kept constant. In the scenario of load increment for all the load buses, we will

study the effect of the change of the measurement vector on the convergence property of the WLS state estimation, including adding PMU voltage magnitude and angle measurements. PMU measurements are used as the regular measurements, although with higher weights in WLS state estimation considering that PMU measurements are much more accurate than SCADA measurements.

In addition, this chapter also studies the convergence property of WLS state estimation when a topology error occurs in a line with the increasing power flow. This is caused by an increasing single load at one terminal of the line and the increasing generation at the other terminal to feed the load through the line. PMU measurements are gradually added in the state estimation to study if they can improve state estimation accuracy.

3.2 State Estimation Considering Load Increment for All the Load Buses

The simulation approach implemented in Section 2.2 is still utilized in this section except the change of measurements. The used measurements include voltage magnitude at bus 1, power injections at all the buses, branch flows in all the branches except the one with topology error. The typical standard deviation setting of the measurement errors is shown in Table 3.1. In the next subsection, more voltage magnitudes are added in the measurement vector to study the change of the divergence rate. Fig. 3.1 and 3.2 plots the divergence rate of the case. Fig. 3.1 depicts the overall change of the divergence rate versus load increment. Fig. 3.2 illustrates the zoom-in variation of the divergence rate versus load increment between 160% and 177% for the case so that the audience has a clear impression upon the change of divergence rate during this interval of load increment. These curves are similar to what we have studied in section 2.3.

Table 3.1 Standard deviation setting of the measurement errors

Standard deviation	Value setting
σ_V	0.4%
σ_{Pinj} and σ_{Qinj}	1%
σ_{Pf} and σ_{Qf}	0.8%

where,

σ_V is the standard deviation of voltage magnitude measurement error;

σ_{Pinj} and σ_{Qinj} are the standard deviation of real and reactive power injection measurement errors, respectively;

σ_{Pf} and σ_{Qf} are the standard deviation of real and reactive power flow measurement errors, respectively;

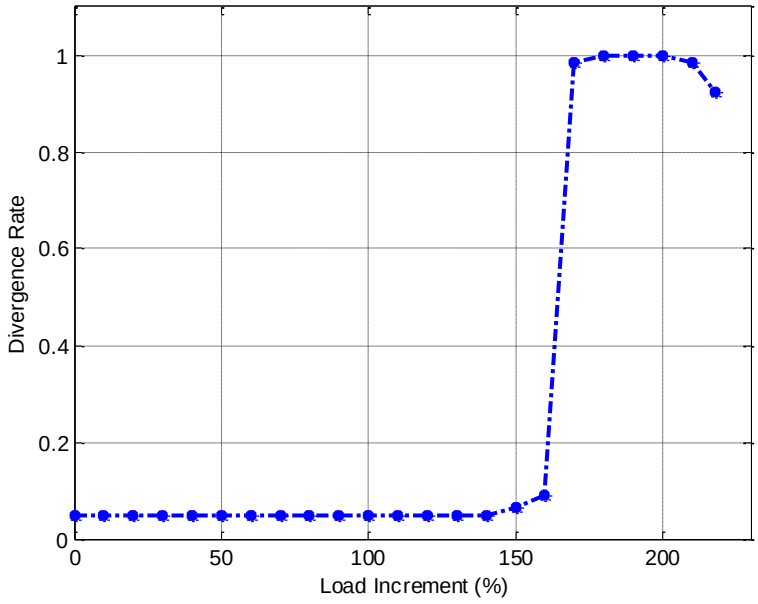

Fig. 3.1 Overall change of the divergence rate

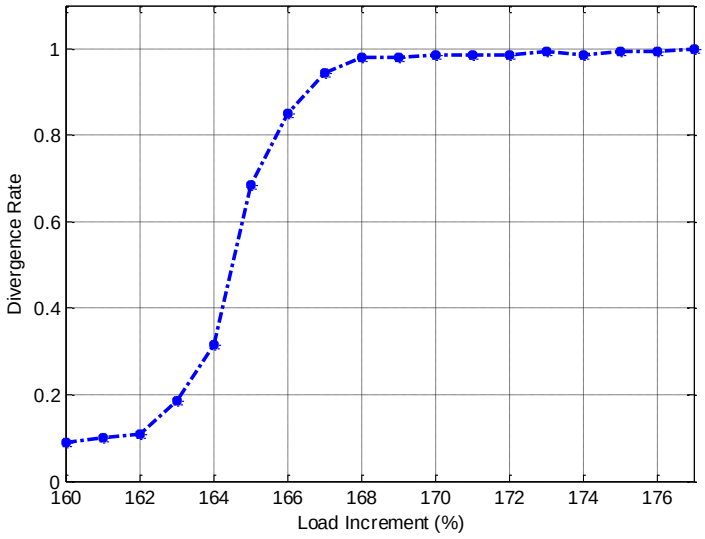

Fig. 3.2 Zoom-in variation of the divergence rate

As can be seen in Fig. 3.1, under this measurement configuration and the standard deviation setting of measurement errors, the divergence rate starts from a small value in the beginning, and then increases to 1.0, or 100% at 177% of load increment as shown in Fig. 3.2. It means that all the cases with random topology errors will diverge.

In order to study the effect of various measurement configurations on the convergence property of the WLS state estimation, section 3.2.1 shows the effect of adding more conventional voltage magnitude measurements to the measurement vector and section 3.2.2 shows the effect of adding more PMU voltage magnitude and angle measurements. It is noted that power injection and flow measurements for the above simulation are kept same as that in Fig. 3.1 and 3.2.

3.2.1 Adding Conventional Voltage Magnitude Measurements in Measurement Vector

In the previous simulation, only voltage magnitude measurement at bus 1 is considered in the measurement vector for state estimation. In the following tests, more voltage

magnitude measurements are added in the measurement vector. Table 3.2 shows the simulation results of 3 case studies through adding different number of voltage magnitude measurements. The method of selecting voltage magnitudes is described as follows. E.g., 8 voltage magnitudes of case 2 are selected, which means one voltage magnitude is selected from every 15 buses of the 118-bus system. Fig. 3.3 shows the comparison of simulation results of 3 case studies.

As seen in Table 3.2, when adding more number of voltage magnitude measurements, the maximum divergence rate of state estimation will decrease. In case 3, the divergence rate is kept at the value of 0.049%, as shown in Fig. 3.3, which means there is only 49 times divergence cases in the running 1000-time state estimation with a random topology error.

Table 3.2 Simulation results of adding voltage magnitudes

Case No.	No. of voltage magnitudes	Maximum divergence rate (%)
1	1	100%
2	8	98.6%
3	20	0.049%

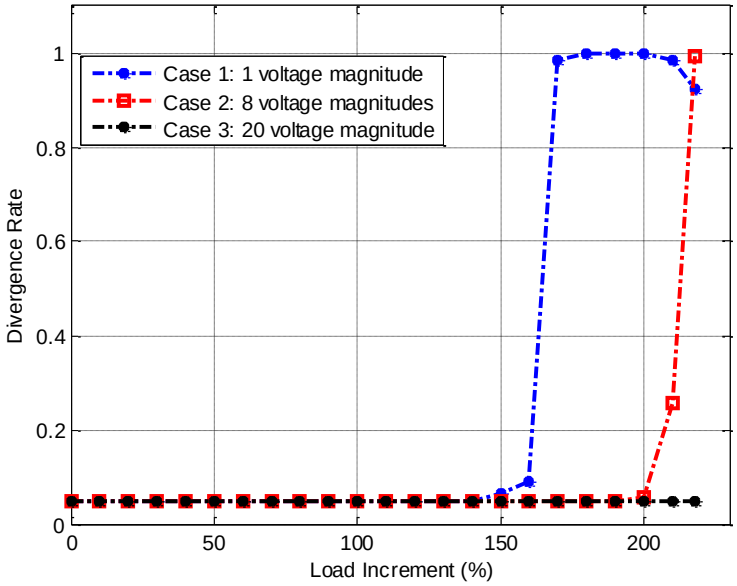

Fig. 3.3 Comparison of 3 case studies

3.2.2 Adding PMU Voltage Phasor Measurements

In this section, PMU voltage magnitude and angle measurements will be added in measurement vector to test if they can eliminate state estimation divergence when a topology error exists. PMU measurements are used along with conventional measurements in the state estimation, albeit with higher weights. It is assumed that bus 1 in the system is considered as the reference bus, at which a PMU is placed to give an accurate angle reference for other buses. The measurement errors of voltage magnitudes and angles are set to have a standard deviation of 0.1%, which means they are more accurate than conventional measurements.

Table 3.3 shows the comparison of the number of divergence cases for running 1000-time state estimation with topology error under the situations with and without PMU measurements. The row 1 of the table represents the number of buses with voltage measurements that will be added in measurement vector. In the case with no PMU

measurements, as shown in row 2, only voltage magnitude measurements are included in measurement vector. There will be 49 divergence cases even adding more bus voltage magnitude measurements. In addition, load increment does not affect the number of divergence cases in this comparison study. In the case with PMU measurements, as shown in row 3, the divergence cases gradually decreases as the more number of buses are equipped with PMUs. Fig. 3.4 depicts the corresponding divergence rate to row 3 of Table 3.3 for running 1000-time state estimation with PMU measurements. For each case, the divergence rate is not affected by the load increment. It is noted that when all the buses have PMUs, there will not exist a divergence case. Although it is unlikely to install every bus with a PMU considering the substantial economic costs, it is still encouraging to find that adding PMU measurements will improve the robustness of WLS state estimation.

Table 3.3. Comparison of the number of divergence cases for running 1000-time state estimation with random topology errors

Number of PMUs	20	40	59	118
No PMU	49	49	49	49
With PMU	43	31	15	0

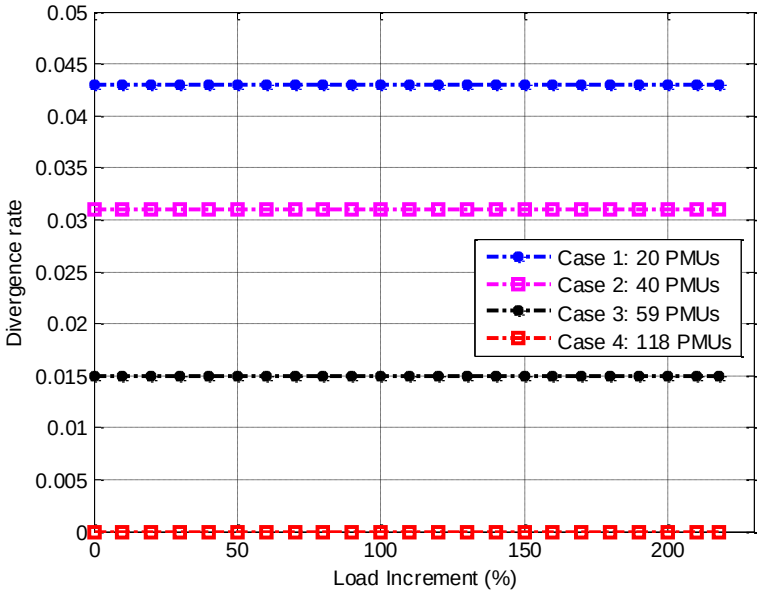

Fig. 3.4 Change of divergence rate for running 1000-time state estimation with different number of PMUs

3.3 Simulation Results Considering Single Load Increment

The previous section simulates the scenario, where all the loads increase at the same time. However, in reality there could be a case that a generator feeds an increasing load through a transmission line, and the topology error occurs in that line. It is interesting to explore the phenomena of state estimation convergence, where the topology error occurs on the line connecting the load and the generator under the load increment.

Fig. 3.5 shows that the topology error occurs on line 98-100 of the IEEE 118-bus system. Line 98-100 is wrongly assumed to be out-of-service in the state estimator as shown in the dash line. Bus 98 is a load bus, and bus 100 is a generator bus.

The detailed simulation procedures are described as follows:

First, the measurements for state estimation are generated. Let us assume that the real and reactive powers of the load bus are increased in proportion, e.g. 10%. Meanwhile, the generator will output the same amount of real power to supply the load through the line. All the other loads and generator are kept unchanged. The Matpower tool is used to generate the power flow results of the 118-bus system to check if it can converge or not when real and reactive powers of the load bus are increased every time. In this way, the maximum load increment under which the power flow program still converges can be found.

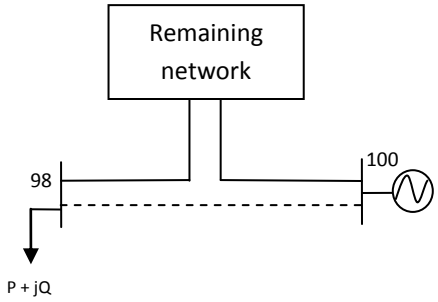

Fig. 3.5 The network with topology error in branch 98-100

Then, the power flow results under the maximum load increment are contaminated with normal distribution noises to form the measurements for state estimation. The measurements comprise 20 voltage magnitudes, all the real and reactive bus injections and line flows, except the line with topology error. In the process of the state estimation, the topology error occurs exactly in the chosen line with load increment. As shown in Fig. 3.5, the topology error occurs in line 98-100, which means this line will be excluded in the formulation of the admittance matrix used for state estimation. The power flow measurements of line 98-100 will also be excluded in the measurement vector. Then, the WLS state estimation program is run and its convergence is checked. In our work, the

maximum iteration number is set to be 50; if the state estimator does not converge within 50 iterations, it is considered to be diverged.

As a comparison, the state estimation program without topology error is also run, and voltage magnitudes and angles of bus 98 and 100 are plotted in Fig. 3.6-3.7, respectively. In Fig. 3.6, the voltage magnitude of load bus 98 will constantly decrease, while voltage magnitude of generator bus 100 will almost keep constant as expected with load increment. Fig. 3.7 shows the voltage angles of bus 98 and 100 in the state estimation with topology error.

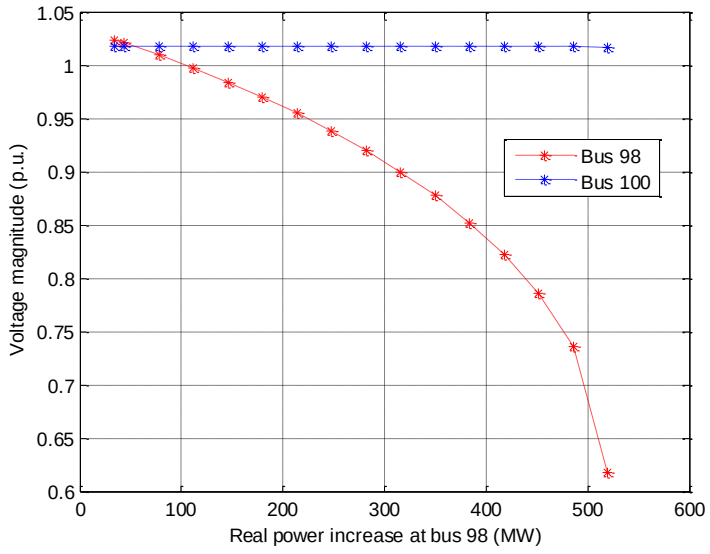

Fig. 3.6 Voltage magnitudes of bus 98 and 100 without topology error

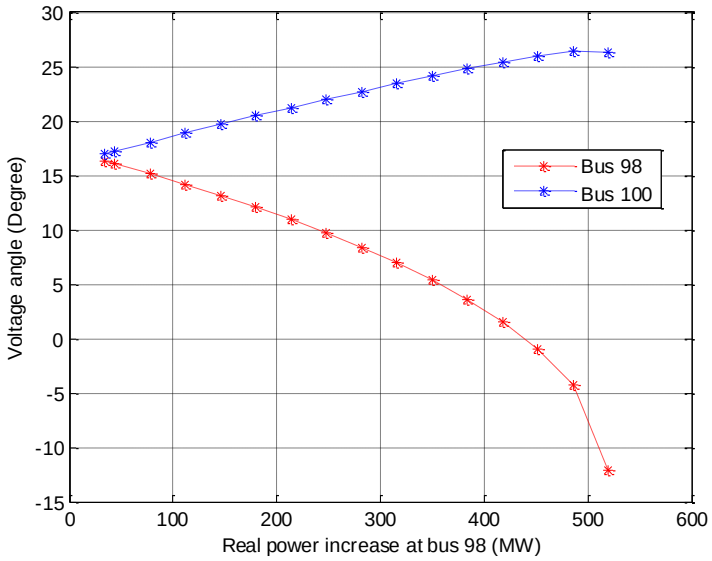

Fig. 3.7 Voltage angles of bus 98 and 100 without topology error

When the topology error occurs in line 98-100, voltage magnitudes and angles of bus 98 and 100 are plotted in Fig. 3.8-3.9, respectively. By comparing Fig. 3.6 and 3.8 obtained from the state estimation without and with topology error, it is found that the biggest difference lies in the change of voltage magnitude of generator bus 100. Without topology error, the state estimation will accurately estimate voltage magnitude of bus 100, which stays almost a constant value. While in the case with topology error as shown in Fig. 3.8, voltage magnitude of bus 100 will increase with load increment, which is incorrect in real world. For the voltage angles of bus 98 and 100, as shown in Fig. 3.7 and 3.9, the trend of the curves is the same although there exists a little change in the degrees of angles.

For other buses of the IEEE 118-bus system, it is tested that they have the same trends as follows. For example, Fig. 3.10 gives the curves of voltage magnitude of bus 63 in the state estimation results with and without topology error. In the state estimation without topology error, the voltage magnitude of bus 63 stays almost a constant value. While in

the situation with topology error, voltage magnitude of bus 63 will increase a little bit with load increment.

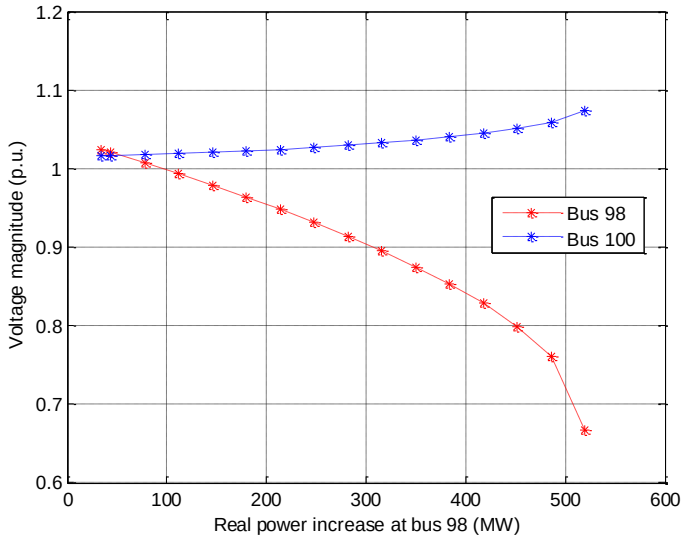

Fig. 3.8 Voltage magnitudes of bus 98 and 100 with topology error

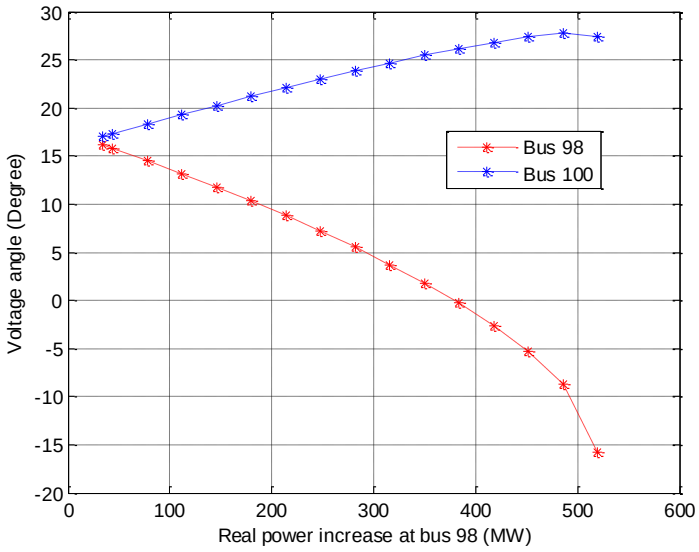

Fig. 3.9 Voltage magnitudes of bus 98 and 100 with topology error

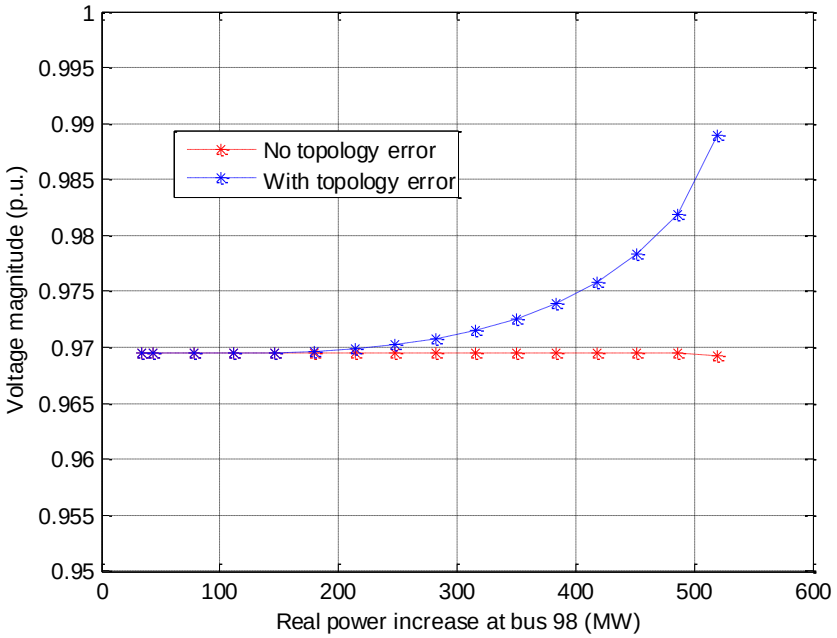

Fig. 3.10 Voltage magnitude of bus 63 in the state estimation with and without topology error

3.4 Effect of Adding PMU Measurements on State Estimation Accuracy

As seen in section 3.3, the topology error will cause the state estimation results to deviate from their correct values. Thus, it is meaningful to test if adding PMU to measurement vector of state estimation can improve state estimation accuracy. To that end, we gradually add more number of PMU measurements to the state estimation, and calculate the average error of voltage magnitudes and angles of bus *i*, respectively. The average error of voltage magnitude of bus *i* is calculated as follows.

$$Error_{ave} = \frac{1}{N}\sum_{n=1}^{N} \frac{\left|V_{SE}^{n} - V_{true}^{n}\right|}{V_{true}^{n}} \times 100 \tag{3.1}$$

where, N is the number of sampling points along the voltage magnitude curve of state estimation results. V_{SE}^{n} is the voltage magnitude of state estimation result at the n-th point. V_{true}^{n} is the voltage magnitude of power flow result at the n-th point. The smaller the error, the closer for state estimation results to the true values.

In addition, maximum error of voltage magnitude is obtained by comparing the values of errors of voltage magnitude from N points and picking the maximum value. Similarly, average and maximum error of voltage angle can be also calculated.

Table 3.4 shows the experiment results of state estimation accuracy improvement. The topology error results in a larger error of voltage angle in state estimation than that of voltage magnitude. As more number of PMU measurements is added in the state estimation, the average error of voltage magnitude is gradually decreasing, so is the value of corresponding maximum error of voltage magnitude. While for the errors of voltage angle, it does not always hold true for voltage angle, as seen in the columns of average and maximum error of voltage angle. But the general trend is that PMU measurements will increase the angle estimation as well.

Table 3.4 Experiment results of state estimation accuracy improvement

No. of PMU measurements	Average error of voltage magnitude (%)	Maximum error of voltage magnitude (%)	Average error of voltage angle (%)	Maximum error of voltage angle (%)
0	1.54	10.50	75.57	509.71
20	0.88	5.55	82.60	559.57
40	0.86	5.09	83.27	565.45
59	0.86	5.03	81.88	556.73
118	0.62	4.04	47.26	316.00

3.5 Conclusion

This chapter studies the convergence property of WLS state estimation under two types of load increment, one is load increment of all load buses, and the other one is a single load increment. Simulation results obtained from a statistical method show that for a certain measurement configuration, state estimation with topology error will diverge when the loads increase to a specific amount. Adding conventional voltage magnitudes in measurement vector can reduce the divergence rate but cannot eliminate that. However, by adding PMU measurements it can finally solve state estimation divergence problem. In addition, we also study the effect of topology error on state estimation when there is a single load increment. Simulation results show that voltage magnitude of generator bus will increase if there is a topology error in the state estimation. It is found that adding PMU measurements in state estimation can reduce the error of voltage magnitude and angle estimation.

Chapter 4 Convergence Property of State estimation with Load Increment on a Specific Line

This chapter is organized as follows. Section 4.1 gives a brief introduction of background knowledge. Section 4.2 presents the formulation of the topology error in state estimation. Section 4.3 describes the simulation results using a simple 3-bus system and the IEEE 118-bus system. Section 4.4 studies the effect of PMU measurements to convergence of WLS state estimation. Section 4.5 gives the future work followed by the conclusion.

4.1 Introduction

In these days the power system is operating to its limit, and the power flow in the grids is approaching to the maximum capability. There exists a possibility that a large load is fed by a generator through a transmission line. The load level on the line is increasing and the generator is also increasing its output to supply the load. It is interesting to explore what will happen when a topology is occurred on the line. The topology error utilized in this chapter is branch exclusion error, which takes place when actually in-service line is excluded in the state estimation model.

As can be expected, the topology error on a line with increasing power flow could finally cause the WLS state estimation to diverge. We are curious about the change in voltage profiles of the generator bus and the load bus. Thus, the simulation on a simple 3-bus system and the IEEE 118-bus system is run to uncover a common law. The increasing

line flow is fulfilled through the change in bus power injections at the two buses of the line. Section 4.2 will explain this from the point view of mathematical equations.

This chapter also investigates the effect of adding PMU voltage phasor measurements to the convergence property of WLS state estimation. The way of incorporating PMU measurements into state estimation is to treat them as conventional measurements but with higher weights. 10 randomly selected cases are tested and reported, and it is found that state estimation with PMU measurements diverges at larger load increment than that without PMU measurements.

4.2 Formulation of Topology Error in WLS State Estimation

The topology errors on transmission line have two situations. In the first one, the line is wrongly modeled as out-of-service in state estimation. In the second situation, the line is wrongly modeled as in-service in state estimation. Fig. 4.1 shows the first topology error.

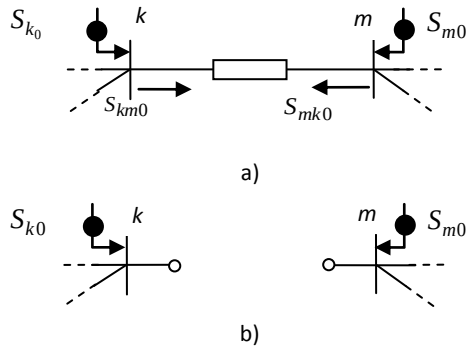

Fig. 4.1 Topology error: a) shows the true situation; b) shows the situation modeled in state estimation

In Fig. 4.1, S_{k0} and S_{m0} is the original power injection measurements at bus *k* and *m* in the base case, respectively. S_{km0} is the complex power flow measurement from bus *k* to

m, which can be expressed as $P_{km0} + jQ_{km0}$. P_{km0} and Q_{km0} are real and reactive power flow measurements, respectively.

In this research, it is assumed that the line bearing a topology error has injection measurements at its two terminals. If there is no injection measurement associated with the topology error, the line with topology errors will not be included in state estimation. In other words, this topology error is not observable to state estimation and could not be detected; thus, it has no impact on state estimation.

Let us assume the topology error occurs on line *k*-*m*. The measurement equation is shown as follows:

$$h(x) = \begin{bmatrix} \vdots \\ V_k \sum_{j\in\Gamma_k} V_j (G_{kj}\cos\theta_{kj} + B_{kj}\sin\theta_{kj}) \\ V_k \sum_{j\in\Gamma_k} V_j (G_{kj}\sin\theta_{kj} - B_{kj}\cos\theta_{kj}) \\ \vdots \\ V_m \sum_{j\in\Gamma_k} V_j (G_{mj}\cos\theta_{mj} + B_{mj}\sin\theta_{mj}) \\ V_m \sum_{j\in\Gamma_k} V_j (G_{mj}\cos\theta_{mj} - B_{mj}\sin\theta_{mj}) \\ \vdots \end{bmatrix} = \begin{bmatrix} \vdots \\ P_{k0} \\ Q_{k0} \\ \vdots \\ P_{m0} \\ Q_{m0} \\ \vdots \end{bmatrix} = z_0 + e \qquad (4.1)$$

where, Γ_k is the set of bus numbers that are directly connected to bus *k*, and it does not include bus *m* due to the topology error on line *k*-*m*. V_k and θ_k are the voltage magnitude and phase angle at bus *k*, $\theta_{kj} = \theta_k - \theta_j$; $G_{kj} + jB_{kj}$ is the *kj*-th element of the admittance matrix Y_{bus}. P_{k0} and Q_{k0} are real and reactive power injection measurements at bus *k* in the base case. z_0 is base measurement vector.

As the power flow on line *k-m* increases, assuming from S_{km0} to $S_{km0} + \Delta S_{km}$, the measurement function will be expressed as follows:

$$h(x) = \begin{bmatrix} \vdots \\ P_{k0} + \Delta P_{mk} \\ Q_{k0} + \Delta Q_{mk} \\ \vdots \\ P_{m0} + \Delta P_{km} \\ Q_{m0} + \Delta Q_{km} \\ \vdots \end{bmatrix} = z_0 + \Delta z + e \tag{4.2}$$

where, ΔP_{mk} and ΔQ_{mk} are the increased real and reactive power flow on line *m-k*. Δz has at most 4 non-zero entries if injection measurements at both terminals are available, and the 4 entries are highly dependent values.

Therefore, this chapter studies the convergence property of the WLS state estimation with the measurement vector changing from z_0 to $z_0 + \Delta z$. In next simulation section, the increasing power flow in a line will be simulated by varying the power injection measurements at two terminals of the line. For the formulation of the second topology error, it is similar to the equation (4.2) and will not be shown again.

4.3 Simulation results

In this section, the simulation results using a simple 3-bus system and the IEEE 118-bus system will be reported.

4.3.1 Test on a Simple 3-bus System

A simple 3-bus system is shown in Fig. 4.2. Bus 1 is the reference bus, bus 2 is the generator bus, and bus 3 is the load bus. The impedances of the lines are shown in the figure. The dashed line 2-3 represents a topology error on the line that is wrongly modeled as out-of-service in state estimation simulation. The detailed simulation procedures are as follows:

First, the base case power flow of the 3-bus system is run to obtain the non-synchronized measurements for the state estimation. The measurements include the voltage magnitude of bus 1, all the real and reactive power injections, and branch flows except the power flow of line 2-3.

Then, let the real and reactive power of the load at bus 3 increase by a certain percentage, e.g. 10%, and the generator at bus 2 will also increase its output with the same amount. Other measurements for state estimation are kept constant. In this way, the increasing power flow on line 2-3 is simulated. The topology error occurs in line 2-3, which means line 2-3 will be excluded in the formulation of the admittance matrix used for state estimation. The power flow measurements of line 2-3 will also be excluded in the measurement vector z. Then, the WLS state estimation program is run and its convergence is checked. In this work, the maximum iteration number is set to be 50; if the state estimator does not converge after 50 iterations, it is considered to be diverged. The standard deviation of measurement errors is set in Table 4.1.

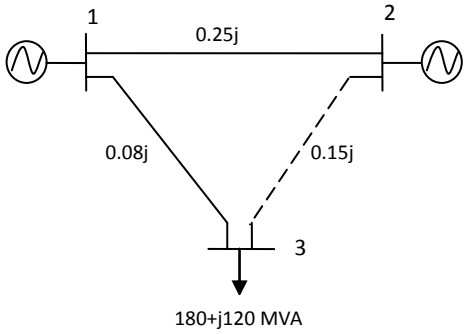

Fig. 4.2 A simple 3-bus system

Table 4.1. Standard deviation setting of measurement errors

Standard deviation	Value setting
σ_V	0.4%
σ_{Pinj} and σ_{Qinj}	1%
σ_{Pf} and σ_{Qf}	0.8%

where,

σ_V is the standard deviation of voltage magnitude measurement error;

σ_{Pinj} and σ_{Qinj} are the standard deviation of real and reactive power injection measurement errors, respectively;

σ_{Pf} and σ_{Qf} are the standard deviation of real and reactive power flow measurement errors, respectively.

The voltage magnitudes in per unit and angles of 3 buses in degree versus real power of the load at bus 3 are shown in Fig. 4.3 - 4.5. The WLS state estimation diverges when the

real power of the load at bus 3 reaches around 1600MW. In Fig. 4.3, the voltage magnitudes of bus 1 and 2 monotonously increase, while for bus 3, the voltage magnitude will decrease at first, and then increase until the state estimator diverges. Fig. 4.4 depicts the change of voltage angles of the three buses.

For clarity, the voltage magnitude of bus 3 is redrawn in Fig. 4.5. The phenomena that the voltage drops first and then rises again could be used to predict the equilibrium when the system reaches a critical operating point.

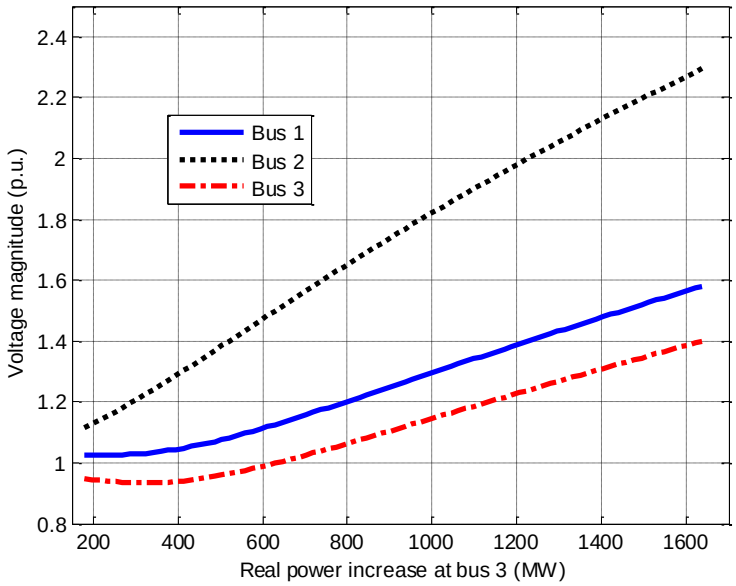

Fig. 4.3 Voltage magnitudes of 3-bus system

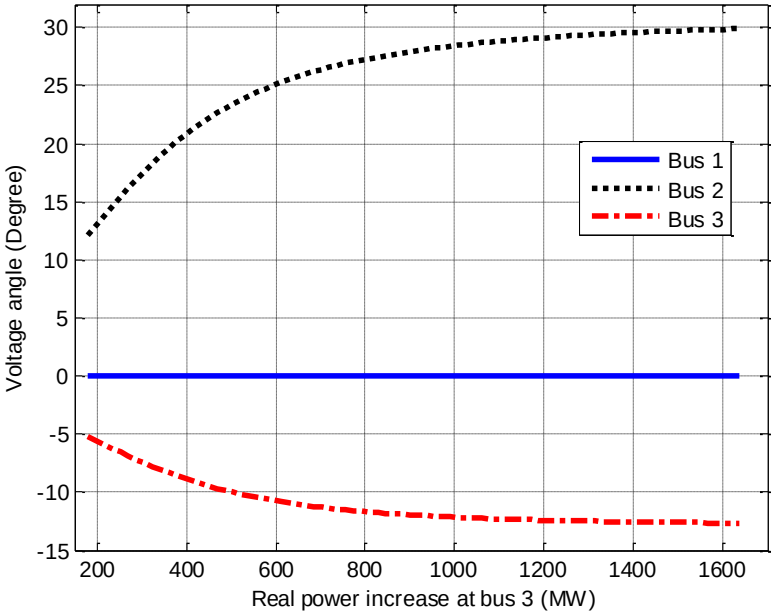

Fig. 4.4 Voltage angles of 3-bus system

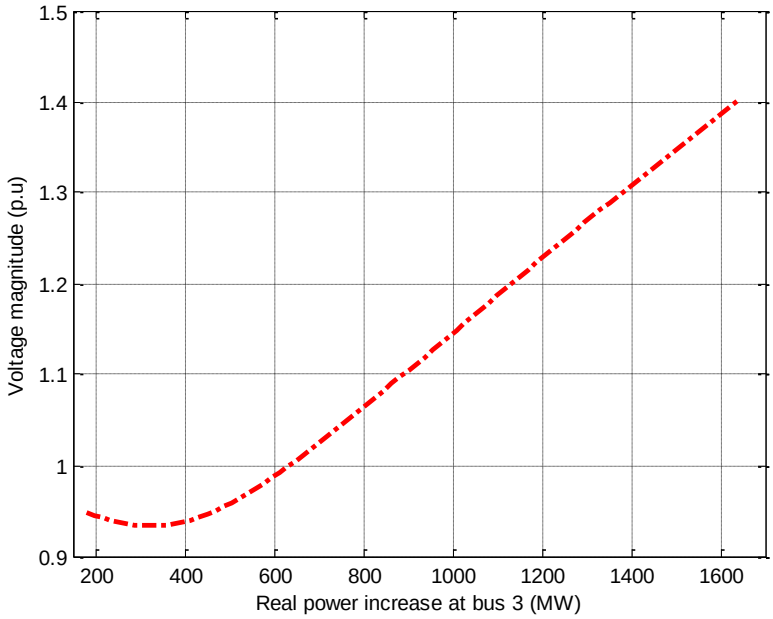

Fig. 4.5 voltage magnitude of bus 3

4.3.2 Test on the IEEE 118-bus system

The IEEE 118-bus system is tested to further verify the above discovery. The test results will include the topology error on a line with heavy and light power flow, respectively.

A. The topology error on a line with heavy power flow

It is assumed that the topology error occurs in line 60-61 in the system as shown in Fig. 4.6. The real power flow in line 60-61 of the base case is about 112MW, which is a relatively heavy power flow compared to that in other lines. For the detailed power flow results of the IEEE 118-bus system, please refer to Appendix A. Line 60-61, actually in service, is wrongly assumed to be out-of-service in the state estimator as shown in dash line. Bus 60 is a load bus, and bus 61 is a generator bus. The state estimation simulation procedures are similar to that in the 3-bus system. The power flow results of the base case are obtained by using the Matpower tool.

In this case, the state estimation measurements are non-synchronized, including 20 voltage magnitudes, all the power injections at the entire system buses, all the line power flows except the line 60-61. Each bus voltage magnitude is selected from every six buses of the total buses. The standard deviation setting of the measurement errors is the same as that listed in Table 4.1.

The simulation results are shown in Fig. 4.7 and 4.8. The WLS state estimation diverges when the real power of bus 60 is close to 2500MW. In Fig. 4.7, the voltage magnitude of bus 60 decreases at first, and then increases until the state estimation diverges. For the voltage magnitude of bus 61, it increases monotonously versus real power increase at bus

60. Fig. 4.8 shows the curves of voltage angles of bus 60 and 61 respectively. For the other buses, they have similar curves of voltage magnitudes and angles to bus 61.

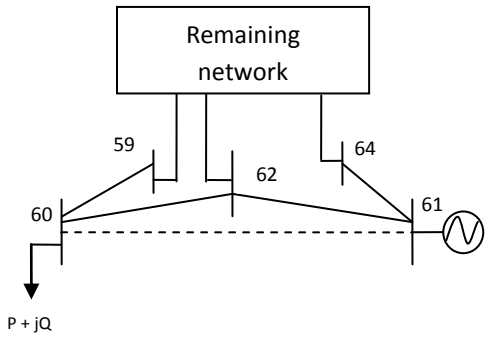

Fig. 4.6 The topology error in branch 60-61 of the IEEE 118-bus system

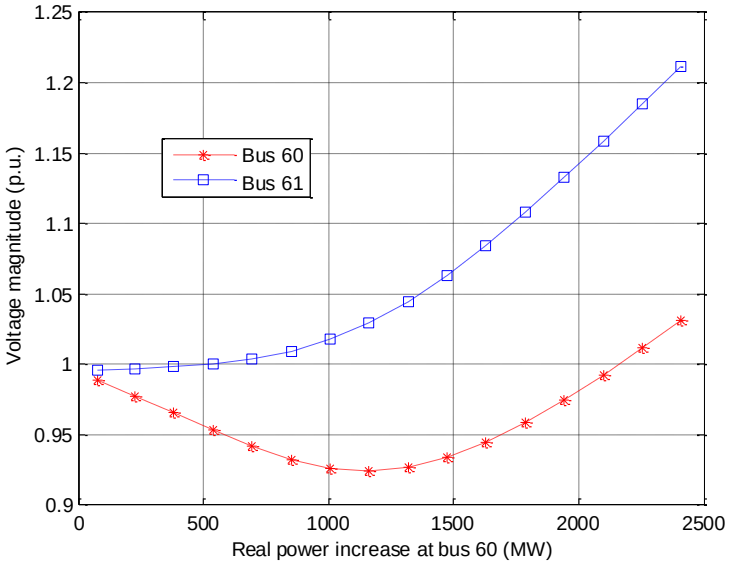

Fig. 4.7 Voltage magnitudes of bus 60 and 61

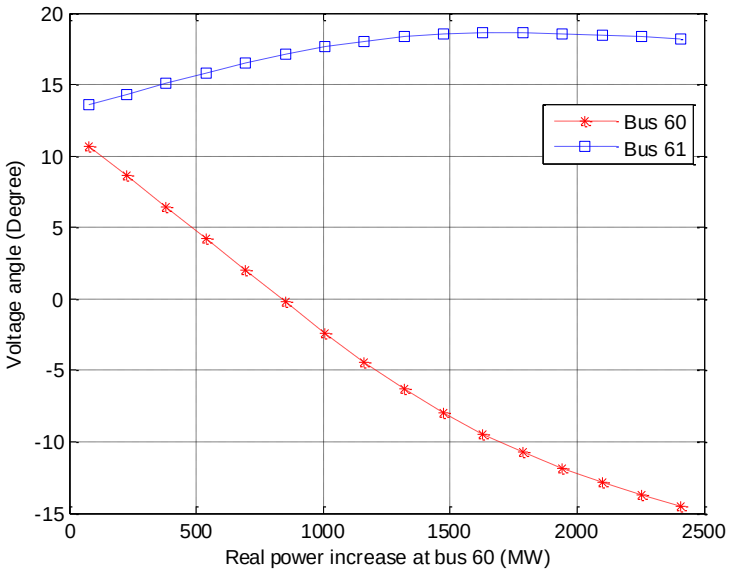

Fig. 4.8 Voltage angles of bus 60 and 61

B. The topology error on a line with light power flow

In this test, the line 98-100 is assumed to have the topology error. Bus 98 is a load bus, and bus 100 is a generator bus. The real power flow in this line of the base case is about 5MW, which is a relatively small value compared to line 60-61. The simulation results are shown in Fig. 4.9 and 4.10.

It can be seen that Fig. 4.9 and 4.10 are similar to Fig. 4.7 and 4.8. The voltage magnitude of bus 98 decreases at first, and then increases until the state estimator diverges. While for bus 100, the voltage magnitude is always increasing as the load increases at bus 98.

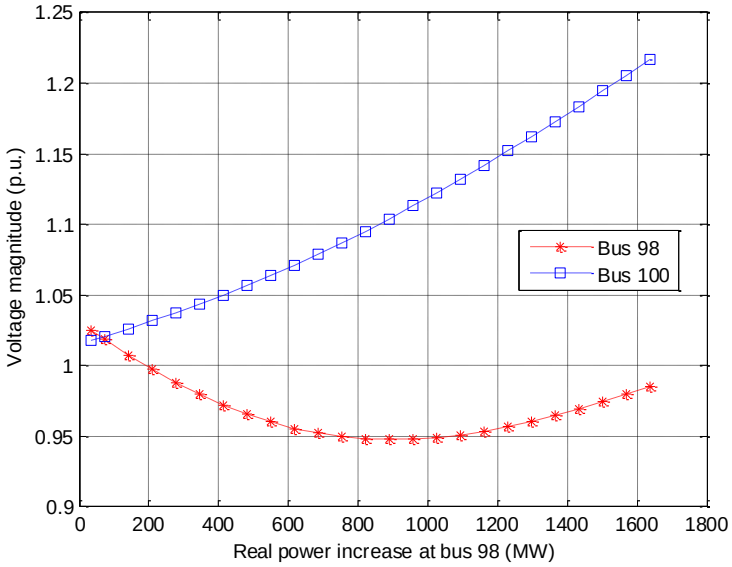

Fig. 4.9 Voltage magnitude of bus 98 and 100

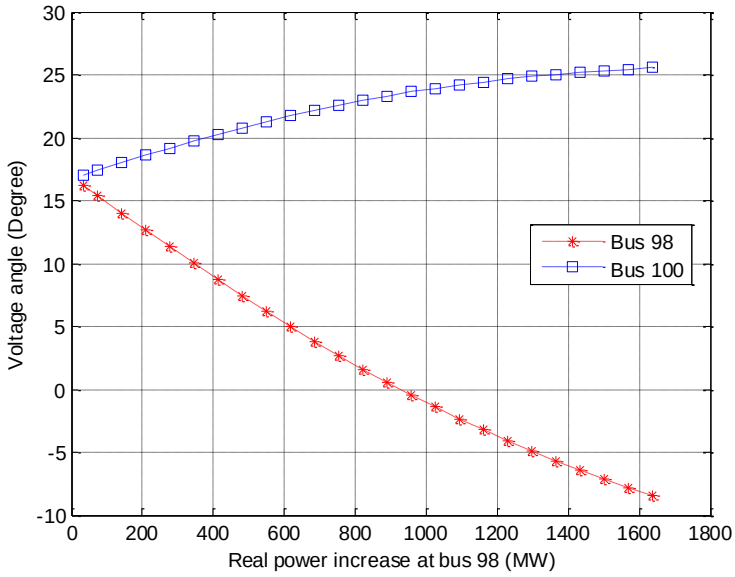

Fig. 4.10 Voltage angles of bus 98 and 100

4.4 Effect of PMU measurements on WLS State Estimation convergence

PMU voltage magnitude and angle measurements are added in the measurement vector of conventional WLS state estimation to test if they will improve the robustness of WLS

state estimation. PMU data are used along with conventional measurements in the state estimation, albeit with higher weights. The measurements used in state estimation will include all the measurements adopted in Section 4.3.2 and the angles of the voltages of the 20 buses. Suppose that bus 1 in the system is considered as the reference bus, at which a PMU is placed to give an accurate angle reference for other buses. The measurements of voltage magnitudes and angles are set to have a standard deviation of 0.1%, which means they are more accurate than conventional measurements.

The topology errors in line 98-100 and 60-61 in the previous section are used as the test cases, and another 8 random lines with topology errors are also studied. The simulation results are shown in Table 4.2 as follows.

Table 4.2 Impacts of PMU measurements on loadability

Line with topology error	Base Line flow (MW)	Maximum real power increment of load bus before divergence (MW)		Loadability Improvement Percentage (%)
		No PMU measurements	With PMU measurements	
Line 98-100	5.26	1,639	1,697	3.54
Line 60-61	112.07	2,410	2,215	N/A
Line 14-15	4.24	2,290	2,369	3.45
Line 88-89	98.93	1,186	1,478	24.62
Line 6-7	35.54	2,367	3,412	44.15
Line 11-12	34.29	2,016	2,345	16.32
Line 17-18	80.27	5,025	3,935	N/A
Line 39-40	26.92	1,023	1,121	9.58
Line 66-67	53.16	1,310	2,220	69.47
Line 79-80	64.74	3,354	4,836	44.19

Column 2 of the table shows the real line flow of the base case in the line that the topology error will occur. Column 3 and 4 give the maximum real power increment of

load bus before divergence for the state estimation without and with PMU measurements, respectively. The last column of the table calculates the loadability improvement percentage, which is obtained as the difference between column 4 and column 3 divided by the value of column 3. It can be seen that except the cases of topology errors in line 60-61 and 17-18, all the other cases show that the state estimation with PMU measurements will diverge at larger load increment than that without PMU measurements. The maximum value of loadability improvement percentage is 69.47%, which occurs in the case of topology error in line 66-67. For the cases of topology error in line 60-61 and 17-18, since adding PMU measurements does not improve the loadability, the loadability improvement percentage is not calculated.

In the case of line 88-89 with topology error, Fig. 4.11 and 4.12 shows the comparison of voltage magnitude of bus 88 and 89 in the state estimation without and with PMU measurements, respectively. It can be seen that state estimation with PMU measurements diverges at larger load increment than that without PMU measurements. All the other cases have similar curves to this case, and thus are not plotted.

4.5 Future work

The simulation results show that the voltage magnitude of load bus will decrease to the lowest voltage magnitude at first, and then increase until the state estimator diverges. The future work will analyze the trend of the load bus curve from the point view of the mathematical equations. Such analysis could provide an analytical solution to finding the critical loading level when state estimation diverges under a certain topology error. If such a solution is found, better design of state estimator that is more robust under stressed operating conditions will be possible. Furthermore, only PMU voltage phasor

measurements are applied in the state estimator. Since PMUs can also measure current phasors, in future PMU current phasor measurements will be considered in state estimation.

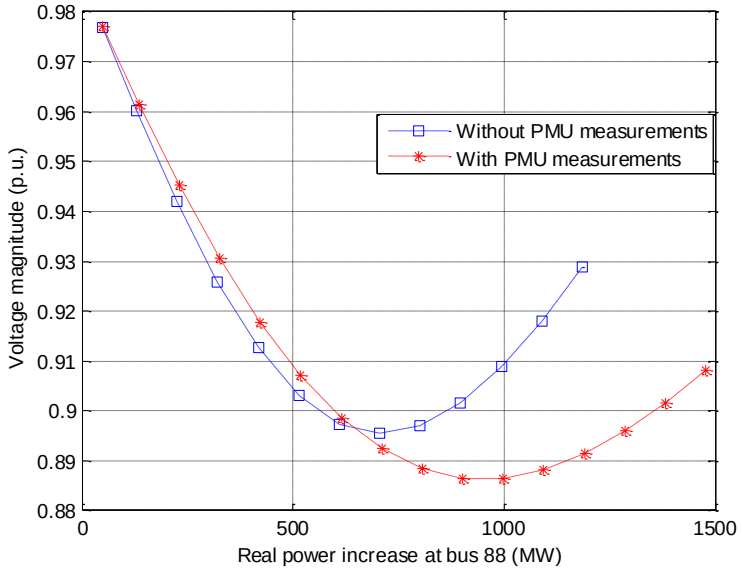

Fig. 4.11 Comparison of voltage magnitude of bus 88

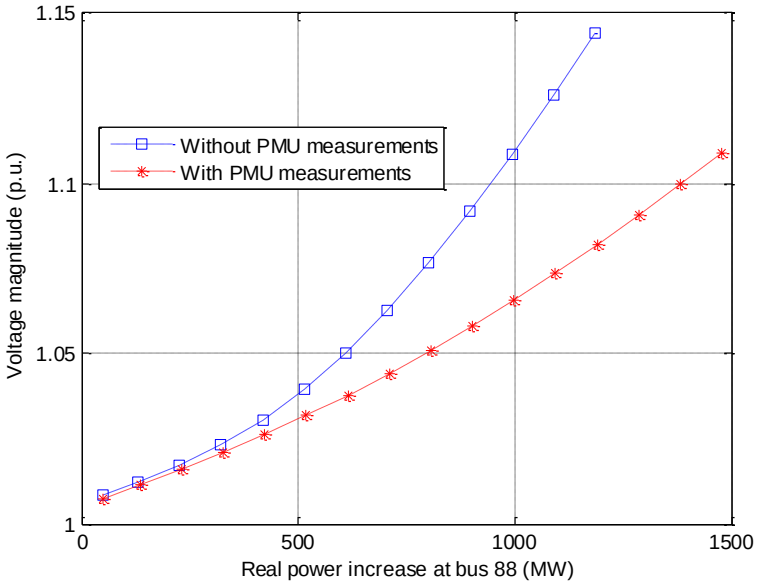

Fig. 4.12 Comparison of voltage magnitude of bus 89

4.6 Conclusion

This chapter investigates the impact of topology error on a line with increasing power flow on the commonly used WLS state estimator. As the power flow on the line increases, the WLS state estimator will diverge at some load level. The simulation results using a simple 3-bus system and the IEEE 118-bus system show that they follow the similar rule. The voltage magnitude of the load bus will decrease at first and then increase until the state estimator diverges. For other buses including the generator buses, the voltage magnitudes will always increase. The mathematical analysis on the change of these curves will be further investigated and results will be reported in the future. In addition, the chapter also studies the effect of adding PMU voltage phasors on the robustness of WLS state estimation. Simulation results show that generally but not always, PMU measurements make the WLS state estimation more robust when the topology error occurs.

Chapter 5 Incorporation of PMU Measurements in WLS State Estimation

This chapter will present new approaches to incorporate PMU measurements in state estimation. These new approaches are able to improve the robustness of the state estimation and thus are expected to be applied in practice in near future. The chapter is organized as follows. Section 5.1 will give a brief introduction of background knowledge. Section 5.2 presents the equality-constrained state estimation with PMU measurements approach. Section 5.3 introduces the Hachtel's matrix state estimation with PMU measurements approach. The comparison of these two methods and conventional WLS state estimation method using the IEEE 14-bus system is illustrated in section 5.4, followed by the conclusion.

5.1 Introduction

The phasor measurement unit (PMU) is considered as one of the most important measuring instruments in the future of power systems. This instrument can receive synchronized sampling clocks from global positioning system (GPS) satellite signals, to accurately measure positive sequence bus voltage phasors as well as branch current phasors incident to the bus at which a PMU is equipped. Voltage phasor measurement can be utilized in the state estimation in terms of voltage magnitude and phase angle. The current phasor measurement used in the state estimation includes real and reactive parts

of the phasor measurement. It can be derived from the general two-port π-circuit model of Fig. 5.1 as follows.

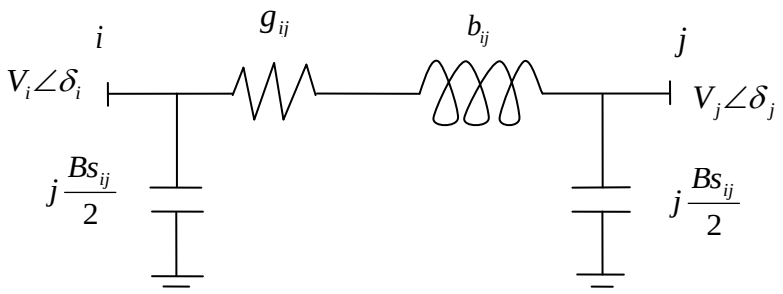

Fig. 5.1. Two-port π-circuit model for a network

The current I_{ij} from bus *i* to *j* is expressed as follows:

$$I_{ij} = (g_{ij} + jb_{ij})(V_i\angle\delta_i - V_j\angle\delta_j) + j\frac{Bs_{ij}}{2}V_i\angle\delta_i \tag{5.1}$$

Hence, the real and imaginary part of the current I_{ij} are

$$\mathrm{Re}(I_{ij}) = g_{ij}\left(V_i\cos\delta_i - V_j\cos\delta_j\right) - b_{ij}\left(V_i\sin\delta_i - V_j\sin\delta_j\right) - \frac{Bs_{ij}}{2}V_i\sin\delta_i \tag{5.2}$$

$$\mathrm{Im}(I_{ij}) = b_{ij}\left(V_i\cos\delta_i - V_j\cos\delta_j\right) + g_{ij}\left(V_i\sin\delta_i - V_j\sin\delta_j\right) - \frac{Bs_{ij}}{2}V_i\cos\delta_i \tag{5.3}$$

where,

V_i and δ_i are the voltage magnitude and phase angle at bus i, respectively;

$g_{ij} + jb_{ij}$ is the admittance of the series branch connecting buses i and *j*;

$\frac{Bs_{ij}}{2}$ is the line-charging susceptance.

The derivative of the current phasor with respect to voltage angle and magnitude is shown in Appendix B. In conventional WLS state estimation, PMU measurements are

treated as the regular measurement with higher weight, which might cause ill-conditioning of the gain matrix. Therefore, the next sections will present new approaches to incorporate PMU measurements in state estimation, which will reduce the condition number of the gain matrix.

5.2 Equality-constrained State Estimation with PMU Measurements Approach

The use of very high weights for modeling very accurate PMU measurements and zero power injections might lead to ill-conditioning of the *G* matrix. Zero power injections are virtual measurements at the switching buses. They represent the perfect measurements, and thus large weights are assigned to them in the state estimation, i.e. 1e12. One way to avoid the use of high weights is to model these measurements as explicit constraints in the WLS state estimation. The constrained WLS state estimation problem is formulated as follows [28]:

$$\text{Minimize} \quad J(x) = \frac{1}{2}[z - h(x)]^T R^{-1}[z - h(x)] \tag{5.4}$$

$$\text{Subject to} \quad c(x) = 0 \tag{5.5}$$

where $c(x) = 0$ represents the accurate PMU and virtual zero power injection measurements, which are now excluded from $h(x)$.

Lagrangian method is utilized to solve this problem, where the following Lagrangian is built:

$$L = J(x) - \lambda^T c(x) \tag{5.6}$$

and the first-order optimality conditions are derived:

$$\partial L(x)/\partial x = 0 \Rightarrow H^T R^{-1}[z - h(x)] + C^T \lambda = 0 \tag{5.7}$$

$$\partial L(x)/\partial \lambda = 0 \Rightarrow c(x) = 0 \tag{5.8}$$

where the Jacobian matrix $C = \partial c(x)/\partial x$, λ is the Lagrange multiplier.

By applying the Gauss-Newton method, the nonlinear set of Equation (5.7) and (5.8) is solved iteratively by means of the following linear system:

$$\begin{bmatrix} H^T R^{-1} H & C^T \\ C & 0 \end{bmatrix} \begin{bmatrix} \Delta x \\ -\lambda \end{bmatrix} = \begin{bmatrix} H^T R^{-1} \Delta z^k \\ -c(x^k) \end{bmatrix} \tag{5.9}$$

where,

$\Delta x = x^{k+1} - x^k$

$\Delta z^k = z - h(x^k)$

It is worth mentioning that the condition number of the coefficient matrix in Equation (5.9) can be further reduced by introducing the scaling factor α, which has no influence on the estimated state. The equation system that must be solved at each iteration is obtained by substituting αR^{-1} for R^{-1}:

$$\begin{bmatrix} \alpha H^T R^{-1} H & C^T \\ C & 0 \end{bmatrix} \begin{bmatrix} \Delta x \\ -\lambda_s \end{bmatrix} = \begin{bmatrix} \alpha H^T R^{-1} \Delta z^k \\ -c(x^k) \end{bmatrix} \tag{5.10}$$

where, $\lambda_s = \alpha \lambda$.

A low condition numbers are obtained when α is chosen as

$$\alpha = \frac{1}{\max R_{ii}^{-1}} \tag{5.11}$$

5.3 Hachtel's Matrix State Estimation With PMU Measurements Approach

The Hachtel's matrix state estimation approach, also called augmented matrix approach, considers the regular measurement equations as equality constraints. In this approach, the WLS problem is formulated as follows [28]:

$$\text{Minimize } J(x) = \frac{1}{2}\gamma^T W \gamma \tag{5.12}$$

$$\text{Subject to } \quad c(x) = 0 \tag{5.13}$$

$$r - z + h(x) = 0 \tag{5.14}$$

Similarly, the Lagrangian method is used to solve the above Equation (5.12) - (5.14), the following system of equations will be obtained:

$$\begin{bmatrix} R & H & 0 \\ H^T & 0 & C^T \\ 0 & C & 0 \end{bmatrix} \begin{bmatrix} \mu \\ \Delta x \\ \lambda \end{bmatrix} = \begin{bmatrix} \Delta z^k \\ 0 \\ -c(x^k) \end{bmatrix} \tag{5.15}$$

The coefficient matrix in Equation (5.15) is called the Hachtel's matrix. Note that Equation (5.15) will become identical to (5.9) if μ is eliminated. Hence, this is the most primitive or augmented formulation which will obtain the lower condition numbers.

Similar to the case of Equation (5.10), the condition number of Hachtel's matrix can be further reduced if the residual weights are properly scaled, which is achieved simply by substituting αR^{-1} for R^{-1} in Equation (5.15).

$$\begin{bmatrix} \alpha^{-1}R & H & 0 \\ H^T & 0 & C^T \\ 0 & C & 0 \end{bmatrix} \begin{bmatrix} \mu_s \\ \Delta x \\ \lambda_s \end{bmatrix} = \begin{bmatrix} \Delta z^k \\ 0 \\ -c(x^k) \end{bmatrix} \tag{5.16}$$

where μ_s and λ_s are the scaled Lagrange multipliers.

5.4 Simulation result of the IEEE 14-bus system

Fig. 5.1 shows the IEEE 14-bus system with PMU measurements at bus 1, 6 and 10. Therefore, the voltage and current phasor measurements related to these three PMU buses are included in the explicit constraint equation $c(x)$. PMU voltage phasor measurements at bus 1, 6, and 10 are included in $c(x)$. PMU current phasor measurements comprise of branch 1-2, 1-5, 5-6, 6-11, 6-12, 9-10 and 10-11. Besides, there is a zero power injection measurement at bus 7, and this measurement will be included in $c(x)$ as well.

For the other regular measurements, they include the voltage magnitudes of the remaining buses, the power injections of the remaining buses. This redundant set of measurements will make the Jacobian *H* of full rank.

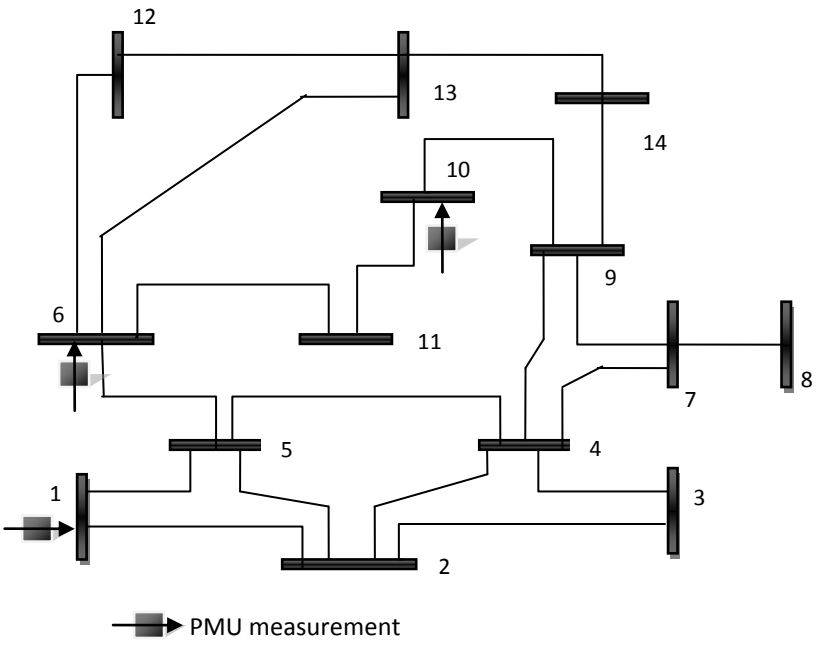

Fig. 5.1 IEEE 14-bus system with PMU measurements

The typical standard deviation setting of the measurement errors is shown in Table 5.1. The simulation results of the condition number of gain matrix *G* for the three methods are given in Table 5.2. The conventional WLS state estimation method incorporates PMU measurements and virtual zero power injections along with other regular measurements together in state estimation. Thus, the condition number of gain matrix *G* is relatively large. Besides, this method does not apply the scalar α . For the other two methods, it can be seen that when applying the scalar α , the condition number will further decrease. The Hachtel's matrix method is better than the equality-constrained method as it can obtain the minimum condition number.

Table 5.1 Standard deviation setting of the measurement errors

Measurements	Standard deviation setting
Regular voltage magnitudes	0.4%
Power injections	1%
PMU voltage and current phasors	0.01%
Virtual zero power injecitons	0.001%

Table 5.2 Simulation results of the condition number of gain matrix G

	Conventional WLS SE method	Equality-constrained method	Hachtel's matrix method
No scalar α	4.9044E7	5.0967E16	8.0569E10
With scalar α		1.3049E7	1.353E6

As comparison, the standard deviations of PMU measurements are set as 0.1% and 0.001%, the results are shown as shows.

Table 5.3 Simulation results for 0.1% of the standard deviation of PMU measurements

	Conventional WLS SE method	Equality-constrained method	Hachtel's matrix method
No scalar α	7.6877E7	4.6538E16	7.4121E10
With scalar α		1.3049E7	1.2451E6

Table 5.4 Simulation results for 0.001% of the standard deviation of PMU measurements

	Conventional WLS SE method	Equality-constrained method	Hachtel's matrix method
No scalar α	4.915E7	5.1425E16	8.1232E10
With scalar α		1.3166E7	1.3640E6

As can be seen from Table 5.2-5.4, by applying the Hachtel's matrix method with scalar α, it can achieve the least condition number in state estimation.

It is important to make sure that the Jacobian matrix *C* has full rank, otherwise the equality-constrained and Hachtel's matrix methods can't be implemented. In some cases there exist linear dependent vectors in matrix *C*. For example, when bus 1 and 5 has PMUs, the measurements include voltage magnitudes and angles of bus 1 and 5, current phasor measurements in branch 1-2, 1-5, 5-2, 5-4, and 5-6, as shown in Fig. 5.1. With the knowledge of linear independent vector in mind, if vector $C_3 = \alpha C_1 + \beta C_2$ where C_1 and C_2 are linear independent vectors, C_3 is a linear dependent vector in the condition that α and β are not both equal to zero. When checking the vectors of the Jacobian matrix *C*, it is observed that there exists linear dependent relationship between current phasor measurement 1-5 and voltage magnitudes and angles of bus 1 and 5.

$$C_{I_{1-5}} = \alpha C_{V_1} + \beta C_{V_5} + \gamma C_{\delta_5} \tag{5.17}$$

where,

$C_{I_{1-5}}$ is the vector of derivative of current phasor measurement with respect to state variables.

C_{V_1} is the vector of derivative of voltage magnitude measurement of bus 1 with respect to state variables.

C_{V_5} is the vector of derivative of voltage magnitude measurement of bus 5 with respect to state variables.

C_{δ_5} is the vector of derivative of voltage angle measurement of bus 5 with respect to state variables.

α, β and γ are real numbers.

Thus, to make matrix *C* of full rank, it is necessary to remove current phasor measurement 1-5 from $c(x)$.

5.5 Conclusion

This chapter presents the new approaches of incorporating PMU measurements into the state estimation to reduce the condition number of gain matrix *G*. Through the comparison of the new approaches and the conventional state estimation approach, the Hachtel's matrix state estimation with PMU measurements approach can obtain the minimum condition number of the coefficient matrix in the state estimation. In addition, the singularity problem of *C* matrix is investigated, and the solution is proposed to solve the problem.

Chapter 6 Optimal Placement of Phasor Measurement Units for Improving Power System State Estimation Accuracy

This chapter is organized as follows. Section 6.1 gives a brief introduction. Section 6.2 illustrates two methods of adding PMU measurements to the state estimator. Section 6.3 proposes a heuristic PMU placement approach. Section 6.4 gives the simulation results on the IEEE 14-bus system, followed by the conclusion [64].

6.1 Introduction

With the installation of PMUs in power systems, the state estimator has two more types of voltage and current phasors measurements, and they are much more accurate than the conventional measurements. If all the substations in power systems are installed with PMUs, the state estimator will directly utilize PMU measurements to obtain the best state estimation results of the system. However, due to cost consideration currently less than 1% of substations in United States are installed with PMUs. Hence, the supervision of the power network is still mainly based on conventional SCADA telemetry in place. The current existing SCADA measurement configuration in the system usually makes the network fully observable, and power grid utilities are interested in the knowledge of how to find the best places to add extra limited numbers of PMUs to their systems in order to enhance state estimation performance [58]. Accordingly, the state estimator will use conventional SCADA measurements along with PMU measurements to perform state estimation.

One way to enhance the performance of state estimation is to reduce state estimation error by optimal placement of PMUs. In paper [58], authors apply the incremental placement algorithm, which is first proposed in [59], to improve the estimation accuracy. The covariance matrix of state vector from the inverse of the gain matrix in weighted least square (WLS) method is used to evaluate the estimation accuracy. Note that the paper only considers the PMU voltage phasor measurements, and current phasor measurements are excluded to reduce state estimation computation burden. Paper [60] proposes a greedy approach to find the optimal PMU places. The authors formulate the problem of optimal PMU placement as an optimal experiment design with a class of optimality criteria in the statistics. The state estimator used in this paper considers only PMU voltage angular measurements, which simplify the state estimation computation process but might not achieve accurate estimation results. In addition, one problem with the greedy approach is that it does not search the candidate buses exhaustively, and might not achieve the global minimum.

In this chapter, a heuristic PMU placement approach is proposed to improve the state estimation accuracy, which is evaluated by the performance index of average Mean Average Percentage Error ($MAPE_{ave}$). The approach will search all the candidate buses exhaustively, and find the minimum number of PMUs in order to most improve state estimation accuracy, as well as their optimal locations. In the state estimator, two methods for incorporating PMU measurements into the state estimator are studied, one is to mix the conventional measurements and PMU measurements in the traditional EMS state estimation software, and the other is to add PMU measurements through a post-processing step [61]. It is necessary to point out that the former method needs to modify

the EMS state estimation software during each state estimation calculation, while the latter one will utilize the results of traditional state estimator to obtain the final estimation results with PMU measurements in the post-processing step without modifying EMS software. Two methods will achieve very similar results of state estimation but have quite different computation efficiency as shown in later studies. Furthermore, to best use the PMU measurements, both voltage and current phasors are considered in the PMU placement approach.

6. 2 State estimation with PMU measurements

The traditional state estimator utilizes conventional SCADA measurements including voltage magnitudes, power flows and power injections, to calculate the best estimates. The system measurement equation is given as follows [28]:

$$z_1 = h_1(x) + e_1 \tag{6.1}$$

where, z_1 is the SCADA measurement vector (m x 1). x is the estimated state vector (n x 1). h_1 is a vector of nonlinear functions that relate the states to the measurements. e_1 is the measurement error vector (m x 1). It is necessary that $m \geq n$ and the Jacobian matrix of $h_1(x)$ has rank n.

By taking partial derivative of $h_1(x)$ with respect to state vector x, we can obtain the Jacobian matrix $[H_1]$

$$[H_1] = \frac{\partial h_1(x)}{\partial x} \tag{6.2}$$

The state vector *x* is initialized as a flat start. The weighted least square (WLS) iterative state estimation approach is employed to obtain the best estimates. Assuming x_k is the state vector at *k*th iteration, and the next iteration x_{k+1} is calculated as follows:

$$x_{k+1} = x_k + \Delta x = x_k + \left[H_1{}^T R_1^{-1} H_1\right]^{-1} H_1{}^T R_1^{-1}\left[z_1 - h_1(x_k)\right] \tag{6.3}$$

where, Δx is the measurement mismatch, and R_1 is the error covariance matrix of SCADA measurements.

The iteration will be terminated when the measurement mismatch reaches a prescribed low value, e.g. 1e-4. Assuming V_{SCADA} is used to denote the converged estimate of the above equation, the error covariance matrix of the estimate V_{SCADA} will be given as follows [58]:

$$W_1 = \left[H_1^T R_1^{-1} H_1\right]^{-1} \tag{6.4}$$

In the following two subsections, two methods for adding PMU measurements to the state estimator will be introduced.

6.2.1 Method I: Mixing PMU Measurements with Conventional Measurements in the Estimator

Let z_2 denote PMU measurements, which include voltage magnitudes, voltage angles, real and imaginary parts of current phasors. The measurement error covariance matrix of z_2 is assumed to be R_2. The new measurement set z is obtained by adding PMU measurements z_2 to the previous conventional measurement vector z_1

$$z = \begin{bmatrix} z_1 \\ z_2 \end{bmatrix} \equiv \begin{bmatrix} z_1 \\ V_{PMU\_mag} \\ V_{PMU\_ang} \\ I_{PMU\_r} \\ I_{PMU\_i} \end{bmatrix} \tag{6.5}$$

where, V_{PMU_mag} and V_{PMU_ang} are respective PMU voltage magnitude and angle measurements. I_{PMU_r} and I_{PMU_i} are respective real and imaginary parts of PMU current phasors, which are introduced in Chapter 5.

Let $h(x)$ and $h_2(x)$ be the nonlinear equations of new measurement set z and PMU measurements z_2, respectively. The new Jacobian matrix corresponding to the measurement set z will be given as follows [61]:

$$H = \begin{bmatrix} H_1 \\ H_2 \end{bmatrix} = \begin{bmatrix} \dfrac{\partial h_1(x)}{\partial x} \\ \dfrac{\partial h_2(x)}{\partial x} \end{bmatrix} \tag{6.6}$$

Accordingly, the WLS state estimation solution proceeds as before and can be written as follows:

$$x_{k+1} = x_k + \left[H^T W^{-1} H\right]^{-1} H^T W^{-1} \left[z - h(x_k)\right] \tag{6.7}$$

where, the error covariance matrix of measurement set z in method I is

$$W = \begin{bmatrix} R_1 & 0 \\ 0 & R_2 \end{bmatrix} \tag{6.8}$$

6.2.2 Method II: Incorporating PMU measurements through a post-processing step

Method II, as proposed in paper [61], employs the WLS state estimation approach to obtain bus voltage magnitudes and angles by using SCADA measurements. The estimated results are then treated as pseudo measurements and further processed together with the PMU measurements. The estimated voltage magnitudes and angles are obtained in polar coordinates, while the state vector of the post-processing step is in rectangular coordinates. The error covariance matrix W_1 of the estimate V_{SCADA} corresponding to polar coordinates should be modified to reflect the transformation of the state variables from polar to rectangular coordinates. To derive the transformation rule, we can express the real and imaginary parts of voltage phasor at bus *j* in terms of polar coordinates as follows:

$$V_r(j) = |V_j|\cos(\delta_j) \tag{6.9}$$

$$V_i(j) = |V_j|\sin(\delta_j) \tag{6.10}$$

Take the whole derivative of both sides in above equations, we get

$$dV_r(j) = -|V_j|\sin(\delta_j)d\delta_j + \cos(\delta_j)d|V_j| \tag{6.11}$$

$$dV_i(j) = |V_j|\cos(\delta_j)d\delta_j + \sin(\delta_j)d|V_j| \tag{6.12}$$

Bus 1 in a *N*-bus system is considered as the reference bus, and its voltage angle is set as 0 degree. The relationship between incremental representation in polar and rectangular coordinates can be expressed as follows [61]:

$$\begin{bmatrix} dV_r(1) \\ dV_r(2) \\ \vdots \\ dV_r(n) \\ dV_i(2) \\ dV_i(3) \\ \vdots \\ dV_i(n) \end{bmatrix} = R_{m1}dx = \begin{bmatrix} 0 & 0 & 0 & 0 & \cos(\delta_1) & 0 & 0 & 0 \\ -|V_2|\sin(\delta_2) & 0 & 0 & 0 & 0 & \cos(\delta_2) & 0 & 0 \\ 0 & \cdots & \ddots & 0 & 0 & 0 & \ddots & 0 \\ 0 & 0 & 0 & -|V_n|\sin(\delta_n) & 0 & 0 & 0 & \cos(\delta_n) \\ |V_2|\cos(\delta_2) & 0 & 0 & 0 & 0 & \sin(\delta_2) & 0 & 0 \\ 0 & |V_3|\cos(\delta_3) & 0 & 0 & 0 & 0 & \ddots & 0 \\ 0 & 0 & \ddots & 0 & 0 & 0 & \ddots & 0 \\ 0 & 0 & 0 & |V_n|\cos(\delta_n) & 0 & 0 & 0 & \sin(\delta_n) \end{bmatrix} \begin{bmatrix} d\delta_2 \\ d\delta_3 \\ \vdots \\ d\delta_n \\ d|V_1| \\ d|V_2| \\ \vdots \\ d|V_n| \end{bmatrix} \quad (6.13)$$

Hence, the error covariance matrix of the estimated results of traditional state estimator corresponding to rectangular coordinates will be

$$W_1^{'} = R_{m1} W_1 (R_{m1})^T \quad (6.14)$$

In method I, PMU voltage phasor measurements are expressed as voltage magnitude and angle in polar coordinates, and their error covariance matrix is assumed to be W_V. When they are expressed as real and imaginary parts of voltage phasors in method II, their error covariance matrix $W_V^{'}$ corresponding to rectangular coordinates will be

$$W_V^{'} = R_{m2} W_V R_{m2}^T \quad (6.15)$$

where, the transformation matrix R_{m2} is similar to matrix R_{m1} although different in detail and size.

By substituting Equation (6.9) and (6.10) into Equation (5.2) and (5.3) of Chapter 5, real and imaginary parts of line current from bus i to j can be expressed in rectangular coordinates as

$$I_{ij\_r} = g_{ij}\left(V_r(i) - V_r(j)\right) - b_{ij}\left(V_i(i) - V_i(j)\right) - \frac{Bs_{ij}}{2} V_i(i) \quad (6.16)$$

$$I_{ij\_i} = b_{ij}\left(V_r(i) - V_r(j)\right) + g_{ij}\left(V_i(i) - V_i(j)\right) + \frac{Bs_{ij}}{2} V_r(i) \tag{6.17}$$

where, $V_r(i)$ and $V_i(i)$ are real and imaginary parts of voltage phasors at bus i, respectively.

Assuming the measurement error covariance matrix of current phasor measurements z_I is W_I. The state vector x in rectangular coordinates is expressed as vector $\begin{bmatrix} V_r \\ V_i \end{bmatrix}$. The measurement equation for equation (6.5) can be modified as follows [61]:

$$z = \begin{bmatrix} z_1 \\ z_2 \end{bmatrix} = \begin{bmatrix} V_{SCADA\_r} \\ V_{SCADA\_i} \\ V_{PMU\_r} \\ V_{PMU\_i} \\ I_{PMU\_r} \\ I_{PMU\_i} \end{bmatrix} = \begin{bmatrix} 1 & 0 \\ 0 & 1 \\ 1' & 0 \\ 0 & 1' \\ A_{5\_1} & A_{5\_2} \\ A_{6\_1} & A_{6\_2} \end{bmatrix} \begin{bmatrix} V_r \\ V_i \end{bmatrix} \equiv \begin{bmatrix} A_1 \\ A_2 \\ A_3 \end{bmatrix} \begin{bmatrix} V_r \\ V_i \end{bmatrix} \tag{6.18}$$

where, the "1" in the above equation represents a unit matrix, whereas the "$1'$" represents a matrix with ones in the corresponding columns where the related voltage phasors have been chosen by the heuristic PMU placement approach. The submatrices A_{5_1} through A_{6_2} are linear, and they are composed of line conductance and susceptance. The submatrices A_1, A_2 and A_3 are the Jacobian matrix of V_{SCADA}, PMU voltage and current phasor measurements, respectively. The error covariance matrix W_{II} in method II will be

$$W_{II} = \begin{bmatrix} W_1' & 0 & 0 \\ 0 & W_V' & 0 \\ 0 & 0 & W_I \end{bmatrix} \tag{6.19}$$

Accordingly, the WLS state estimation solution for the system state will be

$$V_C = G^{-1}\left\{\left[A_1^T (W_1^{'})^{-1}\right]V_{SCADA} + \left[A_2^T (W_V^{'})^{-1}\right]z_V + \left[A_3^T (W_I)^{-1}\right]z_I\right\} \tag{6.20}$$

where, the gain matrix G will be written as follow:

$$G = A_1^T (W_1^{'})^{-1} A_1 + A_2^T (W_V^{'})^{-1} A_2 + A_3^T (W_I)^{-1} A_3 \tag{6.21}$$

Paper in [61] also proves that method I and II are equivalent to each other, and they can achieve very similar state estimation results.

6. 3 Heuristic PMU placement algorithm

Now we consider the optimal PMU placement problem for improving state estimation accuracy. Assuming m PMUs need to be placed in a power system of n buses ($m < n$). Each bus can only have one PMU. After each placement of PMUs, state estimation algorithm is implemented to obtain voltage magnitudes and angles, denoted as SV_{mag} and SV_{del}, respectively. The state estimation accuracy is evaluated by a value of average Mean Absolute Percentage Error, denoted as $MAPE_{ave}$, which is calculated as follows:

$$MAPE_{ave} = (MAPE_{V_{mag}} + MAPE_{V_{del}})/2 \tag{6.22}$$

where,

$$MAPE_{V_{mag}} = \frac{1}{n}\sum_{t=1}^{n}\left|\frac{AV_{mag\_t} - SV_{mag\_t}}{SV_{mag\_t}}\right| \times 100\% \tag{6.23}$$

$$MAPE_{V_{del}} = \frac{1}{n}\sum_{t=1}^{n}\left|\frac{AV_{del\_t} - SV_{del\_t}}{SV_{del\_t}}\right| \times 100\% \tag{6.24}$$

$MAPE_{V_{mag}}$ and $MAPE_{V_{del}}$ are MAPE values of voltage magnitude and angle, respectively. AV_{mag_t} and AV_{del_t} are actual voltage magnitude and angle of bus *t* from power flow results, respectively. SV_{mag_t} and SV_{del_t} are voltage magnitude and angle of state estimation at bus *t*, respectively. In the equation of evaluating the value of $MAPE_{ave}$, the weights of $MAPE_{V_{mag}}$ and $MAPE_{V_{del}}$ are set to 0.5.

Supposing bus 1 in the system is considered as the reference bus, at which a PMU is placed to give an accurate reference for other buses, and this PMU is not counted in the problem of PMU placement. To place m PMUs in the rest $(n-1)$ buses in the system, the total number of possibilities of placements in Mathematics will be

$$A_{n-1}^{m} = (n-1)(n-2)(n-3)\cdots(n-m) = \frac{(n-1)!}{(n-m-1)!} \tag{6.25}$$

Each placement of *m* PMUs has a $MAPE_{ave}$ value. A smaller $MAPE_{ave}$ value indicates the more accurate state estimation of voltage magnitude and angle. The optimal placement of PMUs should have the minimum $MAPE_{ave}$ value.

A heuristic PMU placement approach is proposed to solve the above placement problem. In order to better understand the algorithm, we first define the variables used in the algorithm as follows, and then describe the algorithm procedures. For step 2 and 10, a detailed explanation is followed after the algorithm procedures.

Defining

z_{ori}: the original measurement data vector from power flow results;

Ri_{ori}: the original measurement data error variance vector;

Z: the measurement data vector with noise;

Ri: the measurement error variance vector;

m: number of PMUs needed to place in the system;

AllBus: the vector that contains all the candidate bus numbers;

BusWithPMU: the vector that contains the bus numbers which has been placed with PMUs;

BusToPlace: the vector that contains the bus numbers that will be placed with PMUs. It is obtained by excluding *BusWithPMU* from *AllBus*;

Num: the length of vector *BusToPlace*;

BusNum: the variable that contains the bus number that will be placed with a PMU;

KnownPMUBus: the vector that is formed by combining vector *BusWithPMU* and variable *BusNum*;

MAPE_array: the vector that contains $MAPE_{ave}$ values of state estimation;

The detailed algorithm procedures:

1. Read line data and construct the bus admittance matrix.
2. Read original measurement data from power flow results. The noise is then added to generate new measurement data with mean z_{ori} and error variance Ri_{ori}. Use the

new measurement to construct initial measurement data vector *z* and measurement error variance vector *Ri*.

3. Read the number of PMUs *m* and vector *AllBus* that contains all the candidate bus numbers.
4. Initialize vector *BusWithPMU* with null elements.
5. Set iteration count $i = 1$.
6. Obtain the vector *BusToPlace* that stores the bus numbers that will be placed with PMUs by excluding the elements of vector *BusWithPMU* from vector *AllBus.*
7. Find the length of vector *BusToPlace* and assign it to variable *Num*. Initialize a vector *MAPE_array* of length *Num* to store $MAPE_{ave}$ value of state estimation.
8. Set index count $k = 1$.
9. Read the *k*th value of vector *BusToPlace* and assign it to variable *BusNum*, and obtain vector *KnownPMUBus* by combining the elements of vector *BusWithPMU* and *BusNum*.
10. Modify the initial measurement data vector *z* and measurement error variance vector *Ri* by adding voltage magnitudes and angles as well as current measurements corresponding to buses from vector *KnownPMUBus*.
11. Implement state estimation to obtain $MAPE_{ave}$ value, and store the value in the *k*th element of the vector *MAPE_array*.
12. If $k \leq Num$, increment the index count by 1 and go to step 9; otherwise go to step 13.
13. Find the bus number with the minimum $MAPE_{ave}$ value from vector *MAPE_array*, and add the bus number to vector *BusWithPMU*.

14. If $i \leq m$, increment the iteration count i by 1 and go to step 6; otherwise go to step 15.
15. Print results and stop.

The following discussion gives in-depth analysis about some important steps of the above algorithm:

- In step 2, the original measurement data z_{ori} obtained from Newton Raphson power flow method are considered as true values. The new measurement data z_{new} can be obtained by adding noise to generate a normal distribution with mean z_{ori} and variance Ri_{ori} expressed using Matlab as follows:

$$z_{new} = z_{ori} + \sqrt{Ri_{ori}} .* randn(length(z_{ori}),1) \tag{6.26}$$

  The new measurement data includes real and reactive power injection, real and reactive power flow, voltage magnitude, voltage angle, real and reactive current measurement, and they are listed in order. Among them, power injection and power flow are from SCADA measurements; voltage and current phasor measurements are from PMU measurements.

- In step 10, it is required to add PMU measurements to the initial measurement data vector *z* and error vector *Ri* according to vector *KnownPMUBus*. Assuming vector *KnownPMUBus* has elements of 2 and 4, which means bus 2 and 4 are installed with PMUs. Hence voltage magnitudes and angles as well as current measurement data incident to these two buses will be added to vector *z* and *Ri*.

6.4 Simulation results

In this section we simulate the performance of the proposed heuristic PMU placement algorithm using the IEEE 14-bus system as shown in Fig. 6.1. The Newton Raphson load flow solution is utilized as the basis for generating the measurements with the appropriate normal distribution noise added. The initial conventional measurements are added to Fig. 6.1 such that the system is fully observable [62]. It includes 8 pairs of real and reactive power injection measurements and 12 pairs of real and reactive power flow measurements. As mentioned in section 6.3, one PMU is installed at the reference bus in order to provide the accurate angular reference for the other buses, and the PMU voltage magnitude of the reference bus is also included in the initial measurements. It is assumed that the errors of conventional measurements have a standard deviation equal to 1% of the actual measured values. Since PMUs can measure more accurate voltage and current measurements, PMU measurement errors are assumed to have the standard deviation of 0.1%.

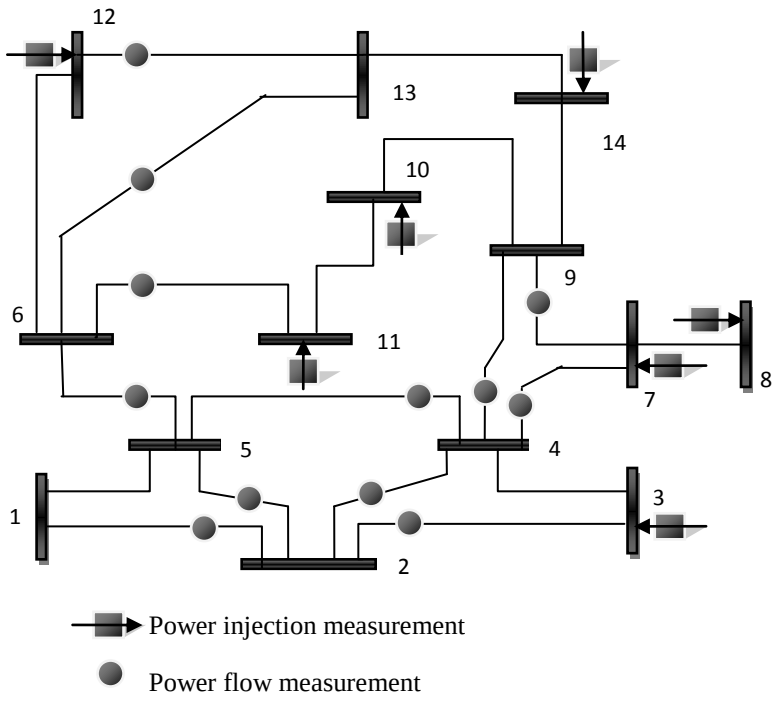

Fig. 6.1 IEEE 14-bus system with initial measurements

The simulation is implemented in Matlab environment. With the initial measurements, we run WLS state estimation Matlab program and obtain the $MAPE_{ave}$ value of 0.6195%. In order to study the results of proposed algorithm with regard to adding different parts of PMU measurements to the initial measurements, 4 cases are designed as follows:

- Case 1: adding PMU voltage magnitude measurements.
- Case 2: adding PMU voltage angle measurements.
- Case 3: adding PMU voltage magnitude and angle measurements.
- Case 4: adding PMU voltage magnitude and angle as well as current measurements.

Method I for incorporating PMU measurements into the estimator is used in the heuristic PMU placement approach to obtain the state estimation results. Fig. 6.2 shows the

simulation results of the above 4 case studies, and their corresponding data table is given in table 6.1.

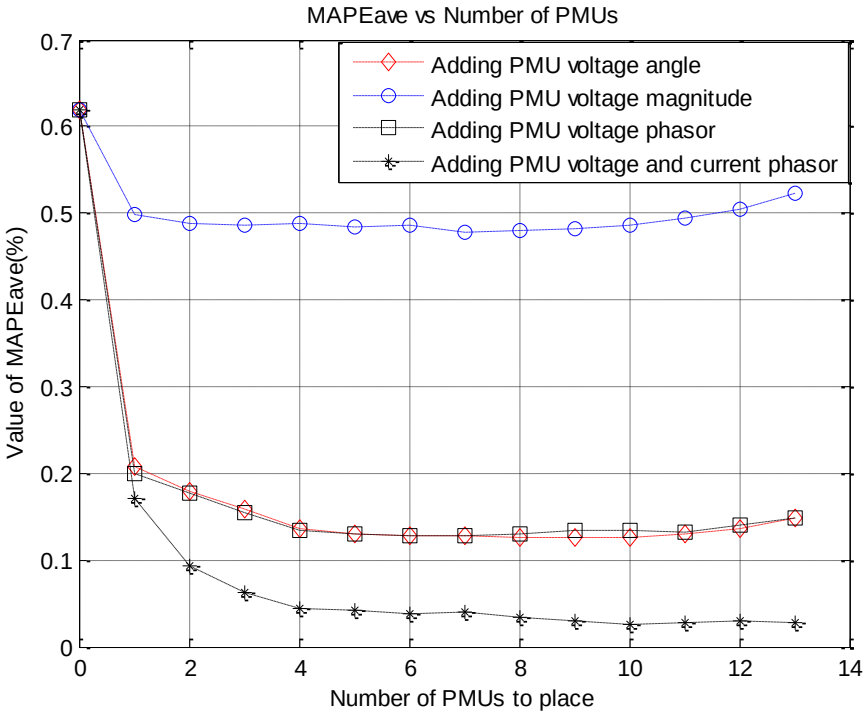

Fig. 6.2 Simulation results of 4 case studies

Table 6.1 The corresponding data table of the above figure.

No. of PMUs	Case 1		Case 2		Case 3		Case 4	
	$MAPE_{ave}$	Bus No.	$MAPE_{ave}$	Bus No.	$MAPE_{ave}$	Bus No.	$MAPE_{ave}$	Bus No.
1	0.4994	4	0.2069	6	0.1989	6	0.171	13
2	0.4885	2	0.1791	3	0.1776	2	0.094	4
3	0.487	6	0.159	8	0.1547	8	0.0623	10
4	0.4878	10	0.1354	4	0.1336	3	0.0436	5
5	0.4845	7	0.1305	12	0.1292	12	0.0411	6
6	0.4857	11	0.128	2	0.1272	4	0.0378	8
7	0.4779	13	0.1279	9	0.1287	13	0.0392	12
8	0.48	12	0.1269	7	0.1307	7	0.0343	9
9	0.4823	8	0.1266	10	0.1342	9	0.0302	14
10	0.4856	14	0.1251	13	0.1345	10	0.0246	7
11	0.4942	9	0.1307	14	0.1318	11	0.0271	3
12	0.5043	3	0.1365	11	0.1403	5	0.0298	2
13	0.5234	5	0.1475	5	0.1491	14	0.028	11

In Fig. 6.2, four curves start from the point that is computed with no PMU placed in the system, and then reduce gradually but seem to saturate as the PMUs are increased beyond a number. Case 4 of adding PMU voltage and current phasor measurements can achieve relatively small $MAPE_{ave}$ value. When placing the 10^{th} PMU at bus 7, we can obtain the minimum $MAPE_{ave}$ value, which is 0.0246%. It is also found that the curves of case 2 and 3 are almost coincided to each other. This means that adding PMU voltage magnitude measurements based on case 2 cannot significantly reduce the value of $MAPE_{ave}$.

Fig. 6.2 may be applied in the optimal placement of PMUs in practical. For example, assuming we only have 5 PMUs in reality to place in the system due to the high cost of PMUs, if we pursue the most accurate state estimation results and ignore the computation complexity of state estimation, case 4 can be adopted. The $MAPE_{ave}$ value is 0.0411%. The optimal places are bus 13, 4, 10, 5, and 6. On the other hand, if we want to reduce the computation complexity but also pursue relatively small MAPE value of about 0.13%, we can utilize case 2 or 3. If case 2 is used since its computation is simpler than case 3, the optimal places will be bus 6, 3, 8, 4 and 12. It can achieve the $MAPE_{ave}$ value of 0.1305%.

In order to improve computation efficiency of the PMU placement approach, method II for adding PMU measurements through a post-processing step is utilized to calculate state estimation results in the PMU placement approach. Table 2 gives the time comparison of two methods running on the four case studies. The simulation tests are implemented on the ThinkPad Edge laptop with Intel i3 CPU at 2.67 GHz. As shown in table 2, the running time by method II can almost reduce 50% on the 4 case studies

compare to method I. Hence, method II is a time-efficient method, and it is preferred to utilize in the heuristic PMU placement approach.

Table 6.2 Time comparison of two methods running on the 4 case studies

	Case 1	Case 2	Case 3	Case 4
Method I (Sec)	1.4260	1.4179	1.3823	1.9344
Method II (Sec)	0.5686	0.7374	0.6665	1.0928

6.5 Conclusion

In this chapter, a heuristic PMU placement approach is proposed to improve state estimation accuracy. The proposed PMU placement algorithm has been tested using IEEE 14-bus system. The simulation results show that adding PMU measurements can improve state estimation accuracy. The obtained PMU placement table and figure might help planning engineers determine the optimal placement of PMUs when they have only a limited number of PMUs to place in the system. In addition, two methods for calculating state estimation results are utilized in the PMU placement approach. It is observed that method II for adding PMU measurements through a post-processing step can significantly improve the computation efficiency of the proposed approach. In addition, this method only needs additional program outside the EMS state estimation software to calculate the final estimates, and does not have to modify the EMS software.

Chapter 7 Conclusion

The WLS state estimation method is the most commonly used in the power industry, and its convergence property has been one of the hot research topics. This dissertation investigates the impacts of the topology errors and the load levels on the WLS state estimator. The simulation shows that as the load level increases, the divergence rate of the state estimation may increase to 1.0 if the standard deviations of the measurements take certain values. The influence of the topology errors on the system is also studied from the point view of the condition number of the gain matrix. Case studies show that the topology errors and measurement standard deviations have impacts on the converged $cond(G)$.

Furthermore, the impacts of the topology errors on the condition number of the converged gain matrix will differ case by case. The locus of the condition number versus the load increment follows a similar trend for the cases with and without topology errors, and the state estimation for cases with topology error will need more number of iterations to converge than cases without topology error. In addition, to indicate the distance between the studied operating point and state estimation divergence, the minimum singular value of the gain matrix is proposed to be used as the gain matrix stability index.

Two types of load increment are used to study their impacts on the convergence property of WLS state estimation, one is load increment of all load buses, and the other one is a single load increment. Simulation results show that adding conventional voltage magnitudes in measurement vector can reduce the divergence rate caused by load

increment but cannot eliminate that, which can be solved by adding PMU measurements. In addition, we also study the effect of topology error on state estimation when there is a single load increment. Voltage magnitude of generator bus will increase if there is a topology error in the state estimation. It is found that adding PMU measurements in state estimation can reduce the error of voltage magnitude and angle estimation.

The impact of topology error on a line with increasing power flow is also investigated. It is observed that the voltage magnitude of the load bus will decrease at first and then increase until the state estimator diverges. For other buses including the generator buses, the voltage magnitudes will always increase. The mathematical analysis on the change of these curves will be further investigated and results will be reported in near future. In addition, the simulation shows that generally but not always, PMU measurements make the WLS state estimation more robust when the topology error occurs.

The condition number of the gain matrix will become large when the state estimator approaches divergence, and adding PMU measurements will reduce the condition number. The equality-constrained and the Hachtel's matrix state estimation with PMU measurements approaches are proposed to incorporate PMU measurements into the state estimator. Through the comparison of the new approaches and the conventional state estimation approach, the Hachtel's matrix approach can obtain the minimum condition number of the coefficient matrix in the state estimation. In addition, the singularity problem of C matrix is investigated, and the solution is proposed to solve the problem.

Finally, a heuristic optimal PMU placement approach is proposed to improve state estimation accuracy. The obtained PMU placement table and figure could help planning

engineers determine the optimal placement of PMUs when they have only a limited number of PMUs to place in the system. In the process of calculating the state estimation results with PMU measurements, two approaches are considered and the approach through a post-processing step can significantly improve the computation efficiency of the proposed approach. This method only needs additional program outside the EMS state estimation software to calculate the final estimates, and does not have to modify the EMS software.

Appendix A

Power Flow Solution of the IEEE 118-bus System

Matpower tool is used to obtain the power flow results of the IEEE 118-bus system. The results are shown as follows.

```
MATPOWER Version 4.1, 14-Dec-2011 -- AC Power Flow (Newton)
Newton's method power flow converged in 3 iterations.
Converged in 0.15 seconds
================================================================================
|     System Summary
|
================================================================================
How many?                How much?              P (MW)            Q (MVAr)
---------------------    -------------------  -------------  -----------------
Buses             118    Total Gen Capacity    9966.2       -7345.0 to 11777.0
Generators         54    On-line Capacity      9966.2       -7345.0 to 11777.0
Committed Gens     54    Generation (actual)   4374.9             795.7
Loads              99    Load                  4242.0            1438.0
Fixed              99    Fixed                 4242.0            1438.0
Dispatchable        0    Dispatchable            -0.0 of -0.0      -0.0
Shunts             14    Shunt (inj)             -0.0              84.4
Branches          186    Losses (I^2 * Z)       132.86            783.79
Transformers        9    Branch Charging (inj)     -              1341.7
Inter-ties          0    Total Inter-tie Flow     0.0                0.0
Areas               1

                         Minimum                      Maximum
                  -------------------------  --------------------------------
Voltage Magnitude   0.943 p.u. @ bus 76          1.050 p.u. @ bus 10
Voltage Angle       7.05 deg   @ bus 41          39.75 deg   @ bus 89
P Losses (I^2*R)             -                  6.40 MW    @ line 25-27
Q Losses (I^2*X)             -                  59.22 MVAr  @ line 9-10

================================================================================
|     Bus Data
|
================================================================================
   Bus      Voltage          Generation             Load
    #     Mag(pu) Ang(deg)    P (MW)   Q (MVAr)    P (MW)   Q (MVAr)
-----    ------- ---------  --------  --------    --------  --------
    1    0.955   10.973       0.00     -3.10      51.00     27.00
    2    0.971   11.513        -         -         20.00      9.00
    3    0.968   11.856        -         -         39.00     10.00
    4    0.998   15.574       0.00    -15.01      39.00     12.00
    5    1.002   16.019        -         -          -         -
    6    0.990   13.292       0.00     15.93      52.00     22.00
    7    0.989   12.847        -         -         19.00      2.00
    8    1.015   21.041       0.00     63.14      28.00      0.00
    9    1.043   28.295        -         -          -         -
   10    1.050   35.876     450.00    -51.04        -         -
   11    0.985   13.006        -         -         70.00     23.00
   12    0.990   12.489      85.00     91.29      47.00     10.00
   13    0.968   11.630        -         -         34.00     16.00
   14    0.984   11.771        -         -         14.00      1.00
   15    0.970   11.474       0.00      7.16      90.00     30.00
   16    0.984   12.187        -         -         25.00     10.00
   17    0.995   13.995        -         -         11.00      3.00
   18    0.973   11.781       0.00     28.43      60.00     34.00
```

19	0.962	11.315	0.00	-14.27	45.00	25.00
20	0.957	12.191	-	-	18.00	3.00
21	0.958	13.778	-	-	14.00	8.00
22	0.969	16.332	-	-	10.00	5.00
23	0.999	21.249	-	-	7.00	3.00
24	0.992	21.114	0.00	-14.91	13.00	0.00
25	1.050	28.180	220.00	50.04	-	-
26	1.015	29.960	314.00	10.12	-	-
27	0.968	15.604	0.00	3.98	71.00	13.00
28	0.962	13.879	-	-	17.00	7.00
29	0.963	12.885	-	-	24.00	4.00
30	0.985	19.034	-	-	-	-
31	0.967	13.002	7.00	32.59	43.00	27.00
32	0.963	15.061	0.00	-16.28	59.00	23.00
33	0.971	10.854	-	-	23.00	9.00
34	0.984	11.511	0.00	-20.83	59.00	26.00
35	0.980	11.055	-	-	33.00	9.00
36	0.980	11.056	0.00	7.73	31.00	17.00
37	0.991	11.967	-	-	-	-
38	0.961	17.108	-	-	-	-
39	0.970	8.577	-	-	27.00	11.00
40	0.970	7.496	0.00	28.45	66.00	23.00
41	0.967	7.052	-	-	37.00	10.00
42	0.985	8.653	0.00	41.03	96.00	23.00
43	0.977	11.460	-	-	18.00	7.00
44	0.984	13.943	-	-	16.00	8.00
45	0.986	15.773	-	-	53.00	22.00
46	1.005	18.576	19.00	-5.03	28.00	10.00
47	1.017	20.799	-	-	34.00	0.00
48	1.021	20.019	-	-	20.00	11.00
49	1.025	21.022	204.00	115.85	87.00	30.00
50	1.001	18.983	-	-	17.00	4.00
51	0.967	16.364	-	-	17.00	8.00
52	0.957	15.411	-	-	18.00	5.00
53	0.946	14.436	-	-	23.00	11.00
54	0.955	15.348	48.00	3.90	113.00	32.00
55	0.952	15.058	0.00	4.66	63.00	22.00
56	0.954	15.245	0.00	-2.29	84.00	18.00
57	0.971	16.449	-	-	12.00	3.00
58	0.959	15.592	-	-	12.00	3.00
59	0.985	19.448	155.00	76.83	277.00	113.00
60	0.993	23.230	-	-	78.00	3.00
61	0.995	24.121	160.00	-40.39	-	-
62	0.998	23.505	0.00	1.26	77.00	14.00
63	0.969	22.827	-	-	-	-
64	0.984	24.593	-	-	-	-
65	1.005	27.719	391.00	81.51	-	-
66	1.050	27.559	392.00	-1.96	39.00	18.00
67	1.020	24.919	-	-	28.00	7.00
68	1.003	27.598	-	-	-	-
69	1.035	30.000*	513.86	-82.42	-	-
70	0.984	22.618	0.00	9.67	66.00	20.00
71	0.987	22.207	-	-	-	-
72	0.980	21.109	0.00	-11.13	12.00	0.00
73	0.991	21.995	0.00	9.65	6.00	0.00
74	0.958	21.669	0.00	-5.63	68.00	27.00
75	0.967	22.930	-	-	47.00	11.00
76	0.943	21.799	0.00	5.27	68.00	36.00
77	1.006	26.751	0.00	12.17	61.00	28.00
78	1.003	26.447	-	-	71.00	26.00
79	1.009	26.745	-	-	39.00	32.00
80	1.040	28.990	477.00	105.47	130.00	26.00

81	0.997	28.145	-	-	-	-
82	0.989	27.272	-	-	54.00	27.00
83	0.984	28.464	-	-	20.00	10.00
84	0.980	31.000	-	-	11.00	7.00
85	0.985	32.556	0.00	-5.61	24.00	15.00
86	0.987	31.186	-	-	21.00	10.00
87	1.015	31.445	4.00	11.02	-	-
88	0.987	35.690	-	-	48.00	10.00
89	1.005	39.748	607.00	-5.90	-	-
90	0.985	33.338	0.00	59.31	163.00	42.00
91	0.980	33.351	0.00	-13.09	10.00	0.00
92	0.990	33.881	0.00	-13.96	65.00	10.00
93	0.985	30.849	-	-	12.00	7.00
94	0.990	28.682	-	-	30.00	16.00
95	0.980	27.710	-	-	42.00	31.00
96	0.992	27.543	-	-	38.00	15.00
97	1.011	27.916	-	-	15.00	9.00
98	1.024	27.433	-	-	34.00	8.00
99	1.010	27.067	0.00	-17.54	42.00	0.00
100	1.017	28.059	252.00	95.55	37.00	18.00
101	0.991	29.647	-	-	22.00	15.00
102	0.989	32.365	-	-	5.00	3.00
103	1.010	24.318	40.00	75.42	23.00	16.00
104	0.971	21.748	0.00	2.39	38.00	25.00
105	0.965	20.644	0.00	-18.33	31.00	26.00
106	0.961	20.383	-	-	43.00	16.00
107	0.952	17.583	0.00	6.56	50.00	12.00
108	0.966	19.443	-	-	2.00	1.00
109	0.967	18.991	-	-	8.00	3.00
110	0.973	18.144	0.00	0.28	39.00	30.00
111	0.980	19.789	36.00	-1.84	-	-
112	0.975	15.045	0.00	41.51	68.00	13.00
113	0.993	13.993	0.00	6.75	6.00	0.00
114	0.960	14.726	-	-	8.00	3.00
115	0.960	14.718	-	-	22.00	7.00
116	1.005	27.163	0.00	51.32	184.00	0.00
117	0.974	10.948	-	-	20.00	8.00
118	0.949	21.942	-	-	33.00	15.00
			---	---	---	---
		Total:	4374.86	795.68	4242.00	1438.00

Branch Data

Brnch #	From Bus	To Bus	From Bus Injection P (MW)	From Bus Injection Q (MVAr)	To Bus Injection P (MW)	To Bus Injection Q (MVAr)	Loss (I^2 * Z) P (MW)	Loss (I^2 * Z) Q (MVAr)
1	1	2	-12.35	-13.04	12.45	11.01	0.098	0.32
2	1	3	-38.65	-17.06	38.90	16.88	0.250	0.82
3	4	5	-103.23	-26.79	103.43	27.49	0.201	0.91
4	3	5	-68.11	-14.49	69.35	17.28	1.238	5.55
5	5	6	88.47	4.11	-87.54	-1.30	0.930	4.22
6	6	7	35.54	-4.77	-35.48	4.51	0.060	0.27
7	8	9	-440.64	-89.73	445.25	24.43	4.620	57.75
8	8	5	338.47	124.73	-338.47	-92.01	0.000	32.72
9	9	10	-445.25	-24.43	450.00	-51.04	4.745	59.22
10	4	11	64.23	-0.22	-63.36	1.35	0.866	2.85
11	5	11	77.22	2.97	-76.02	-0.62	1.209	4.06
12	11	12	34.29	-35.14	-34.15	35.13	0.147	0.48

13	2	12	-32.45	-20.01	32.73	19.42	0.282	0.93
14	3	12	-9.79	-12.40	9.89	8.86	0.106	0.35
15	7	12	16.48	-6.51	-16.45	5.76	0.027	0.11
16	11	13	35.09	11.41	-34.77	-12.16	0.317	1.04
17	12	14	18.31	2.62	-18.24	-4.14	0.076	0.25
18	13	15	0.77	-3.84	-0.77	-2.04	0.001	0.00
19	14	15	4.24	3.14	-4.21	-7.83	0.030	0.10
20	12	16	7.51	4.30	-7.49	-6.32	0.018	0.07
21	15	17	-103.86	-24.27	105.44	25.22	1.582	5.24
22	16	17	-17.51	-3.68	17.66	-0.30	0.145	0.57
23	17	18	80.27	24.76	-79.39	-22.40	0.881	3.62
24	18	19	19.39	16.83	-19.31	-17.55	0.080	0.35
25	19	20	-10.62	5.17	10.67	-7.71	0.042	0.20
26	15	19	11.53	15.72	-11.47	-16.50	0.050	0.17
27	20	21	-28.67	4.71	28.84	-5.90	0.171	0.79
28	21	22	-42.84	-2.10	43.26	1.76	0.418	1.94
29	22	23	-53.26	-6.76	54.30	7.69	1.042	4.84
30	23	24	8.28	10.42	-8.25	-15.24	0.032	0.12
31	23	25	-162.56	-26.16	166.76	38.63	4.201	21.55
32	26	25	90.29	21.58	-90.29	-18.64	0.000	2.94
33	25	27	143.52	30.06	-137.13	-15.25	6.398	32.79
34	27	28	32.88	-0.59	-32.66	-0.43	0.221	0.99
35	28	29	15.66	-6.57	-15.58	4.64	0.070	0.28
36	30	17	231.19	92.97	-231.19	-70.10	0.000	22.87
37	8	30	74.16	28.15	-73.81	-75.42	0.355	4.15
38	26	30	223.71	-11.46	-219.73	-36.57	3.978	42.82
39	17	31	14.77	11.52	-14.57	-14.73	0.192	0.63
40	29	31	-8.42	-8.64	8.43	7.92	0.016	0.05
41	23	32	92.98	5.05	-90.20	-6.24	2.781	10.12
42	31	32	-29.86	12.40	30.20	-13.60	0.343	1.13
43	27	32	12.53	1.76	-12.49	-3.43	0.040	0.13
44	15	33	7.31	-4.42	-7.28	1.49	0.025	0.08
45	19	34	-3.59	-10.40	3.65	4.60	0.056	0.18
46	35	36	0.84	4.04	-0.84	-4.29	0.000	0.00
47	35	37	-33.84	-13.04	33.99	12.43	0.149	0.67
48	33	37	-15.72	-10.49	15.86	7.46	0.143	0.49
49	34	36	30.25	4.70	-30.16	-4.98	0.085	0.26
50	34	37	-94.31	-44.20	94.59	44.29	0.286	1.05
51	38	37	243.37	113.60	-243.37	-88.01	0.000	25.59
52	37	39	54.91	2.98	-53.92	-2.30	0.992	3.28
53	37	40	44.02	-3.68	-42.85	2.96	1.172	3.32
54	30	38	62.35	19.03	-62.09	-55.98	0.260	3.03
55	39	40	26.92	-8.70	-26.76	7.75	0.154	0.51
56	40	41	15.45	1.19	-15.41	-2.21	0.037	0.13
57	40	42	-11.84	-6.45	11.93	2.30	0.093	0.31
58	41	42	-21.59	-7.79	21.81	5.24	0.221	0.73
59	43	44	-16.59	-1.33	16.77	-3.79	0.177	0.71
60	34	43	1.41	1.63	-1.41	-5.67	0.007	0.03
61	44	45	-32.77	5.48	33.03	-6.62	0.258	1.04
62	45	46	-36.33	-3.57	36.87	2.12	0.544	1.84
63	46	47	-31.11	-1.22	31.48	-0.79	0.364	1.22
64	46	48	-14.76	-5.83	14.90	1.42	0.137	0.43
65	47	49	-9.54	-10.84	9.57	9.28	0.035	0.12
66	42	49	-64.87	5.24	68.04	0.37	3.167	14.30
67	42	49	-64.87	5.24	68.04	0.37	3.167	14.30
68	45	49	-49.70	-2.08	51.44	2.31	1.737	4.72
69	48	49	-34.90	3.21	35.11	-3.93	0.212	0.60
70	49	50	53.66	13.43	-52.88	-13.14	0.785	2.21
71	49	51	66.63	20.44	-64.35	-17.40	2.282	6.43
72	51	52	28.56	6.25	-28.37	-6.99	0.187	0.54
73	52	53	10.37	1.99	-10.32	-5.45	0.054	0.22
74	53	54	-12.68	-5.55	12.74	2.99	0.052	0.24

75	49	54	37.77	13.07	-36.58	-15.60	1.191	4.71
76	49	54	37.74	11.20	-36.38	-13.79	1.365	4.57
77	54	55	7.07	1.46	-7.06	-3.25	0.010	0.04
78	54	56	18.53	4.35	-18.52	-4.98	0.011	0.04
79	55	56	-21.42	-5.82	21.45	5.57	0.026	0.08
80	56	57	-22.99	-9.10	23.21	7.49	0.223	0.63
81	50	57	35.88	9.14	-35.21	-10.49	0.664	1.88
82	56	58	-6.67	-3.69	6.69	1.53	0.019	0.05
83	51	58	18.79	3.16	-18.69	-4.53	0.101	0.28
84	54	59	-30.38	-7.51	30.90	4.26	0.522	2.38
85	56	59	-27.96	-4.17	28.67	0.99	0.711	2.16
86	56	59	-29.31	-3.91	30.07	1.13	0.760	2.26
87	55	59	-34.52	-8.26	35.16	5.88	0.640	2.91
88	59	60	-43.32	3.57	43.94	-4.40	0.623	2.85
89	59	61	-51.72	5.03	52.64	-4.63	0.920	4.21
90	60	61	-112.07	8.52	112.41	-8.23	0.338	1.73
91	60	62	-9.87	-7.11	9.89	5.74	0.017	0.08
92	61	62	25.49	-13.86	-25.42	13.20	0.069	0.31
93	63	59	151.77	67.48	-151.77	-57.02	0.000	10.46
94	63	64	-151.77	-67.48	152.25	52.51	0.482	5.61
95	64	61	30.54	13.99	-30.54	-13.68	0.000	0.30
96	38	65	-181.28	-57.63	184.49	-8.37	3.213	35.16
97	64	65	-182.79	-66.49	183.78	40.06	0.993	11.15
98	49	66	-132.22	4.33	135.22	8.32	3.001	15.32
99	49	66	-132.22	4.33	135.22	8.32	3.001	15.32
100	62	66	-37.16	-17.26	37.93	14.68	0.768	3.48
101	62	67	-24.30	-14.41	24.50	12.15	0.196	0.89
102	65	66	8.54	72.25	-8.54	-70.55	0.000	1.70
103	66	67	53.16	19.27	-52.50	-19.15	0.662	3.00
104	65	68	14.18	-22.43	-14.18	-41.85	0.004	0.05
105	47	69	-55.94	11.63	58.68	-10.07	2.744	9.03
106	49	69	-46.54	10.65	48.78	-12.06	2.242	7.37
107	68	69	-125.80	112.82	125.80	-103.64	0.000	9.18
108	69	70	108.38	16.07	-104.94	-13.98	3.432	14.53
109	24	70	-6.22	-2.97	6.22	-6.80	0.001	0.18
110	70	71	16.65	-12.38	-16.61	11.68	0.038	0.15
111	24	72	1.47	3.31	-1.45	-7.98	0.017	0.07
112	71	72	10.60	-0.94	-10.55	-3.15	0.052	0.21
113	71	73	6.01	-10.74	-6.00	9.65	0.012	0.07
114	70	74	16.21	12.89	-16.01	-15.42	0.196	0.65
115	70	75	-0.13	9.94	0.19	-13.17	0.060	0.20
116	69	75	110.01	20.49	-105.16	-18.31	4.854	14.62
117	74	75	-51.99	-6.19	52.36	6.44	0.367	1.21
118	76	77	-61.15	-21.04	63.21	24.39	2.055	6.85
119	69	77	62.21	6.78	-61.05	-13.80	1.160	3.79
120	75	77	-34.61	-9.55	35.41	7.38	0.803	2.67
121	77	78	45.39	6.61	-45.32	-7.63	0.079	0.26
122	78	79	-25.68	-18.37	25.74	17.95	0.053	0.24
123	77	80	-96.57	-37.41	98.34	37.53	1.773	5.06
124	77	80	-44.37	-20.55	45.05	20.59	0.681	2.43
125	79	80	-64.74	-29.58	65.50	31.08	0.767	3.46
126	68	81	-44.15	-4.61	44.20	-75.54	0.056	0.65
127	81	80	-44.20	75.54	44.20	-73.05	0.000	2.49
128	77	82	-3.03	17.55	3.17	-25.28	0.141	0.40
129	82	83	-47.22	24.39	47.56	-26.99	0.335	1.09
130	83	84	-24.79	14.69	25.35	-15.99	0.560	1.18
131	83	85	-42.77	12.00	43.67	-12.29	0.895	3.08
132	84	85	-36.35	8.99	36.79	-9.24	0.445	0.94
133	85	86	17.17	-7.35	-17.05	5.09	0.119	0.42
134	86	87	-3.95	-15.09	4.00	11.02	0.053	0.39
135	85	88	-50.39	7.60	50.93	-7.53	0.540	2.75
136	85	89	-71.24	0.68	72.49	3.73	1.252	9.06

137	88	89	-98.93	-2.47	100.33	7.70	1.396	7.15
138	89	90	58.22	-4.72	-56.48	5.81	1.740	6.32
139	89	90	110.83	-5.44	-107.93	7.07	2.894	12.12
140	90	91	1.41	4.42	-1.40	-6.46	0.008	0.03
141	89	92	201.54	-2.10	-197.56	16.96	3.981	20.31
142	89	92	63.59	-5.07	-62.02	7.29	1.577	6.34
143	91	92	-8.60	-6.63	8.64	3.59	0.040	0.13
144	92	93	57.62	-11.66	-56.72	12.50	0.904	2.97
145	92	94	52.17	-15.21	-50.75	15.91	1.422	4.67
146	93	94	44.72	-19.50	-44.18	19.44	0.539	1.77
147	94	95	40.86	9.01	-40.62	-9.31	0.237	0.78
148	80	96	18.97	21.07	-18.66	-24.62	0.304	1.55
149	82	96	-9.94	-6.57	9.96	1.29	0.019	0.06
150	94	96	19.79	-9.82	-19.66	7.98	0.128	0.41
151	80	97	26.42	25.75	-26.18	-27.19	0.243	1.24
152	80	98	28.95	8.32	-28.74	-10.43	0.206	0.93
153	80	99	19.56	8.17	-19.35	-12.94	0.213	0.96
154	92	100	31.50	-16.53	-30.71	15.37	0.790	3.59
155	94	100	4.28	-50.54	-3.87	45.81	0.415	1.35
156	95	96	-1.38	-21.69	1.45	20.51	0.079	0.25
157	96	97	-11.10	-20.16	11.18	18.19	0.085	0.43
158	98	100	-5.26	2.43	5.28	-7.30	0.020	0.09
159	99	100	-22.65	-4.59	22.74	2.79	0.093	0.42
160	100	101	-16.74	22.90	16.98	-25.13	0.237	1.08
161	92	102	44.65	-8.39	-44.39	8.13	0.258	1.17
162	101	102	-38.98	10.13	39.39	-11.13	0.414	1.88
163	100	103	121.75	-22.15	-119.40	24.36	2.351	7.72
164	100	104	56.18	10.65	-54.73	-9.41	1.455	6.58
165	103	104	32.45	13.87	-31.85	-15.83	0.597	2.03
166	103	105	43.35	12.85	-42.25	-13.48	1.103	3.35
167	100	106	60.36	9.48	-58.14	-7.12	2.225	8.42
168	104	105	48.58	2.63	-48.33	-2.61	0.250	0.95
169	105	106	8.86	3.88	-8.85	-5.15	0.015	0.06
170	105	107	26.75	-2.37	-26.35	-0.55	0.407	1.41
171	105	108	23.97	-11.13	-23.77	9.92	0.191	0.51
172	106	107	23.98	-3.73	-23.65	0.55	0.331	1.14
173	108	109	21.77	-10.92	-21.71	10.39	0.066	0.18
174	103	110	60.60	8.35	-59.15	-6.15	1.450	6.73
175	109	110	13.71	-13.39	-13.61	11.77	0.102	0.28
176	110	111	-35.70	0.96	36.00	-1.84	0.297	1.02
177	110	112	69.46	-30.61	-68.00	28.51	1.459	3.78
178	17	113	2.06	5.90	-2.05	-6.65	0.004	0.01
179	32	113	4.12	-17.80	-3.95	13.40	0.168	0.56
180	32	114	9.37	1.78	-9.36	-3.22	0.014	0.06
181	27	115	20.72	5.06	-20.64	-6.53	0.081	0.37
182	114	115	1.36	0.22	-1.36	-0.47	0.000	0.00
183	68	116	184.13	-66.36	-184.00	51.32	0.126	1.50
184	12	117	20.15	5.20	-20.00	-8.00	0.153	0.65
185	75	118	40.21	23.59	-39.87	-23.56	0.341	1.13
186	76	118	-6.85	-9.69	6.87	8.56	0.024	0.08
							--------	--------
						Total:	132.863	783.79

Appendix B

Derivative of the current phasor

The derivative of the real and reactive parts of the current phasor is shown as follows:

- Elements corresponding to real power flow measurements $\mathrm{Re}(I_{ij})$:

$$\frac{\partial \mathrm{Re}(I_{ij})}{\partial \delta_i} = -g_{ij}V_i \sin\delta_i - b_{ij}V_i \cos\delta_i - \frac{Bs_{ij}}{2}V_i \cos\delta_i$$

$$\frac{\partial \mathrm{Re}(I_{ij})}{\partial \delta_j} = g_{ij}V_j \sin\delta_j + b_{ij}V_j \cos\delta_i$$

$$\frac{\partial \mathrm{Re}(I_{ij})}{\partial V_i} = -g_{ij} \cos\delta_i - b_{ij} \sin\delta_i - \frac{Bs_{ij}}{2}\sin\delta_i$$

$$\frac{\partial \mathrm{Re}(I_{ij})}{\partial V_j} = -g_{ij} \cos\delta_j + b_{ij} \sin\delta_i$$

- Elements corresponding to real power flow measurements $\mathrm{Im}(I_{ij})$:

$$\frac{\partial \mathrm{Im}(I_{ij})}{\partial \delta_i} = -b_{ij}V_i \sin\delta_i + g_{ij}V_i \cos\delta_i + \frac{Bs_{ij}}{2}V_i \sin\delta_i$$

$$\frac{\partial \mathrm{Im}(I_{ij})}{\partial \delta_j} = b_{ij}V_j \sin\delta_j - g_{ij}V_j \cos\delta_i$$

$$\frac{\partial \mathrm{Im}(I_{ij})}{\partial V_i} = b_{ij} \cos\delta_i + g_{ij} \sin\delta_i - \frac{Bs_{ij}}{2}\cos\delta_i$$

$$\frac{\partial \operatorname{Im}(I_{ij})}{\partial V_j} = -b_{ij}\cos\delta_j - g_{ij}\sin\delta_i$$

where,

V_i and δ_i are the voltage magnitude and phase angle at bus i, respectively;

$g_{ij} + jb_{ij}$ is the admittance of the series branch connecting buses *i* and *j*.

$\frac{Bs_{ij}}{2}$ is the line-charging susceptance.

References

[1] Schweppe F.C. and Wildes J., "Power System Static-State Estimation, Part I: Exact Model", IEEE Transactions on Power Apparatus and Systems, Vol.PAS-89, January 1970, pp. 120-125.

[2] Schweppe F.C. and Rom D.B., "Power System Static-State Estimation, Part II: Approximate Model", IEEE Transactions on Power Apparatus and Systems, Vol.PAS-89, January 1970, pp.125-130.

[3] Schweppe F.C., "Power System Static-State Estimation, Part III: Implementation", IEEE Transactions on Power Apparatus and Systems, Vol.PAS-89, January 1970, pp. 130-135.

[4] R. Miller, Power System Operation, second edition, McGraw-Hill, New York, 1983.

[5] G. Kusic, Computer Aided Power System Analysis, Prentice-Hall, Englewood Cliffs, NJ, 1986.

[6] H. Rustebakke, Electric Utility Systems and Practices, fourth edition, John Wiley & Sons, New York, 1983.

[7] M. Sterling, Power System Control, Peter Peregrinus, LTD, London, 1978.

[8] Greg Kohn, The New IEEE Standard Dictionary of Electrical and Electronics Terms, sixth edition, Inst of Elect & Electronic, 1997.

[9] A. Monticelli, State Estimation in Electric Power Systems, A Generalized Approach, Kluwer, Boston, 1999.

[10] A. G. Phadke, “Synchronized phasor measurements in power systems”, IEEE Computer Applications in Power, Vol. 6, Issue 2, pp. 10-15, April 1993.

[11] Phadke A. G., and Thorp J. S., Synchronized Phasor Measurements and Their Applications, Springer: New York, 2008.

[12] GE Power Systems Engineering, "Assessment of Applications and Benefits of Phasor Measurement Technology in Power Systems", EPRI Final Report, April, 1997.

[13] V. Centero, J. De La Ree, A. G. Phadke and G. Michel, “Adaptive out-of-step relaying using phasor measurement techniques”, IEEE Computer Application in Power Magazine, vol. 6, no. 4, pp. 12-17, October 1993.

[14] B. Bhargava, “Synchronized Phasor Measurement System project at Southern California Edison Co”, in Proceedings of Power Engineering Society Summer Meeting, vol. 1, pp. 16-22, Edmonton, Canada, 1999.

[15] M. Kezunovic and B. Perunicic, “An accurate fault location using synchronized sampling,” Electric Power System Research Journal, vol. 29, no. 3, pp. 161-169, May 1994.

[16] A. Gomez-Exposito, A. Abur, P. Rousseaux, A. de la Villa Jaen, and C. Gomez-Quiles, "On the use of PMUs in power system state estimation," Proc. 17th Power Systems Computation Conference, Stockholm, Sweden, Aug. 22-26, 2011.

[17] J. S. Thorp, A. G. Phadke and K. J. Karimi, “Real time voltage-phasor measurements for static state estimation,” IEEE Trans. Power Apparatus and Systems, vol. PAS-104, no. 11, August, 1985.

[18] A. G. Phadke, J. S. Thorp and K. J. Karimi, “State estimation with phasor measurements,” IEEE Transactions on Power Systems, vol. 1, no. 1, pp. 233-241, Feb. 1986.

[19] T. L. Baldwin, L. Mili, M. B. Boisen and R. Adapa, “Power system observability with minimal phasor measurement placement,” IEEE Transactions on Power Systems, vol. 8, no. 2, pp. 707-715, May 1993.

[20] L. Zhao and A. Abur, “Multi area state estimation using synchronized phasor measurements,” IEEE Transactions on Power Systems, vol. 20, no. 2, pp. 611-617, May 2005.

[21] K. Pflieger, P. K. Enge, and K. A. Clements, “Improving power network state estimation using GPS time transfer,” in Proceedings of Position Location and Navigation Symposium, pp. 188-193, Piscataway, NJ, March 1992.

[22] Final Report on the August 14, 2003, Blackout in the United States and Canada: Causes and Recommendations. U.S.-Canada Power System Outage Task Force. [Online]. Available: https://reports.energy.gov/.

[23] J. Stuller, An Electric Revolution: Reforming Monopolies, Reinventing the Grid and Giving Power to the People, Galvin Electricity Initiative, 2010.

[24] F. Wu, "Power system estimation: a survey", Electrical Power & Energy Systems, vol. 12, no. 2, pp. 80-87, April 1990.

[25] L. Holten, A. Gjelsvik, S. Adm, F.F.Wu, and W.E. Liu, "Comparison of different methods for state estimation," IEEE Transaction on Power Systems, vol. 3, no. 4, pp. 1798-1806, November 1988.

[26] Monticelli A and A. Garcia, "Fast decoupled state estimations," IEEE Transactions on Power Systems, vol. 5, no. 2, pp. 556-564, May 1990.

[27] J. Grainger and W. Stevenson, “Power System Analysis”, New York: McGraw-Hill, 1994.

[28] A. Abur and A. G. Exposito, Power System State Estimation: Theory and Implementation. New York: Mercel Dekker, 2004.

[29] A.G. Exposito and A. Abur, "Generalized Observability Analysis and Measurement Classification", TREE Trans, on Power .Systems, Vol.13, No.3, August 1998, pp. 1090-1096.

[30] A. Monticelli and F.F. Wu, "Network Observability: Theory", IEEE Transactions on Power Apparatus and Systems, Vol. PAS-104, No.5, May 1985, pp.1042-1048.

[31] A. Monticelli and F.F. Wu, "Network Observability: Identification of Observable Islands and Measurement Placement", IEEE Transaction on Power Apparatus and Systems, Vol. PAS-104, No.5, May 1985, pp.1035-1041.

[32] G.R. Krumpholz, K.A. Clements and P.W. Davis, "Power System Observability: A Practical Algorithm Using Network Topology", JEFF Trans, on Power Apparatus and Systems, Vol. PAS-99, No.4, July/Aug. 1980, pp. 1534-1542.

[33] K.A. Clements, G.R. Krumpholz and P.W. Davis, "Power System State Estimation with Measurement Deficiency: An Observability/Measurement Placement Algorithm", IEEE Trans, on Power Apparatus and Systems, Vol. 102(7), 1983, pp.2012 - 2020.

[34] K.A. Clements, G.R. Krumpholz and P.W. Davis, "Power System State Estimation with Measurement Deficiency: An Algorithm that Determines the Maximal Observable Subnetwork", IEEE Trans, on Power Apparatus and Systems, Vol. 101(7), 1982, pp.3044 - 3052.

[35] K.A. Clements, G.R. Krumpholz and P.W. Davis, "Power System State Estimation Residual Analysis: An Algorithm Using Network Topology", IEEE Trans, on Power Power Apparatus and Systems, Vol. 100, No.4, April 1981, pp.1779 - 1787.

[36] Gou Bei and Abur, A., "An Improved Measurement Placement Algorithm for Network Observability", IEEE Trans, on Power Systems, Vol.16, No.4, November 2001, pp.819-824.

[37] L. Mili and Th. Van Cutsem, "Implementation of HTI Method in Power System State Estimation", TREE Trans. on Power Systems, Vol.3, No.3, Aug. 1988, pp.887-893.

[38] E. Handschin, F.C. Schweppe, J. Kohlas and A. Fiechter, "Bad Data Analysis for Power System State Estimation", IEEE Trans, on Power Apparatus and Systems, Vol.PAS-94, No. 2, pp. 329-337, 1975.

[39] N. Xian, S. Wang and E. Yu, "A New Approach for Detection and Identification of Multiple Bad Data in Power System State Estimation", TRRE Trans, on Power Apparatus and Systems, Vol.PAS-101, No.2, pp.454-462, 1982.

[40] A. Garcia, A. Monticelli and P. Abreu, "Fast Decoupled State Estimation and Bad Data Processing" , IEEE Trans, on Power Apparatus and Systems, Vol. PAS-98, pp. 1645-1652, September 1979.

[41] K. A. Clements and P. W. Davis, "Multiple Bad Data Detectability and Identifiability: a Geometric Approach", TREE Trans, on Power delivery, Vol.PWRD-1, No. 3, July 1986.

[42] U.S. Department of Energy Report, DOE/ET/29362-1, "Contribution to Power System State Estimation and Transient Stability Analysis", February 1984.

[43] H. M. Merrill and F. C. Schweppe, "Bad Data Suppression in Power System Static Estimation", TREE Trans, on Power Apparatus and Systems, Vol.PAS-90, pp.2718-2725, Nov. /Dec. 1971.

[44] R. Ebrahimian and R. Baldick, “State estimator condition number analysis,” IEEE Trans. Power Syst., vol. 16, no. 2, pp. 273–279, May 2001.

[45] J. W. Gu, K. A. Clements, G. R. Krumpholz, and P. W. Davis, “The solution of ill-conditioned power system state estimation problems via the method of Peter and Wilkinson,” IEEE Trans. Power App. Syst., vol. 102, no. 10, pp. 3473–3480, Oct. 1983.

[46] Vempati M., Slutsker I., Tinney W., "Enhancements to Givens Rotations for Power System State Estimation". 7EEE Transactions on Power .Systems, Vol. 6(2), pp. 842-849, May 1991.

[47] J. Wang, V. Quintana, "A Decoupled Orthogonal Row Processing Algorithm for Power System State Estimation". 7EEE Transactors on Power Apparatus and Systems, Vol. PAS-103, pp. 2337-2344, August, 1984.

[48] Gu J., Clements K., Krumpholz G., Davis P., "The Solution of Ill-conditioned Power System State Estimation Problems Via the Method of Peters and Wilkinson" . PICA Conference Proceedings, Houston, pp. 239-246, May 1983.

[49] Clements K.A., Davis P. W., "Detection and Identification of Topology Errors in Electric Power Systems" , IEEE Transactions on Power systems, Vol. 3, No. 4, pp. 1748-1753, November 1988.

[50] Matpower: A Matlab Power System Simulation Package. Available at: http://www.pserc.cornell.edu/matpower/.

[51] Power Systems Test Case Archive, University of Washington. [Online]. Available at: http://www.ee.washington.edu/research/pstca/.

[52] R. Ebrahimian and R. Baldick , "State estimator condition number analysis", IEEE Trans. Power Syst., vol. 16, pp.273, 2001.

[53] J. Meng, C. L. Demarco, "Application of Optimal Multiplier Method in Weighted Least-Squares State Estimation, Part I: Theory", The 31st North American Power Symposium, San Luis Obispo, California, October, 1999.

[54] J. Meng, C. L. Demarco, "Application of Optimal Multiplier Method in Weighted Least-Squares State Estimation, Part II: Simulation", The 31st North American Power Symposium, San Luis Obispo, California, October, 1999.

[55] C.L. Lawson and R.J. Hanson, Solving Least Squares Problems, Prentice Hall, Englewood Cliffs, NJ, 1974.

[56] G. H. Golub and C.F. Van Loan, Math computations, North Oxford Academic, Oxford, 1983.

[57] G. Dahlquist, A. Bjorck, and N. Andersson, Numerical Methods, Prentice Hall, Englewood Cliffs, NJ, 1974.

[58] Z. Kun, L Nordstrom, L Ekstam, "Application and analysis of optimum PMU placement methods with application to state estimation accuracy", IEEE Power Energy Society General Meeting, pp. 1 - 7, July, 2009.

[59] M. Çelik and W. Liu, "An incremental measurement placement algorithm for state estimation," IEEE Trans. Power Systems, vol. 10, no 3, pp. 1698- 1730, Aug, 1995.

[60] Q. Li, R. Negi, and M. D. Ilic, "Phasor measurement units placement for power system state estimation: a greedy approach," Power and Energy Society general Meeting, 2011 IEEE, pp. 1-8, 2011.

[61] M. Zhou, V. A. Centeno, J. S. Thorp, A. G. Phadke, "An Alternative for Including Phasor Measurements in State Estimators", IEEE Transactions on Power Systems, Vol.21, No.4, pp. 1930-1937, November 2006.

[62] A. Monticelli and F. F. Wu, "Network Observability: Theory," IEEE Trans. Power Appar. G Syst., Vol. PAS-104, May 1985, pp.1042 – 1048.

[63] J. Chen, Y. Liao, B. Gou, and K. Yocum, “Impacts of load levels and topology errors on WLS state estimation”, North American Power Symposium (NAPS), Champaign, IL, October, 2012.

[64] J. Chen and Y. Liao, "Optimal Placement of Phasor Measurement Units for Improving Power System State Estimation Accuracy: A Heuristic Approach", Journal of Electrical Engineering & Electronic Technology, September, 2012.

VITA

Jiaxiong Chen

Place of birth: Fuqing, Fujian, China

Educational institutions attended and degrees awarded
August 2010 - present
University of Kentucky, Ph.D. candidate in Electric Power Systems Engineering, 2013 (expected)

September 2008 - May 2010
University of Kentucky, M.S. in Electrical Engineering, 2010

September 2004 - June 2008
Hunan University, China, B.S. in Electrical Engineering, 2008

Professional Publications
J. Chen, Y. Liao, B. Gou, and K. Yocum, “Impacts of load levels and topology errors on WLS state estimation”, North American Power Symposium (NAPS), Champaign, IL, October, 2012.

J. Chen and Y. Liao, "Optimal Placement of Phasor Measurement Units for Improving Power System State Estimation Accuracy: A Heuristic Approach", Journal of Electrical Engineering & Electronic Technology, September, 2012.

J. Chen and Y. Liao, "State estimation and power flow analysis of power systems", Journal of Computers, vol. 7, no. 3, 2012.